SONOGENETIC MODULATION TO REVERSE DEPRESSION-RELATED BEHAVIORS

TING LEI

PhD

The Hong Kong Polytechnic University

2025

The Hong Kong Polytechnic University

Department of Biomedical Engineering

Sonogenetic Modulation to Reverse Depression-related Behaviors

Ting Lei

A thesis submitted in partial fulfilment of the requirements for the degree of Doctor of Philosophy

November 2023

CERTIFICATE OF ORIGINALITY

I hereby declare that this thesis is my own work and that, to the best of my knowledge and belief, it reproduces no material previously published or written, nor material that has been accepted for the award of any other degree or diploma, except where due acknowledgment has been made in the text.

(Signed)

Ting Lei **(Name of Student)**

ABSTRACT

Sonogenetics combines genetic tools and low-intensity ultrasound to non-invasively modulate specific neuronal populations and circuits, exhibiting potential for treating brain diseases. This study examines sonogenetics' potential in a mouse depression model, targeting excitatory medial prefrontal cortex (mPFC) neurons that project to its downstream brain area - dorsal raphe nucleus (DRN). Projecting neurons were induced to express a mechanosensitive ion channel, ultrasound was applied, and alterations in patterns of neuronal activation and depressive behaviors were evaluated. Sonogenetics selectively activated targeted excitatory mPFC neurons projecting to the DRN, enhancing real-time DRN neuronal activity and serotonin release, with no observed tissue damage or astrocytic/microglial activation. Tail suspension and forced swim tests revealed that sonogenetically activating this pathway rapidly reversed despair-like behaviors in stressed mice, whereas antidepressant effects observed upon mPFC sonication were abrogated by functionally silencing the downstream DRN neurons. Subsequently, we investigated the direct manipulation of sonogenetic modulation of DRN serotoninergic (5-HT^{DRN}) neurons. We found that sonogenetic modulation of 5-HT^{DRN} neurons significantly increased the neuronal activity and the level of serotonin in the DRN, and alleviated despair-like phenotypes in a real-time manner. There was also no sign of tissue damage or abnormal activation of microglia and astrocytes. Collectively, this study constitutes the first demonstration of the potential for a circuit-targeted sonogenetic therapeutic approach for depression.

ACKNOWLEDGEMENTS

I sincerely appreciate my supervisor Prof. SUN Lei who gave me the opportunity to be a Ph.D. student at this prestigious university and a member of this promising scientific team. I would like to appreciate not only Prof. Sun but also Dr. GUO Jinghui, Dr. QIU Zhihai, Dr. XIAN Quanxiang, Dr. HOU Xuandi, Dr. ZHU Jiejun, Dr. ZHU Ting, WU Yong, SU Min, JIANG Yizhou, JI Jianing, HUANG Xiaohui, ZHAO Xinyi, LIU Langzhou, ZHAO Dongshuai, LI Danni, GONG Zhiyong for their great help towards this research project.

I thank the Warden-Tutor Team of Hall, who provided me with a family vibe, especially Ms. Sanduni. She is not only my colleague as a hall tutor but also one of my best friends. We organized hall activities together, visited many tour sites, enjoyed various foods from different countries, and discussed opinions and feelings toward religions, philosophies, and life. Although we are always busy with our research projects and hall affairs, the little time we spend with each other makes life more colorful.

Here, I express my deepest appreciation to my parents, my intimates, and all family members. They are good models in my life, with attractive qualities and a stable mentality. Whenever I encountered any difficulties, their patience, care, love, and wisdom were like a light in the darkness so that I could always confront these challenges with this powerful light. Their boundless love and support give me enormous encouragement and make my life fulfilled.

TABLE OF CONTENTS

INDEX OF ABBREVIATIONS

Abbreviation	Explanation
5-HT	5-hydroxytryptamine
5-HT^{DRN}	Serotoninergic neurons in the DRN
AD	Alzheimer's disease
AC	Auditory cortex
BLA	Basolateral amygdala
BBB	Blood-brain barrier
Best1	Glutamate-releasing bestrophin-1
BDNF	Brain-derived neurotrophic factor
CLS	Closed-loop deep brain stimulation
CNO	Clozapine-N-oxide
CNS	Central nervous system
CPZ	Chlorpromazine
CRS	Chronic restraint stress
CSF	Cerebrospinal fluid
DA	Dopamine
DBS	Deep brain stimulation
DRN	Dorsal raphe nucleus
ECT	Electroconvulsive therapy
FDA	The United States Food and Drug Administration
FST	Forced swimming test
GBA	Gut-brain axis
GCs	Glucocorticoids
GFAP	Glial fibrillary acidic protein
HPA	Hypothalamus-pituitary-adrenal
IL-1β	Interleukin 1 beta
IL-6	Interleukin 6
LHb	Lateral habenula
LIUS	Low-intensity ultrasound stimulation

(Continued)

Abbreviation	Explanation
LPS	Lipopolysaccharides
MAO	Monoamine oxidase
MDD	Major depressive disorder
MscL	The mechanosensitive channel of large conductance
mPFC	Medial prefrontal cortex
MST	Magnetic seizure therapy
NK	Natural killer
NE	Norepinephrine
OFT	Open field test
PBM	Photobiomodulation
PD	Parkinson’ diseases
RMTg	Rostromedial tegmental nucleus
SNRIs	Serotonin and norepinephrine reuptake inhibitors
SSRIs	Selective serotonin reuptake inhibitors
TM	Transmembrane domains
TMS	Transcranial magnetic stimulation
TNS	Trigeminal nerve stimulation
TPH2	Tryptophan hydroxylase 2
TRD	Treatment-resistance depression
TRP	Transient receptor potential
TST	Tail suspension test
TNF-a	Tumor necrosis factor-alpha
US	Ultrasonic stimulation
VNS	Vagus nerve stimulation
VTA	Ventral tegmental area

CHAPTER 1: Background

Major depressive disorder (MDD) is a prevalent yet challenging mental health condition, plaguing ~3.8% of the population worldwide [1] and becoming the second most important factor in chronic disease burden [2]. Its symptoms include a persistent lack of interest in activities once found enjoyable, coupled with enduring feelings of despair, which can tragically lead to suicidal thoughts and behaviors [1]. Upsettingly, around 800,000 humans die each year because of suicide, and the highest mortality of unnatural causes is depression (30%) [3]. Various types of therapies for depression, including psychotherapy, medications, and neuromodulation methods, are available in clinical practice, but there is still around one-third of patients do not remit after all treatments [4].

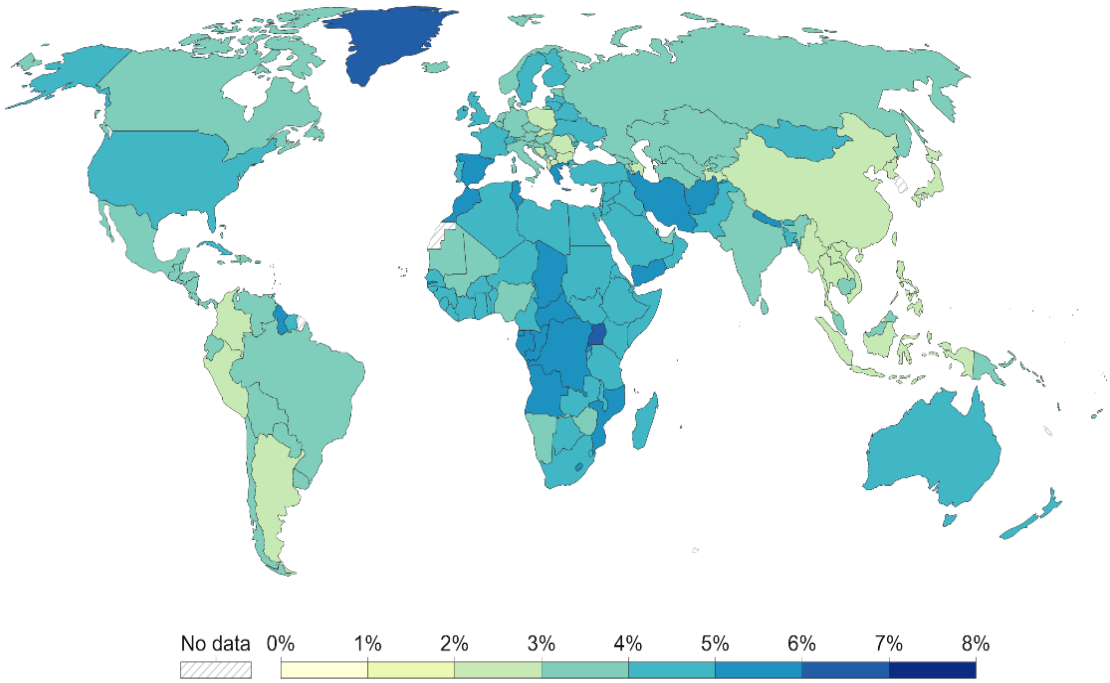

Figure 1. Prevalence of depressive disorders worldwide (adapted from [5]).

1.1 The pathophysiology of depression

Depression is multifactorial; no established mechanism, to date, can unveil all facets of it. Several proposed factors may contribute to depression, including genetic and epigenetic factors, deficient monoamine, dysregulated neuroendocrinology, and neuroimmune system, altered brain structure and neuroplasticity, and abnormal communications among brain circuits.

1.1.1 Genetic and epigenetic factors

Abundant evidence from family and twin epidemiological studies indicates that genetic factors may be a critical contributor to depression [6]. Genome-wide association studies observed higher heritability of depression in families and twins [6]. Populations who are the first-degree relatives of depressive patients show around three-fold higher rates of depression than those from healthy control groups [7]. The published meta-analysis data, the heritability rate of depression is about 35% [8]. However, the specific genetic differences that cause depression have not been revealed partly due to the complicated genetic loci and their complex interaction in this multifactor heterogeneous mental disorder [9].

Recently, several studies indicated the implication of epigenetic changes in depression, in which the gene's functional state is modified while its coding sequences are without changes, such as histone modification and DNA methylation. It was reported that exposure to social stress in early life induced persistent epigenetic changes and depression-related behaviors [10,11]. Prenatal exposure to stress altered the

methylation status of a glucocorticoid receptor in newborns as well as depression-related behaviors [12]. Postmortem studies have identified significant variations in DNA methylation in the frontal cortex when comparing individuals with depression to a healthy control group [13]. These observations collectively indicated that genetic and epigenetic factors contributed to the progress of depression, but how they contribute to depression is waiting for further investigation.

1.1.2 Monoamine hypothesis

This typical hypothesis suggests MDD is primarily resulted from insufficient levels of neurotransmitters, including 5-HT, DA, and NE in the CNS [14]. Historically, the key phenomena supporting the hypothesis were observed in the 1950s. Reserpine, a compound derived from the roots of the Rauwolfia serpentina plant (commonly known as Indian snakeroot), was one of the first effective drugs for treating hypertension at that time; however, it was found to result in depression-related symptoms in some patients [15]. Later, reserpine was demonstrated to inhibit vesicular monoamine, causing the synaptic depletion of 5-HT, DA, and NE [15]. Furthermore, administration of monoamine precursors was effective in reversing reserpine-induced depression-related syndromes, putting monoamine levels in the brain as a crucial mechanism underlying depression [16].

At the same time, other supportive evidence has been discovered. Iproniazid, an antibiotic effective in treating tuberculosis previously, was serendipitously discovered to improve the mood of patients with tuberculosis [17]. In 1957, psychiatrist Nathan S.

Kline and his colleagues first demonstrated the antidepressant role of iproniazid in depressed humans with non-tuberculosis [18]. Additionally, iproniazid has been investigated by chemists and was found to be a type of MAO inhibitors, which functioned by decreasing the degradation of monoamine neurotransmitters once reabsorbed thereby increasing their concentration in the CNS [19]. In parallel to these discoveries, the chemical modification of the structure of polycyclic phenothiazine ring gained unprecedented attention in the 1950s due to the attractive therapeutic success of chlorpromazine (CPZ) as a psychotropic drug [20]. In 1958, Roland Kuhn first reported the antidepressant effects of imipramine, a tricyclics derived from CPZ, in patients with severe depression [21]. The mechanism underlying its therapeutic effects is thought to pharmacologically inhibit the presynaptic norepinephrine and serotonin reuptake transporters thereby elevating the level of NE and 5-HT in synaptic [22]. These millstone discoveries not only defined the first-generation antidepressant drugs targeting the monoaminergic system but also paved the way for the naissance of current biological/molecular psychiatry [23].

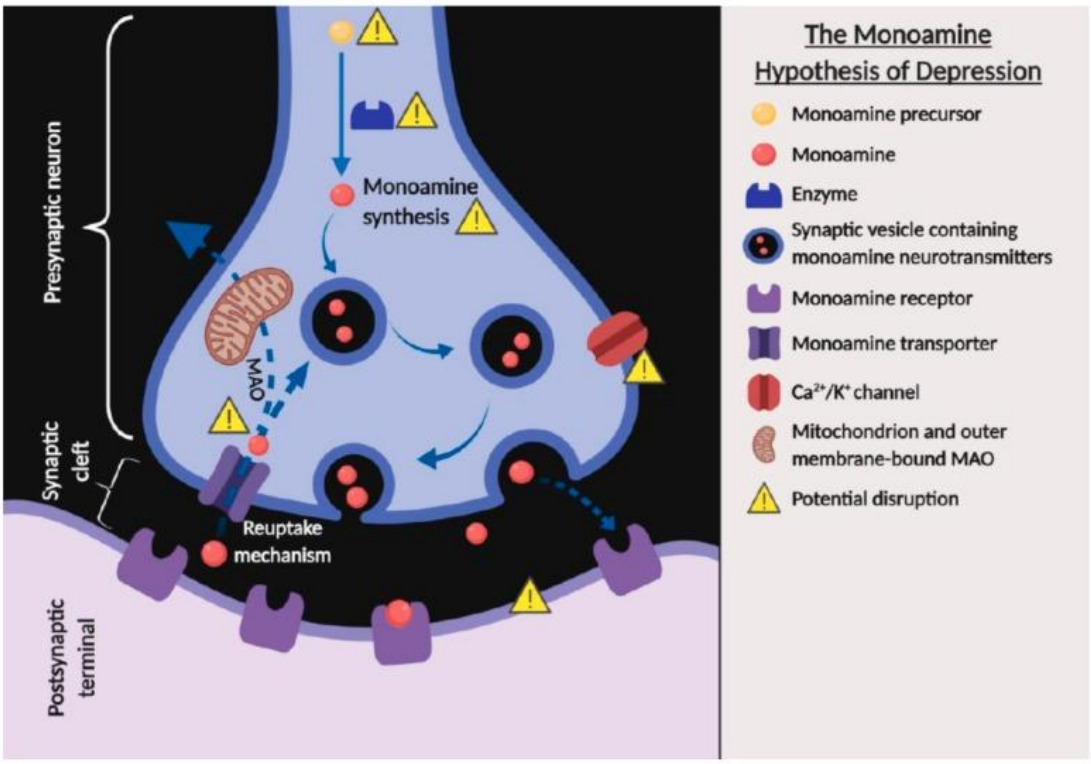

Figure 2. The monoamine hypothesis of depression (adapted from [24]).

1.1.3 Neuroendocrinology and neuroimmunology

Depression alters brain activity and affects the peripheral body as well. Many observations of the abnormalities of hormones in depressive patients indicated that endocrine disturbances might participate in the development of depression [25]. It was consistently reported that the level of cortisol (a glucocorticoid hormone produced by the adrenal cortex) in depressive patients significantly increased [26,27]. The hypersecretion of hypothalamic CRH from the cerebrospinal fluid (CSF) in depressive patients was also observed [28], indicating the implication of the HPA axis in depression.

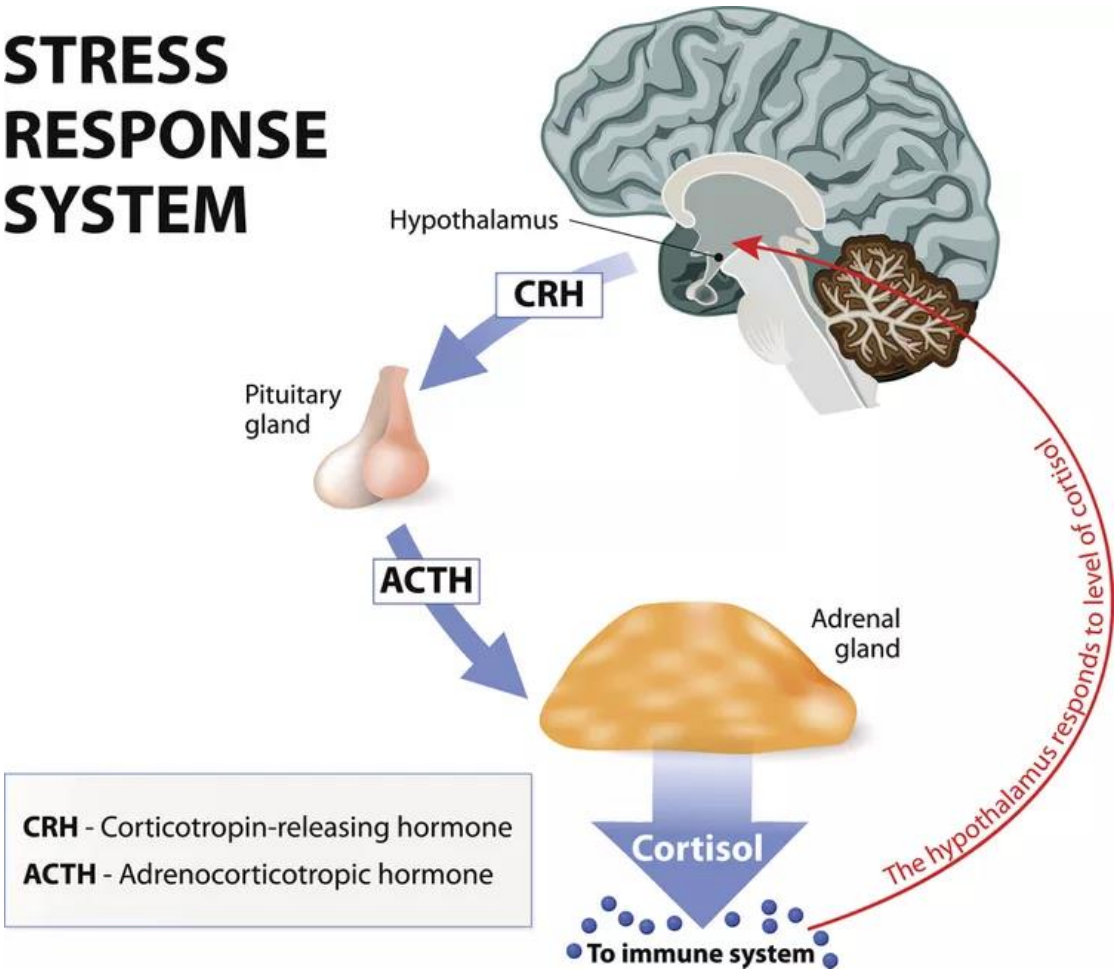

Figure 3. The structure of the HPA axis (adapted from [29]).

Glucocorticoid receptors are naturally present in immune cells [30]. When the HPA axis is activated, the systemic release of glucocorticoids increases, playing a role in regulating the inflammatory system [31]. Additionally, many clinical studies consistently found an increased level of multiple inflammatory immune biomarkers in patients with depression, including IL-1β [32,33], IL-6 [32-34], and TNF-a [32]. Pre-clinical studies have also noted profoundly increased pro-inflammatory immune biomarkers as abovementioned in different animal models of depression [35]. Furthermore, it was reported that intracranial administration of IL-1β [36] or IL-6 [37] into the hippocampus induced depressive-like behaviors, while specific administration of antibodies of IL-

1β [36] or IL-6 [37] reversed these behaviors. In addition, it was also reported the activation of immune cells, like leukocytes, monocytes, and neutrophilia [38], T cell proliferative capacity [39], and reduced natural killer (NK) cell cytotoxicity [40] in clinical depressive patients. These phenomena further cause the elevation of inflammatory cytokines [41].

Peripheral cytokines and immune cells also regulate the activity of the CNS, especially glial cells which endogenously express inflammatory mediator receptors [42] [35]. When mice were exposed to the stress of social defeat, monocytes infiltrated specific brain regions and differentiated into microglia-like cells to induce inflammatory activation [43]. In contrast, preventing monocyte trafficking by decreasing the chemokine CCR2 ameliorated depressive-like behaviors in mice [43]. Microglia isolated from stressed mice secreted more cytokines, like IL-1β and IL-6, when exposed to lipopolysaccharides (LPS) [44]. In clinical studies, increased recruitment of peripheral monocytes into the brain [45] and microglia activation [46] was observed in depressive patients. Post-mortem analysis of brain tissue also showed an increased microglia activation in suicidal than non-suicidal depressive patients [47,48]. Moreover, blood circulating cytokines can affect astrocytes' transcriptome profiles and then change their end feet on the blood-brain barrier (BBB) to further alter its permeation and make leakage of cytokines thereby changing the activity of surrounding neurons and affecting behaviors [35]. The evidence indicated that stress induced both the hyperactivity of the HPA axis and the immune system's unbalance.

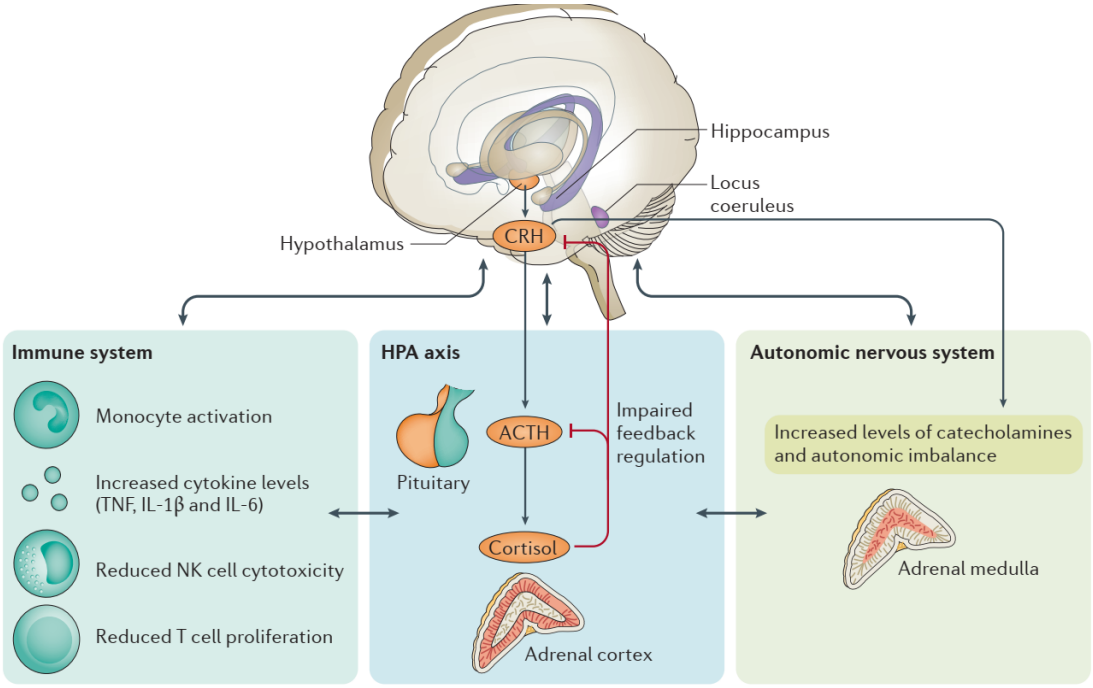

Figure 4. The neuroendocrine and immune system (adapted from [6]).

1.1.4 The dysbiosis of gut microbiota

Gut microbiota consists of microorganisms that reside on the surface of digestive tracts and engage in mutual interactions with their host animals [49]. Gut dysbiosis is involved in mental disorder via the gut-brain axis (GBA) in which metabolites produced by gut microbiota, such as immune factors, neurotransmitters, fatty acids, and hormones, pass through the epithelial barrier, initiate inflammation, act on the CNS, and eventually influence mental states [50]. It was reported that inflammatory factors induced by gut dysbiosis impaired the function of the HPA axis and dysregulated cortisol, which further influenced the intestinal environment surrounding gut microbiota [50].

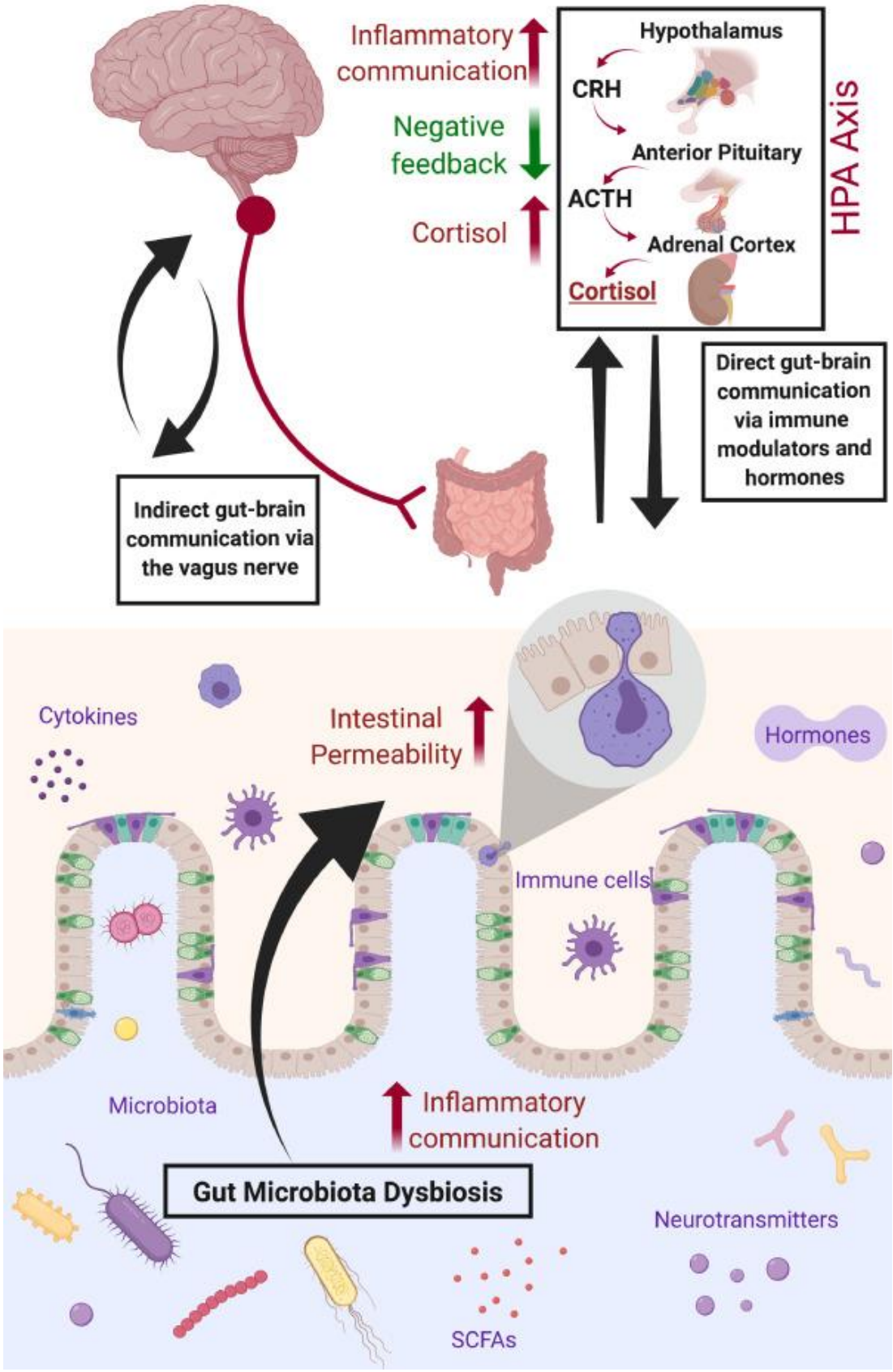

Figure 5. Gut microbiota dysbiosis (adapted from [50]).

Interestingly, the comorbidity rate between depression and irritable bowel

syndrome (a common gastrointestinal disorder) has been reported to be over 84% [51]. Recent reports have shown that the composition of gut microbiota differs significantly between depressive patients and healthy individuals [52]. Transplanting faecal microbiota of mice exhibited depressive phenotype into wide-type mice induced depressive-like behaviours, and vice versa [53]. However, the exact mechanisms by which gut microbiota influence depression remain unclear, necessitating further research to better understand their role.

1.1.5 Neuroplasticity and structural alterations

The altered cortisol levels and the dysregulated immune system affect neuroplasticity and brain function [6]. Immune cells and cytokines were reported to regulate the formation of synaptic structures and neuronal connections primarily via modulating the neurotrophic factors [54]; neurotrophic factors are endogenous biomolecules that control and support the growth and survival of both developing and mature neurons [55]. Preclinical studies demonstrated that chronic stress reduced the expression of BDNF as well as the hippocampal neurogenesis [56,57], while administration of BDNF or other MAOIs and TCAs prevented stress-induced decreased BNDF levels and ameliorated depressive-like behaviors in rodents [58,59]. In addition, BDNF fosters the growth and enhances the function of serotonergic neurons and further elevates the serotonin levels in synaptic clefts [60]. Consistently, systematic reviews and meta-analyses of clinical studies indicated that BDNF from serum was abnormally reduced in depressive patients, which was normalized after receiving

antidepressants [61]. These findings collectively put the abnormal level of BDNF as a manifestation of depression.

The alterations in molecular and cellular levels may ultimately affect the structure of the brain in depressive patients [6]. Lots of neuroimaging evidence has indeed observed the volume changes of many brain regions correlated with depression, including the frontal lobe, thalamus, hippocampus, and striatum [62]. Thereinto, the frontal lobe is a crucial brain area regulating emotion-related behaviors; its lesion has been considered to cause depression or other mental disorders [63]. The thickness of the frontal lobe is reduced in patients with depression [64]. The volume of gray matter is also decreased in depressive patients [65], which can be normalized after treatment [66]. The thalamus, a brain area that has anatomic connections with the frontal lobe, has also been reported to reduce volume in depressive patients [67]. In addition, depressive patients who committed suicide showed a reduced density of gray matter in the striatum [68-70]. The volume of hippocampus, which strongly correlated with stress and the HPA axis activity, was significantly smaller (17%) in depressive patients [71,72]. Importantly, the volume of gray matter in the hippocampus increased following depression treatment [73]. These observations collectively suggest that the structural alteration of the brain was strongly correlated with depression, which has the potential to be a diagnosis marker for depression in clinics.

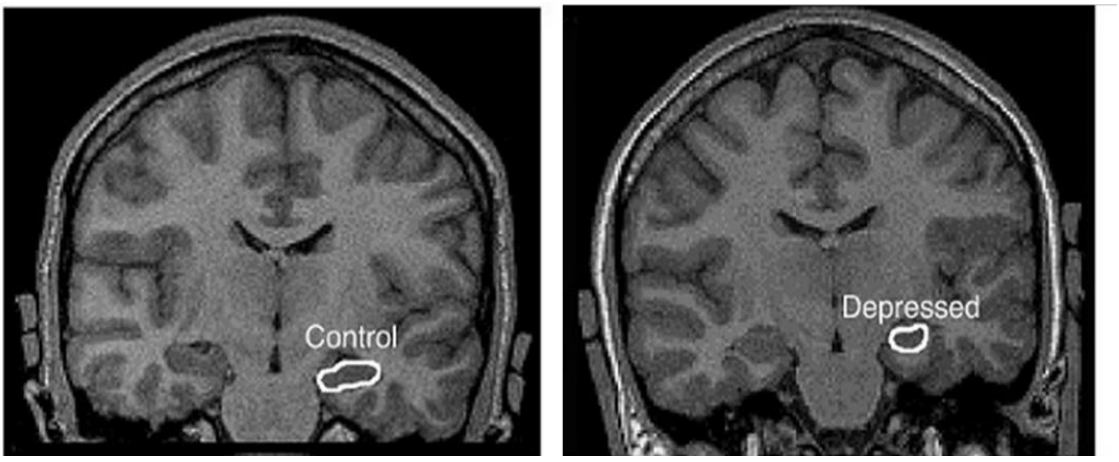

Figure 6. The atrophy of the hippocampus (adapted from [72]).

1.1.6 Functional brain circuits

The change of the abovementioned factors will ultimately lead to abnormal communication among different brain regions. A revolutionary neuromodulation method - optogenetics - manipulated different specific cell types and neural circuits with a precise spatiotemporal resolution by heterogeneously overexpressing light-sensitive proteins [74], offering a high-fidelity neuromodulatory tool to dissecting the circuit level abnormalities underlying disease, such as depression [75]. The dysfunction of specific brain regions and their abnormal communication with distal brain structures was strongly correlated with depression, mainly including the mPFC, DRN, LHb, hippocampus, NAc, VTA, and amygdala [76]. The mPFC is a critical central hub to process a diverse array of cognitive and emotional changes, strongly implicated in psychiatric disorders [77]. It was reported that the synaptic transmission from the mPFC to the NAc is significantly decreased when mice were susceptible to stress and that specific activation of this circuit in mice induced resilience to stress [78]. It was also demonstrated that selectively optogenetic activating the glutamatergic neurons in

mPFC that projecting to the DRN or the LHb rapidly reversed or triggered despair-like states in rats [79], while indiscriminate optogenetic stimulation of the mPFC has produced mixed results [74,80], highlighting the importance of selectivity. The DRN is the primary source of neurotransmitters -serotonin - in the CNS [81], which regulates reward-, stress-, and emotion-related behaviors [82]. Specific activation of serotoninergic neurons [83,84] or inhibition of GABAergic neurons [85] in the DRN ameliorated depressive-like behaviors in rodents. Optogenetic stimulation of the axonal terminals in the LHb that projected from the DRN inhibited neuronal activity in the LHb, resulting in antidepressant effects in rodents [86]. The LHb modulates the function of the monoamine system in the CNS and regulates motivational and affective emotional states [87]. Optogenetic activation of the circuit – the LHb to the rostromedial tegmental nucleus (RMTg, a GABAergic nucleus that functions as a brake for the midbrain monoamine system) - evoked a despair-like state in a real-time manner, while optogenetic inhibition of this circuit elicited the opposite effects [88]. The hippocampus is a processing center of cognition and memory, which is also involved in depression. Optogenetic activation of the circuit projected from the ventral hippocampus to the mPFC rapidly reversed depression-related behaviors [89]; optogenetic activation of the circuit connecting the ventral hippocampus to the NAc led to depressive-like behaviors [78]. The VTA is a well-known dopaminergic nucleus that regulates reward-related behaviors. Optogenetic activation of dopaminergic neurons in the VTA ameliorated depressive-like behaviors [80]. The amygdala is a critical hub in the CNS to process fear stimuli, which is also associated with

emotional processes [90]. Optogenetic activation of basolateral amygdala (BLA) to the NAc induced depression-related behaviors in mice [91]. All these findings provide fundamental evidence of pathological mechanisms in depression; meanwhile, demonstrations in large animals and humans are still needed in future research.

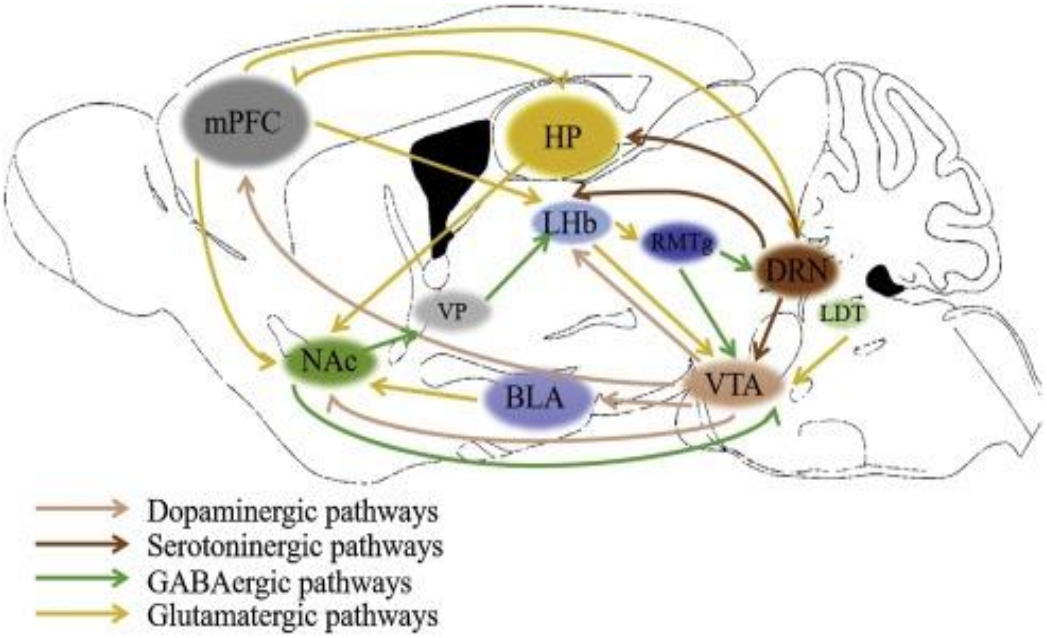

Figure 7. The neural circuits related to depression (adapted from [76]).

1.2 The treatment of depression

In clinics, the first-line intervention at present for depression treatment includes medication, psychotherapy, or a combination of the two. Typically, as for patients with inadequate responses following the above-mentioned therapies (a.k.a., treatment-resistant depression, TRD), alternative non-pharmacologic neuromodulation therapies have also been provided in clinics. The step-care model of depression in the clinic is shown as follows.

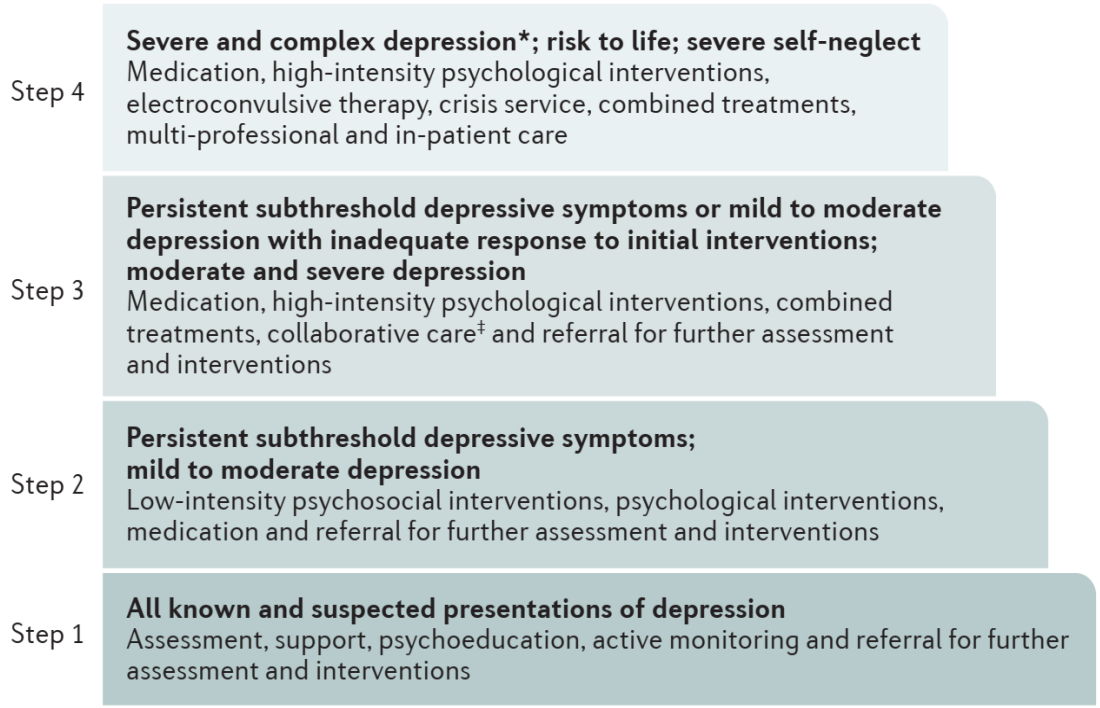

Figure 8. Stepped-care model in the management of depression (adapted from [6]).

1.2.1 Psychotherapy and medications

In the management of depression, psychotherapy can be initially used [6]. There are also various types of antidepressant drugs are available in clinics. These typically include SSRIs, SNRIs, MAO inhibitors, and cyclic antidepressants, which are believed to relieve depressive symptoms mainly by increasing monoamines levels in synapses [92]. Due to fewer side-effects and the efficiency, SSRIs, and SNRIs are the first-line medicine for depressive patients now [92].

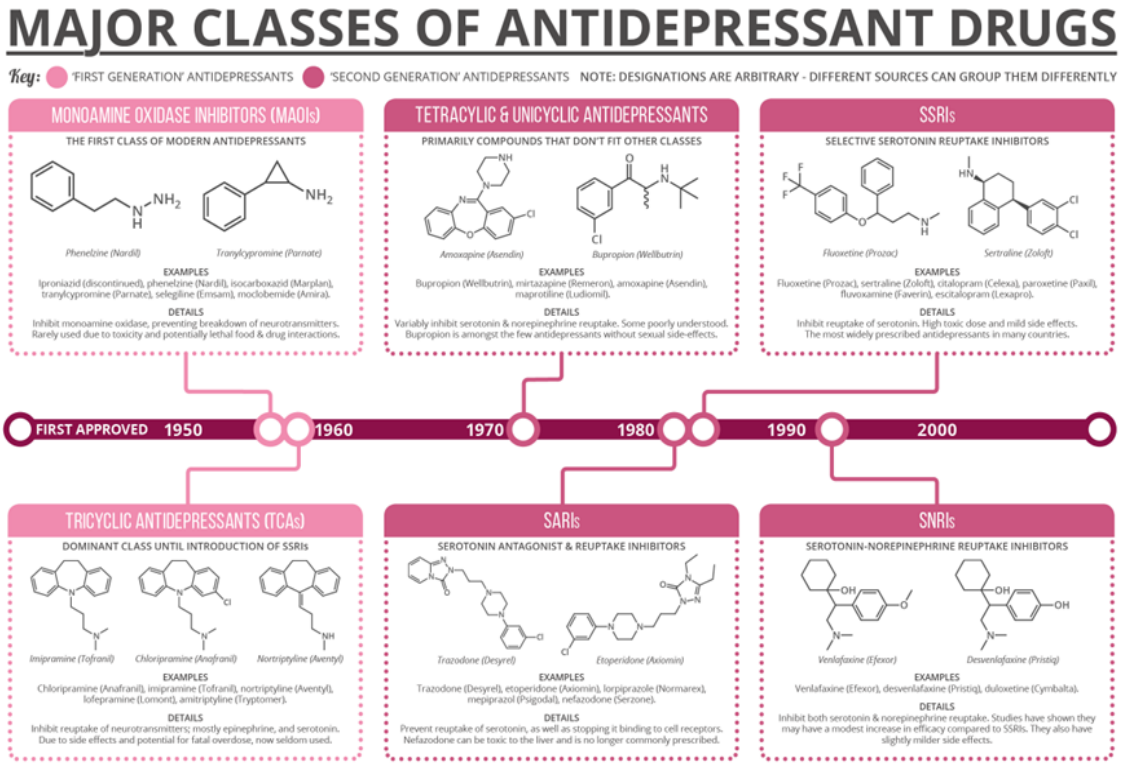

Figure 9. Major classes of antidepressants (adapted from [93]).

Clinical studies also indicated that combined treatment with medication and psychotherapy increased the response rate when compared to monotherapy alone, but there are still more than 50% of patients who don't show response to these treatments [94,95]. As for those patients, there are also alternative neuromodulation therapies.

1.2.2 Neuromodulation therapies

To date, there are three non-pharmacologic neuromodulation therapies for depression treatment have been approved by the FDA [96], including ECT, VNS (only for adults), and TMS [97]. ECT is to utilize a minor electric current to non-invasively stimulate patients' brains under general anesthesia to intentionally induce a generalized seizure thereby relieving depressive symptoms [98], sometimes

accompanied by serval side-effects, such as disorientation, cognitive impairment, or even memory loss [97]. In VNS, a small pulse generator is surgically put into the left thoracic region to continuously stimulate the left vagus nerve for depression treatment [97], commonly accompanied by sign of hoarseness, cough, voice alteration, and paresthesia because of invasive implantations [99]. By contrast, TMS shows rare side-effects, in which non-invasive magnetic fields are used to repeatedly stimulate the medial prefrontal cortex to relieve depressive symptoms [100], but it needs long-circle treatment to trigger antidepressant effects and there are still over 40% of patients are not in remission [101].

Noninvasive Intervention	Pros	Cons
Transcranial Magnetic Stimulation (TMS) FDA-approved office-based treatments using electromagnetic conduction to stimulate areas of the brain, typically the dorsolateral prefrontal cortex	• Pairs well with behavioral activation because it provides daily structure for patient • Patients can continue daily routine (work, driving) • Minimal adverse effects; good option in severe depression without psychosis or acute suicidality if patients worry about effects of ECT	• Time-intensive, requires 4-8 weeks of daily treatment • Small risk for seizures
Electroconvulsive Therapy (ECT) FDA-approved treatment given under general anesthesia using a short burst of electrical stimulation to induce a generalized tonic clonic seizure	• Proven safe and effective in unipolar, bipolar, psychotic, and peripartum depression • Rapid improvement over the span of 2-4 weeks	• Acute cognitive effects limits ability to work and drive • Risk for memory impairment
Invasive Intervention	**Pros**	**Cons**
Vagus Nerve Stimulation (VNS) FDA-approved treatment using a surgically implanted stimulator to deliver repetitive stimulation to the left cervical vagus nerve	• May be effective in a highly treatment-resistant depression population • Good option in patients who respond to ECT but quickly relapse (also effective in ECT nonresponse)	• Surgical risks as well as risks for dysphagia and dysphonia • May require long duration of treatments before response is seen • Not yet covered by most insurance

Figure 10. FDA-approved neuromodulatory approaches for depression (adapted from [102]).

Increasing amounts of neuromodulation techniques for depression treatment are in progress. Magnetic seizure therapy (MST), is a procedure in which a high-frequency transcranial magnetic field is put into the brain to elicit generalized seizure to relieve depressive symptoms (2-3 MST sessions are given per week until remission or a maximum of 24 sessions), without adverse effects on memory [103]. Confirmatory

efficacy and safety trials of MTS for depression treatment under double-blind randomized conditions are ongoing (ClinicalTrials.gov, NCT03191058). Transcutaneous auricular VNS, a potential alternative to implanted VNS, non-invasively applies an electrical signal to stimulate the auricular branch of the vagus nerve around the ears for several weeks to achieve depression remission [104]. Deep brain stimulation (DBS), involving surgically placing electrodes into specific brain areas for electrical stimulation, has been developed for many years and shown treatment efficacy in TRD, but the inconsistent findings reported by clinical studies hinder their advance in clinical practices [97,105]. The interindividual response heterogeneity, at least in part, contributes to this controversial observation [106]. Recently, an intriguing study adopted a CLS in one patient with TRD, in which focal electrical stimulation electrodes and intracranial electrophysiology recording systems were firstly implanted in the brain to find a personalized biomarker and treatment sites, and then a NeuroPace responsive neurostimulation system was implanted to continuously sense neural activity and deliver electrical stimulation triggered by prespecified patterns of neuronal activities, resulting in a rapid and sustained amelioration in depression [106]. The clinal trial investigating CLS in a broader population of depression is ongoing (ClinicalTrials.gov, NCT04004169). Other novel neuromodulation attempts for depression treatment have also been made. Trigeminal nerve stimulation (TNS), a strategy of non-invasively applying an electric current to the trigeminal nerve over the skin of the forehead, is reported to yield an improvement in TRD patients after a 10-day intervention in a recent study [107]. Another innovative

neuromodulation strategy called brain photobiomodulation (PBM) therapy, which non-invasively delivers red to near-infrared light to the brain thereby stimulating mitochondrial respiratory chains, increasing adenosine triphosphate (ATP), and enhancing metabolic capacity of neurons, showing an early improvement in depression after dozens of PBM sessions [108]. More clinical trials applying PBM to treat depressive patients are ongoing [109].

1.3 Ultrasound neuromodulation

Ultrasound neuromodulation, a burgeoning neuromodulation method, has gained widespread attention worldwide due to its high spatiotemporal resolution [110], been widely applied to various brain regions to investigate, restore, and enhance brain function [111].

1.3.1 Ultrasound and its bioeffects

Ultrasound, a mechanical pressure wave, is characterized by a frequency beyond human hearing (> 20 kHz). It originates as a generator of electrical signals, which are then enhanced by an amplifier, and finally converted to acoustic pressure waves via a transducer with piezoelectric elements. The main parameters of ultrasound are frequency, amplitude (i.e., intensity), duty cycle (T1/T2, pulse width/pulse interval), stimulus duration and interval. Thereinto, the frequency is positively correlated with spatial resolution but also tissue attenuation [112]. The intensity can be broadly divided into high- and low-intensity to ablate tissues via thermal effects and

stimulate/modulate cellular populations via non-thermal actions [113].

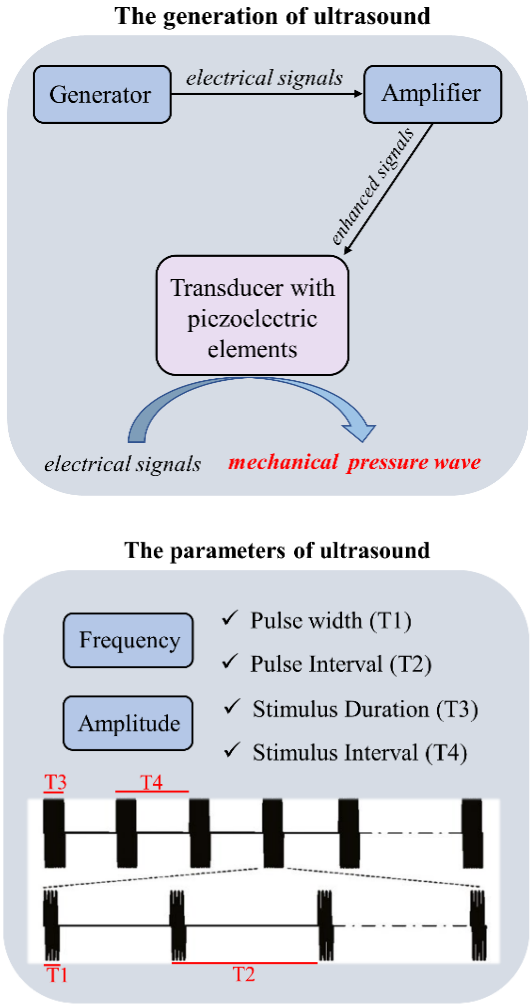

Figure 11. The generation and parameters of ultrasound.

While ablation with high-intensity ultrasound is known to occur via thermal effects, the impact of low-intensity ultrasound on neurons is quite complex. Many studies have indicated minimal or negligible changes in temperature with low-intensity ultrasound stimulation (LIUS) [114-116], suggesting there are other mechanisms mediating its bioeffects. It was reported that LIUS activated auditory pathways to produce neuromodulation effects while destroying it abrogated the bioeffects from LIUS. [117,118]. However, lots of studies have observed that LIUS can directly activate neuronal populations in cultured primary neurons where the auditory pathways did

not exist [119]. Furthermore, many studies observed the neuromodulatory effects of LIUS in mouse models of deafness [120]. The discrepancy among these studies may be because of different ultrasound parameters or recording methods [121,122], but it suggests that LIUS bioeffects are very complicated. Intramembrane cavitation has also been observed when LUIS, in which the oscillation of intramembrane hydrophobic space in response to ultrasound leads to cavitation and leaflets separation thereby altering the membrane characteristics and cellular activity [123,124]. Recently, many studies discovered various mechanosensitive ion channels, such as the mechanosensitive channel of large conductance (MscL) [125], piezo channels [126-128], transient receptor potential (TRP) channels [129-131], potassium channels [132,133], voltage-gated sodium channels [132], which may serve as an important mediator to ultrasound bioeffects [134]. A recent study indicated that ultrasound first activates many TRP channels and thus elicits calcium influx, whose accumulation activates calcium-sensitive sodium channels, induces depolarization of the neuronal membrane, activates voltage-gated calcium and sodium ion channels, and finally excites neurons to fire [135]. Cytoskeletal proteins and integrins may be involved in deforming the membrane in such a way affecting the interaction of ultrasound with ion channels [136,137]. Apart from the short-term effect, LIUS impacts sustained synaptic plasticity, and the influence is varied among different ultrasonic parameters in rats [138]. Taken together, the neuromodulatory effects of LIUS are collectively mediated by various mechanosensitive ion channels in different types of cellular populations, which alter integration and transmission within the sonicated brain region in a manner sufficient to affect behavior.

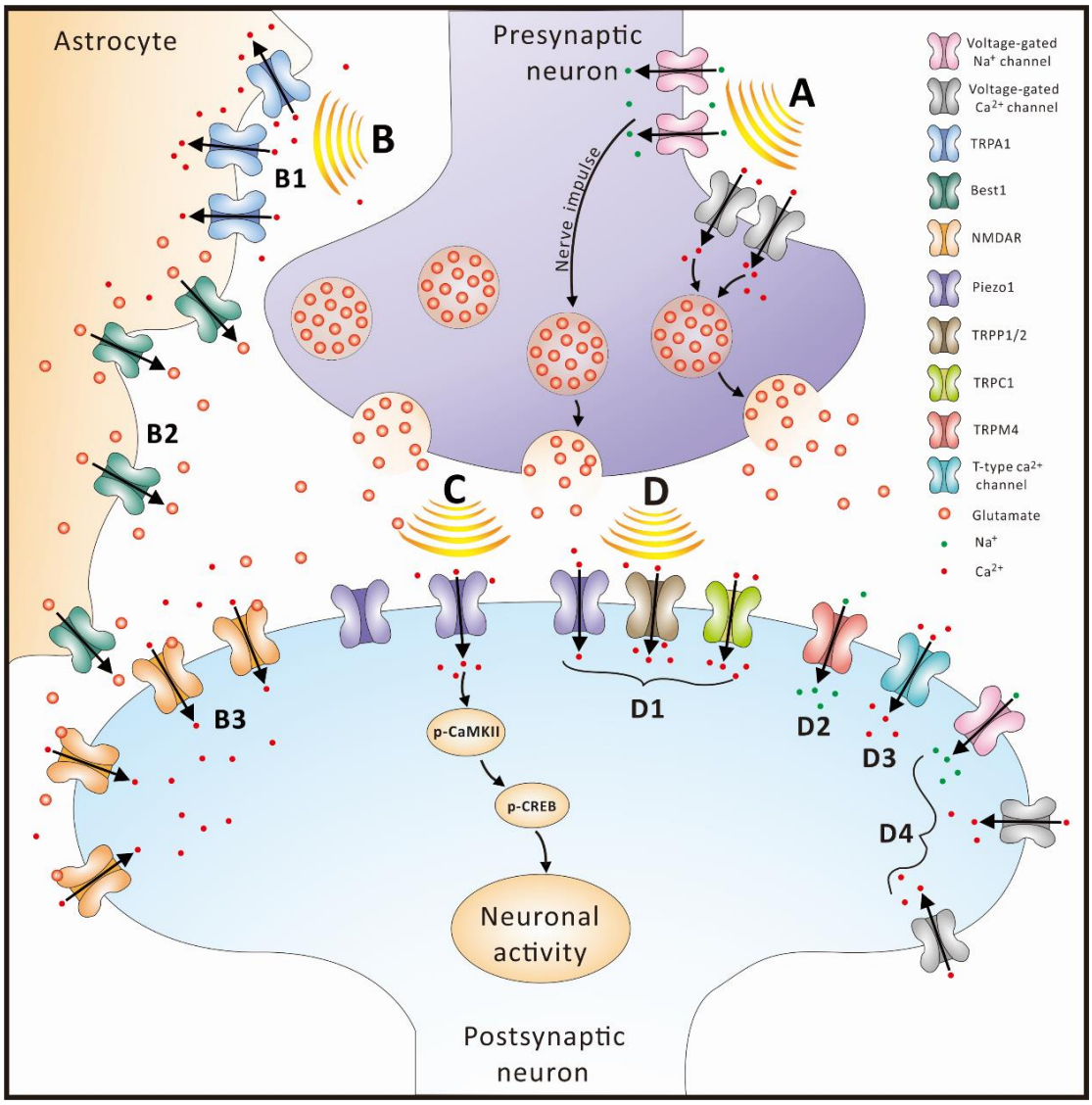

Figure 12. Proposed mechanisms underlying ultrasonic neuromodulation. a) LIUS-activated voltage-gated sodium and calcium channels to stimulate electrical activity and trigger the release of neurotransmitters [134]. **b)** In astrocytes, LIUS activated TRPA1 channels, which induced calcium influx (B1). The accumulated intracellular calcium increased glutamate release through Best1 channels (B2) and then affected NMDA receptors (B3) [131]. **c)** LIUS activated Piezo1 cation channels and enhanced calcium influx thereby activating CaMKII and CREB and affecting neuronal activity [119]. **d)** LIUS activated TRPP1/2, TRPC1, and Piezo1, which elicited calcium influx (D1). The accumulation of calcium calcium-sensitive sodium channels

such as TRPM4 (D2), then T-type calcium channels (D3), which further activated voltage-gated calcium and sodium channels (D4), and finally excited neurons [139].

1.3.2 Current application of ultrasound neuromodulation

Ultrasound can be applied to the brain to alter neuronal activity within specific brain regions to investigate, restore, or enhance brain function. The following sections will discuss various modalities that may be used in vivo.

It was reported that the mood of human beings who received LIUS was significantly improved [140,141]. Several pre-clinical studies also indicated that non-invasive LIUS of the mPFC [142-144] or the DRN [145] (two brain regions that are widely used as targets for depression treatment [80]) for consecutive several weeks ameliorated depression-related behaviors in rodents. In addition, many investigators have attempted to utilize LIUS to treat other brain diseases, including PD [146,147], AD [148], and epilepsy [149-152]. LIUS of the subthalamic nucleus significantly weakened neuronal oscillatory activity [146], and increased levels of striatal dopamine and locomotor ability in the mouse model of PD [147]. Furthermore, LIUS pretreatment prevented cerebral damage and cognitive dysfunction in an aluminum chloride-induced model of AD [148]. In addition, LIUS was reported to inhibit epileptic-like firings and ameliorated epileptic-related behaviors in the kainic acid-induced mouse model of epilepsy [149,150] and pentylenetetrazol-induced rat model of epilepsy [151,152]. But there is much that remains unclear, how mechanosensitive ion channels are distributed throughout the brain, how they interact with ultrasound, how cytoskeletal components mediate these

effects, and finally how all these factors interact in diverse physiological and pathological conditions.

Apart from the direct therapeutic effects of ultrasound neuromodulation, many studies used ultrasound to open the BBB to relief brain diseases or deliver drugs. It was reported that using ultrasound stimulation to open BBB ameliorated cognitive impairment in animal models of AD [153]. Ultrasound has also been used to deliver chemical agents [154] or genes [155] to modulate neuronal activities.

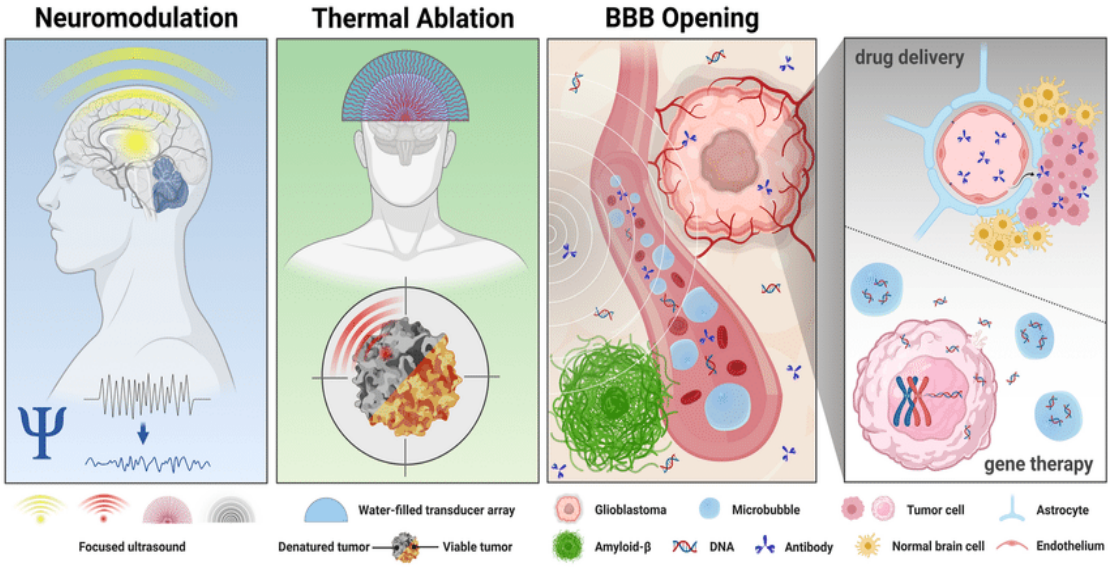

Figure 13. The applications of ultrasound neuromodulation (adapted from [156]).

1.3.3 Sonogenetics

As we mentioned above, endogenous mechanosensitive ion channels can confer ultrasonic mechanical forces on neurons to affect their activity, however, to date, their spatial distribution in the brain is quite unclear. To realize targeting specific neuronal populations with ultrasound, sonogenetics (the counterpart of optogenetics) emerges. Sonogenetics combines ultrasound and genetic modifications. To be specific, it uses

non-invasive ultrasound to manipulate specific neuronal populations genetically modified with ultrasound-sensitive ion channels [110]. This concept was first reported in 2015 that overexpressing ultrasound-responsive TRP-4 ion channels in ASH and AWC sensory neurons, PVD neurons, and AIY neurons specifically sensitized these neuronal populations to ultrasound in *C. elegans*, suggesting that LIUS can serve as a non-invasive method to manipulate specific cell-type neurons [129]. Recently, the same scientific team identified an impactful receptor with an unbiased screen, i.e., *Homo sapiens* transient receptor potential A1 (*hs*TRPA1), which is capable of effectively conferring ultrasound sensitivity to neurons [157]. Low-intensity ultrasound non-invasively activated neurons exogenously overexpressed *hs*TRPA1 both *in vitro* and *in vivo* [157]. Other investigators found that prestin is an ultrasound-responsive protein, which has also been used as a sonogenetic tool [158]. Their recent study suggested that low-intensity ultrasound stimulation of dopaminergic neurons overexpressed prestin significantly alleviated dopaminergic neurodegeneration, attenuated neurotrophic release, and improved Parkinson's symptoms in mice [159].

Another sonogenetic tool that has been verified is MscL. It was first found in *Escherichia coli* and its major physiological function is to protect cells from lysing [160,161] by opening a 3.5 Å-diameter pore for permeation of molecules and ions [160-162]. By large-scale mutational screening, it was found that mutation G22S (substituting a glycine (G) with a serine (S) at site 22) in MscL dramatically altered channel gating [163]. After mutating at hydrophilic residues with serine, MscL-G22S became more sensitive to mechanical forces than wide-type (WT) MscL due to the alterations of its

structural and chemical properties [163]. To be specific, MscL-G22S opens at a gating threshold of ~10.4 mN/m in response to mechanical forces, such as tension or deformation, whereas WT MscL opens at ~5-6 mN/m [164-166]. It was also reported that mechanical forces-induced MscL-G22S activation significantly enhanced Ca^{2+} influx in cultured Schwann cells [164] and enhanced neuronal activity in cultured primary neurons [167]. Given the small gene size and sensitive mechanical response together, it exhibited potential to use MscL-G22S as a sonogenetic tool [168].

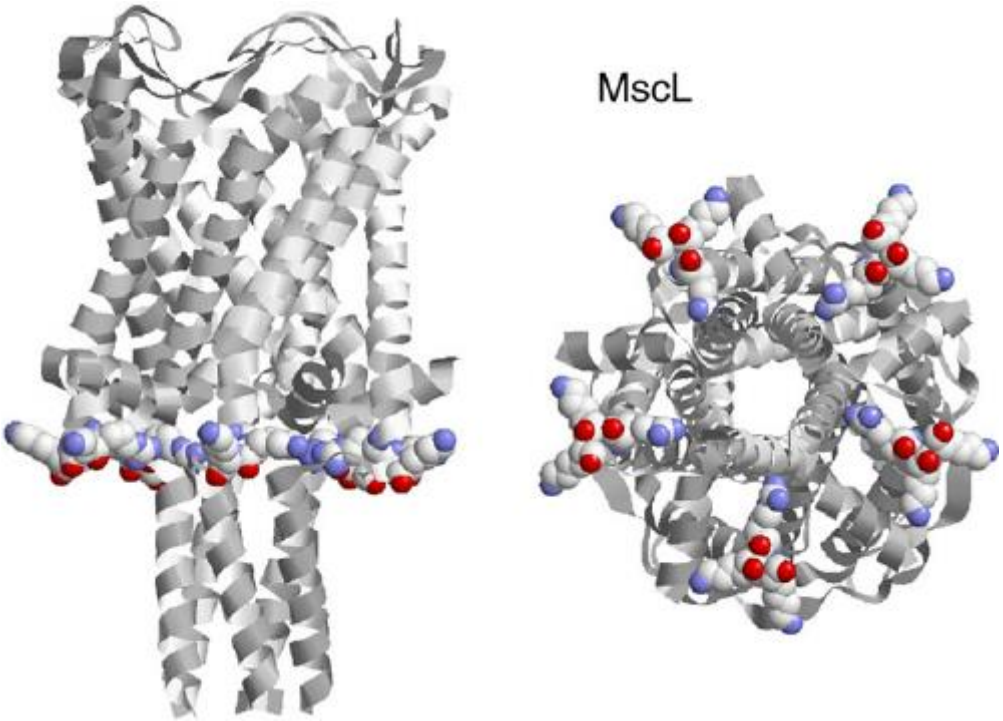

Figure 14. The crystal structure of MscL which is visualized from the plane of the membrane (left) and cytoplasm (right) (adapted from [169]).

Our previous work first verified the feasibility of MscL-G22S as a sonogenetic tool *in vivo*, demonstrating that non-invasive LIUS could induce specific activation of neuronal populations exogenously overexpressed with MscL-G22S [170]. Our latest study further demonstrated that LIUS of neurons heterogeneously overexpressed with

MscL-G22S in the striatum increased locomotion while sonogenetic modulation of dopaminergic neurons in the VTA-induced appetitive conditioning with a real-time modality in awake mice [171]. Another recent work also took MscL-G22S as a sonogenetic tool and showed that sonogenetic activation of the primary visual cortex was sufficient to enhance neuronal activity and restore visual deficits in mice [172]. Taking together, this evidence suggests that LIUS can be utilized to non-invasively activate specific neuronal populations or circuits genetically modified with mechanosensitive ion channels.

Beyond the use of mechanosensitive ion channels, mechanoresponsive particles have also been utilized as sonogenetic tools [173]. In 2014, Shapiro et al. introduced an innovative type of air-filled protein nanostructures known as gas vesicles (GVs), which could augment the mechanical function of ultrasound [174]. Additionally, the researchers genetically engineered GVs to display an RGD peptide on the C terminus of their outer shell protein [175]. This modification enhances the interaction with tumors, leading to significant mechanotherapeutic effects at the tumor site when non-invasive ultrasound stimulation [175]. This application also utilizes mechanical properties of low-intensity ultrasound.

These abovementioned sonogenetic approaches which involve mechanosensitive ion channels or mechanoresponsive particles use low-intensity ultrasound to produce mechanical forces. As we mentioned above, ultrasound can produce mechanical and thermal effects, which mainly depend on its intensity and duty cycle. Apart from thermal ablation, ultrasound can be utilized to produce thermal modulation in cells [173].

A pioneering instance is the mammalian heat shock protein 70 (HSP70), which can be thermally activated in the range of 44-48 ℃, without affecting cell viability [176]. By combining HSP70 with other gene expressions in cells, ultrasound can produce spatial and accurate control over these cellular populations [177]. In addition, thermal-activated channels can be utilized as sonogenetic tools as well. It was reported that non-invasively ultrasonic stimulation of neurons at the striatum that exogenously overexpressed TRPV1 (a typical thermal-activated ion channel) selectively activated these neuronal populations and evoked locomotor behaviors in mice [178]. This application also utilizes thermal properties of relatively high-intensity ultrasound.

Collectively, this novel technology - sonogenetics - can be utilized to non-invasively activate specific neuronal populations or circuits by the combination of non-invasive ultrasound stimulation and ultrasound-responsive mediators. We hypothesized it may provide a new strategy for depression via activating specific depression-related neuronal populations and circuits. This study takes MscL-G22S as the mediator because of its small gene size and sensitive mechanical response and examines sonogenetic modulation in mouse models of depression.

CHAPTER 2: Sonogenetic modulation of the neuronal circuit from excitatory neurons in the mPFC to the DRN elicited rapid antidepressant actions

2.1 Introduction

Major depressive disorder (MDD) is a common but debilitating mental disorder, plaguing an estimated 3.8% of the population worldwide [1] and becoming the second leading contributor to chronic disease burden in the past few decades [2]. MDD is typically characterized by a loss of interest in previously-rewarding activities and persistent despair, likely leading to suicides [1]. It was reported in 2023 that more than 700,000 deaths result from suicide every year and that the highest mortality of unnatural causes was depression (30%) [3,179]. The primary method of medically countering MDD's devastating effects is the use of different classes of antidepressants; these include selective serotonin reuptake inhibitors (SSRIs), serotonin and norepinephrine reuptake inhibitors (SNRIs), monoamine oxidase inhibitors (MAOIs), and tricyclic antidepressants (TCAs). These drugs are understood to relieve depressive symptoms by increasing the availability of neurotransmitters, particularly serotonin (a.k.a., 5-HT), norepinephrine, and dopamine, in the central nervous system (CNS) [92]. Systematic reviews have shown that the response rates of all these antidepressants are around 50%, and several weeks are required for the effective onset of therapeutic effects [6,180].

Simultaneously, several non-pharmacological modalities for more direct neuromodulation have also been under development, with some showing promise as alternative treatments for depression, particularly for patients unresponsive to antidepressant drugs. Some methods have obtained approval from the United States Food and Drug Administration (FDA), including electroconvulsive therapy (ECT), vagus nerve stimulation (VNS) (only for adults), and transcranial magnetic stimulation (TMS) [97]. While these approaches offer possible symptomatic relief to patients who cannot be helped pharmacologically, they each have important limitations, such as the risk of cognitive impairment or even long-lasting memory loss [97], surgical invasiveness [99], and long initiation time or even no response [181]. An important factor contributing to the generation of such side-effects is the inability to accurately target the neuromodulation to specific neuronal populations [80,106]. This insight has led to newer neuromodulation techniques being specifically targeted at specific cell types or circuits which are abnormally altered in pathological states. An optogenetic approach that selectively activated excitatory neurons in the medial prefrontal cortex (mPFC - a central hub for processing cognitive and emotional information [77]) which project to the dorsal raphe nucleus (DRN, the major source of serotonin in the brain [182]) was shown to rapidly reverse despair-like states in rodents [79]. This study also implicated the neuronal pathway from the mPFC to the DRN as a potential intervention target for alleviating depression-related behaviors [79]. However, owing to the opacity of brain tissue, optogenetics requires optical fibers to be invasively implanted into the targeted brain regions to deliver light locally for the

entire duration of the treatment, which hampers its clinical translation [183]. A neuromodulation method capable of combining the advantages of improved targeting - predictable and controllable antidepressant effects with rapid action and minimal side-effects - with greater non-invasiveness and fine spatiotemporal resolution could significantly accelerate the development of next-generation treatments.

Sonogenetics - a method analogous to optogenetics - uses low-intensity ultrasound to non-invasively manipulate specific neuronal populations and circuits by genetically inducing them to overexpress ultrasound-sensitive ion channels [129,155,157,159,168,170-172]. This recently-developed strategy is capable of manipulating neuronal activities and neurotransmitter release in specific neuronal populations and neural circuits [129,155,157,159,168,170-172]. Specifically, sonogenetics can affect mesoscale circuits, even in deeper brain regions, such as the ventral tegmental area (VTA)- nucleus accumbens (NAc) dopaminergic projection pathway [171]. In such a treatment approach, effectively, the only invasion required would be the local delivery of genetic modification agents to the targeted brain region, and all ultrasound treatment would be delivered externally. This offers a potential method of disease management with the added merits of non-invasiveness, selectivity, deep penetration, and fine spatiotemporal resolution [110]. However, this research is still in its early stages, and the feasibility and effectiveness of this approach, particularly with regard to depression-related circuitry, has not yet been comprehensively demonstrated *in vivo*. Putting together these facts, we hypothesized that a sonogenetic neuromodulation approach could be an effective candidate for non-invasively modulating depression-related circuitry, activating

excitatory neurons from the mPFC to the DRN and alleviating depression-related behaviors.

In the present study, we used a mutant of the mechanosensitive channel of large conductance (MscL-G22S) as a sonogenetic mediator to target the circuit from excitatory neurons in the mPFC to the DRN. This sonogenetic approach was applied to a mouse model of depression induced via chronic restraint stress (CRS), and symptoms were monitored at the level of cellular signaling and behavioral tests. We found that sonogenetic modulation of the DRN-projecting excitatory neurons in the mPFC increased DRN neuronal activity and serotonin release in real-time. Importantly, sonogenetic modulation of this circuit rapidly relieved depression-related behaviors in stressed mice, as reflected by spending less time immobile and more time struggling in tail suspension and forced swim tests, which are widely-employed measurements of depression-related behavioral states in rodents [184]. Furthermore, the functional silencing of downstream DRN neurons abrogated the anti-despair effects of sonogenetic modulation applied in the upstream mPFC, indicating the specific and effective sonogenetic activation of this circuit was the major contributor to the observed effects. In addition, there was no sign of tissue damage or abnormal activation of microglia and astrocytes. Taken together, this study is the first attempt to ameliorate depression-related behaviors by sonogenetic modulation of specific neuronal circuits in rodents, laying the groundwork for the future development of new therapeutic methods for depression.

2.2 Materials and methods

2.2.1 Mice

All experiments were conducted on male C57BL/6J mice, housed with adequate food and water at a controlled, comfortable temperature within the Centralized Animal Facilities (CAF) at the Hong Kong Polytechnic University. The experiments adhered to CAF regulations and received approval before commencement.

2.2.2 Viral Vectors

All viruses were obtained from BrainVTA, Wuhan, P.R.C., and were as prepared as follows: AAV2/9-CaMKIIα-DIO-MSCL-G22S-F2A-EGFP, AAV2/9-CaMKIIα-DIO-EGFP, AAV2/9-CaMKIIα-DIO-MSCL-G22S-F2A-mCherry, AAV2/9-CaMKIIα-DIO-mCherry, AAV2/retro-hSyn-Cre, AAV2/9-hSyn-GCaMP6s, AAV2/9-hSyn-5HT2.1, AAV2/9-hSyn-hM4D(Gi)-mCherry, AAV2/9-hSyn-mCherry, AAV2/9-TPH2-TetTox-P2A-mCherry, and AAV2/9-TPH2-mCherry. Diluted virus in 1×10^{12} vg/ml have been used for experiments.

Company	Virus	Experimental Purpose
OBiO Technology	AAV2/9-CaMKIIα-MscL-G22S-EYFP or AAV2/9-CaMKIIα-EYFP	Overexpress MscL-EYFP or EYFP into excitatory neurons in the mPFC
BrainVTA	AAV2/retro-hSyn-Cre & AAV2/9-CaMKIIα-DIO-MSCL-G22S-F2A-EGFP	Overexpress MscL-EGFP into DRN-projecting excitatory neurons in the mPFC
BrainVTA	AAV2/retro-hSyn-Cre & AAV2/9-CaMKIIα-DIO-MSCL-G22S-F2A-mCherry	Overexpress MscL-mCherry into DRN-projecting excitatory neurons in the mPFC
BrainVTA	AAV2/9-hSyn-NES-GCaMP6s	Record calcium activity in the DRN
BrainVTA	AAV2/9-hSyn-5HT2.1	Record serotonin release in the DRN
BrainVTA	AAV2/9-hSyn-hM4D(Gi)-mCherry	Chemogenetic inhibition of DRN neurons
BrainVTA	AAV2/9-TPH2-TetTox-P2A-mCherry	Synaptic inactivation of serotoninergic neurons in the DRN

Table 1. The usage of the virus in Chapter 2.

2.2.3 Stereotaxic surgery

The mice were initially anesthetized using a ketamine/xylazine cocktail (100 mg/kg of ketamine and 10 mg/kg of xylazine). They were then secured on a horizontal stereotaxic apparatus (RWD). Using a sterile surgical blade, the scalp was excised to reveal the bregma and lambda. After cleaning and leveling the skull, we proceeded

with viral injections and the implantation of optical fibers or the installation of ultrasonic collimators, as detailed in subsequent sections. Following the completion of stereotaxic surgery, the mice were promptly placed in a comfortable cage with warm, heated air for ventilation until they regained consciousness. Fiber photometry or behavioral assessments were carried out on the mice at least 7 days post-surgery

***Virus Injection*.** After cleaning and leveling the skull on the stereotaxic apparatus, a tiny hole was drilled with a micro drill in the skull above the targeted brain area. To target DRN-projecting excitatory neurons in the mPFC, a monosynaptic retrograde transport virus encoding Cre recombinase was infused into the DRN (0.5 μL AAV2/retro-hSyn-Cre; AP, -4.4 mm; ML, 0 mm; DV, -3.4 mm) in 5 min. Additionally, a Cre-dependent virus encoding MscL-G22S (AAV2/9-CaMKIIα-DIO-MSCL-G22S-F2A-EGFP or AAV2/9-CaMKIIα-DIO-MSCL-G22S-F2A-mCherry) or their respective control virus were infused into the mPFC (1 μL; AP, 1.8 mm from bregma; ML, ± 0.35 mm; DV, -2.0 mm) in 10 min. The injection needle was left in the targeted brain regions for at least 5 minutes to ensure complete infusion before being withdrawn. Following experiments, to detect the calcium activity or serotonin release in the DRN, 0.5 μL AAV2/9-hSyn-GCaMP6s (a genetically encoded calcium sensor with green fluorescence [185]) or AAV2/9-hSyn-5HT2.1 (a serotonin sensor with green fluorescence [186]) was infused into the DRN. For chemogenetic inhibition, 0.5 μL AAV2/9-hSyn-hM4D(Gi)-mCherry or its control virus was infused into the DRN. For synaptic inactivation, 0.5 μL AAV2/9-TPH2-TetTox-P2A-mCherry or its control virus

was infused into the DRN. Mice were given at least three weeks to recover post-surgery.

***Optic fiber implantation*.** Mice were first placed on a stereotaxic apparatus, and a portion of the scalp was removed to reveal the bregma and lambda. After these points were leveled, a small hole was drilled above the dorsal raphe nucleus (DRN), and the area was rinsed with sterile saline solution. The black fiber optic cannula was then carefully inserted into the DRN (DV, -3.35 mm) using a clamp holder. A screw was placed next to the fiber, and dental cement was applied to anchor both the screw and fiber securely to the skull. After the experiments, brain sections were prepared using a vibrating microtome to examine virus expression and fiber placement under a microscope. Data from mice with incorrectly positioned fibers were excluded from analysis.

Ultrasonic collimator installation. After being fixed on the stereotaxic apparatus, scalp above the mPFC was removed and cleaned. A customized wearable ultrasonic collimator was put onto the intact skull aligned with the targeted brain area and fixed with dental cement. In experiments requiring both a fiber and a collimator, we implanted the fiber with a clamp holder in the DRN and installed the collimator on the mPFC, securing both with dental cement.

2.2.4 Ultrasound system and stimulation

Amplifier’s output was linked to customized wearable transducers. Then, the customized wearable transducer was installed into the collimator coupled with

ultrasound gel. Hydrophone was used to assess acoustic field distribution, and the parameters of ultrasound stimulation were shown as follows (central frequency, 0.8 MHz; intensity, 0.15 or 0.3 MPa; pulse width, 500 μs; pulse repetition frequency, 1 kHz; stimulation duration, 300 ms; stimulation interval, 3 s).

2.2.5 Fiber photometry recording

Mice were kept under continuous anesthesia with approximately 1% isoflurane throughout the entire experiment. A wire connected the recording system to the implanted fiber, and the excitation wavelength for GCaMP6s and 5-HT2.1 was approximately 480 nm. Another fiber linked the recording system with the ultrasound stimulation system to synchronize the signals. The ultrasound transducer was placed on the mPFC to monitor changes in fluorescent intensities in the DRN. In this study, ΔF/F represented the 'fluorescence change,' calculated as $(F-F_0)/F_0$.

2.2.6 Chemogenetic inhibition

Mice heterologously overexpressing hM4D(Gi)-mCherry or mCherry were subjected to a process of habituation, in which intraperitoneal injection with 120 μL sterile saline was conducted daily for 1 week. Then, clozapine-N-oxide (CNO, Tocris, MO, 1 mg/kg) was given before behavioral assessment.

2.2.7 Chronic restraint stress

In chronic restraint stress (CRS) protocol, mice were individually placed into 50 ml conical tubes with manually drilled holes for ventilation for approximately 3 hours

each day (total 14 days), while control mice remained in their home cages [187]. After each session, the restrained mice were promptly returned to cage [187].

2.2.8 Behavioral tests

Tail suspension test (TST).

In this protocol, mice were suspended 25 cm above the floor via attaching their tails with adhesive tape [187]. An observer blinded to animal treatments videotaped and offline analyzed animal behaviors. “Immobility time” was the time that their body and four limbs were still [188]. “Struggling time” was the time that strong movements of body jerks and jumps were observed [188].

Forced swim test (FST).

In this protocol, mouse was placed into a Plexiglas cylinder (12 cm in diameter and 25 cm in height) filled with water at 24 ± 1 °C to a depth of 10 cm, allowing them to swim freely for 6 minutes [189]. An observer who is blinded to animal treatments videotaped and offline analyzed animal behaviors. “Immobility time” was defined as when the mouse was floating without moving or with slight kick for balance its body [190]. “Struggling time” was the time that strong movements of their paws or legs to escape the cylinder were exhibited [190].

Open field test (OFT).

In this protocol, mouse was individually put in the center of a cubic plastic chamber (50 cm^3) and allowed to move freely for 6 minutes [191]. Their behaviors were

videotaped, and their speed during the 6-minute test session was measured using ToxTrac software.

2.2.9 Immunofluorescence staining

After anesthesia, mice were transcardially perfused with PBS (Cat. no., 70011044; Thermo Fisher Scientific Inc., Waltham, USA) followed by a 4% paraformaldehyde (PFA) solution (Cat. no., sc-281692; Santa Cruz Biotechnology Inc., California, USA), and brain was obtained and fixed with the 4% PFA solution overnight in a 4 ℃ refrigerator. Coronal sections containing the mPFC or the DRN with a thickness of 40 μm were attained from the fixed brain by the vibrating microtome (VT1200S; Leica Biosystems GmbH, Wetzlar, Germany). Slices were blocked with blocking solution (10% normal goat serum + 1% BSA + 0.3% Triton in 1X PBS) for 90 min at room temperature (RT) [192] and incubated with prepared primary antibody solution against c-Fos (1:500; Cat. no., 2250; CST, Massachusetts, USA), Iba1 (1:1000; Cat. no., 17198; CST, Massachusetts, USA) or GFAP (1:1000; Cat. no., 12389; CST, Massachusetts, USA) overnight in a 4 ℃ refrigerator. After washing, slices were incubated with secondary antibodies (1:1000; anti-rabbit Alexa Fluor 488 or 633, Thermo Fisher Scientific Inc., Waltham, USA) for around 90 min at RT. After washing, the sections were placed on glass slides to dry naturally. Mounting medium with DAPI was then applied, and the slides were covered with cover glass. The staining sections were visualized by a confocal microscope and analyzed by an observer blinded to animal treatments with ImageJ software.

2.2.10 In vitro electrophysiological recordings.

After anesthetizing, the mouse was transcardially perfused with pre-cooled cutting NMDG-HEPES artificial cerebrospinal fluid (ACSF). Following experiments, its brain was quickly removed and sliced into 300 μm-thick coronal sections in pre-cooled cutting ACSF with a pre-cooled vibrating microtome (VT1200S; Leica Biosystems GmbH, Wetzlar, Germany). Sections containing the DRN were transferred to the holding HEPES ACSF for ten min at an incubation chamber. Subsequently, the sections were transferred to a recording chamber, where continuous oxygenation perfusion was maintained. Then, neurons overexpressing hM4D(Gi)-mCherry in the DRN were observed with an upright fluorescent microscope (Olympus, Japan), and recorded by the patch pipettes with a resistance of ~5 MO. To confirm the hM4D(Gi)-mediated inhibitory effect, action potentials were recorded. After recording firing spikes for 3-5 min, 5 μM CNO (Tocris, MO) was bath-applied for 2 min and subsequently washed.

Component (mM)	NMDG-HEPES ACSF	Holding ACSF	Recording ACSF
NMDG	**92**	**/**	**/**
HCl	**92**	**/**	**/**
NaCl	**/**	**92**	**124**
KCl	**2.5**	**2.5**	**2.5**
NaH2PO4	**1.2**	**1.2**	**1.2**

NaHCO3	**30**	**30**	**24**
HEPES	**20**	**20**	**5**
Glucose	**25**	**25**	**12.5**
Ascorbate	**5**	**5**	**/**
Thiourea	**2**	**2**	**/**
Pyruvate	**3**	**3**	**/**
MgSO4.7H2O	**10**	**2**	**2**
CaCl2.2H2O	**0.5**	**2**	**2**

Table 2. The formula in patch clamp solution.

2.2.11 Hematoxylin and eosin staining

After anesthesia, mice were transcardially perfused with PBS (Cat. no., 70011044; Thermo Fisher Scientific Inc., Waltham, USA) followed by a 4% paraformaldehyde (PFA) solution (Cat. no., sc-281692; Santa Cruz Biotechnology Inc., California, USA). Brain tissues were exacted and fixed with the 4% PFA solution for 24 hours in a 4 ℃ refrigerator and then washed with PBS. Then, brain tissues were dehydrated using a series of alcohol solutions with increasing concentrations (70%, 80%, 90%, 95%, 100%), cleared with xylene, and then embedded in paraffin. After the experiments, coronal brain sections of 5 μm thickness were obtained from paraffin-embedded blocks with a microtome (Leica RM2235) and stained by a hematoxylin and eosin

stain kit (Solarbio G1121). After staining, sections were re-dehydrated with the gradient alcohol, re-hyalinized with xylene, and mounted by resinene for microscopic observation.

2.2.12 Data analysis

Data analysis and figure generation were conducted using GraphPad Prism 7.0, while schematic illustrations were created with CorelDRAW X8. For data analysis, two-tailed unpaired t-tests were employed for comparisons between two experimental groups, and two-way ANOVA with post-hoc Tukey tests were used for multiple group comparisons. Bar charts present the mean ± standard error of the mean (SEMs). *P* values less than 0.05 were considered statistically significant, indicated as follows: * $p < 0.05$, ** $p < 0.01$, *** $p < 0.001$, **** $p < 0.0001$, n.s., not significant. All statistically significant relationships are depicted in the graphs.

2.3 Results and Discussion

2.3.1 Wearable ultrasound system and characteristics

For this study, a wearable transducer was first customized. The central frequency of the transducer is 0.8 MHz, and it fabricated using PZT-5H/Epoxy 1-3 composite material. Tungsten powder was mixed into the epoxy to fabricate the matching layer of the transducer. Its physical dimensions included an outer diameter of 7.8 mm, and the aluminum housing featured three protrusions designed to secure the transducer within the collimator (Figure 15a, b). The collimator had a 5 mm aperture size (Figure

15c). To drive the transducer, an electrical signal was generated with a function generator and amplified by a radio frequency (RF) amplifier, similar to our previous studies [193]. The transducer output intensity and the acoustic distribution profile were measured with a hydrophone scanning system, controlled by a 3D translational motor system (Figure 15d). The lateral acoustic beam profile at 0.3 MPa output intensity, measured 2 mm away from the collimator surface, is shown in Figure 15e. The collimator was installed on the mouse head to align the ultrasound beam with the mPFC right underneath, while the DRN was left uncovered by the collimator (Figure 15f, g). Then, the customized wearable transducer was installed into the collimator, with ultrasound coupling gel filled in the intermediate space (Figure 15h). The parameters of ultrasound stimulation in this study were: central frequency, 0.8 MHz; pulse width, 500 μs; pulse repetition frequency, 1 kHz; stimulation duration, 300 ms; stimulation interval, 3 s; pressure, 0-0.3 MPa (Figure 15i).

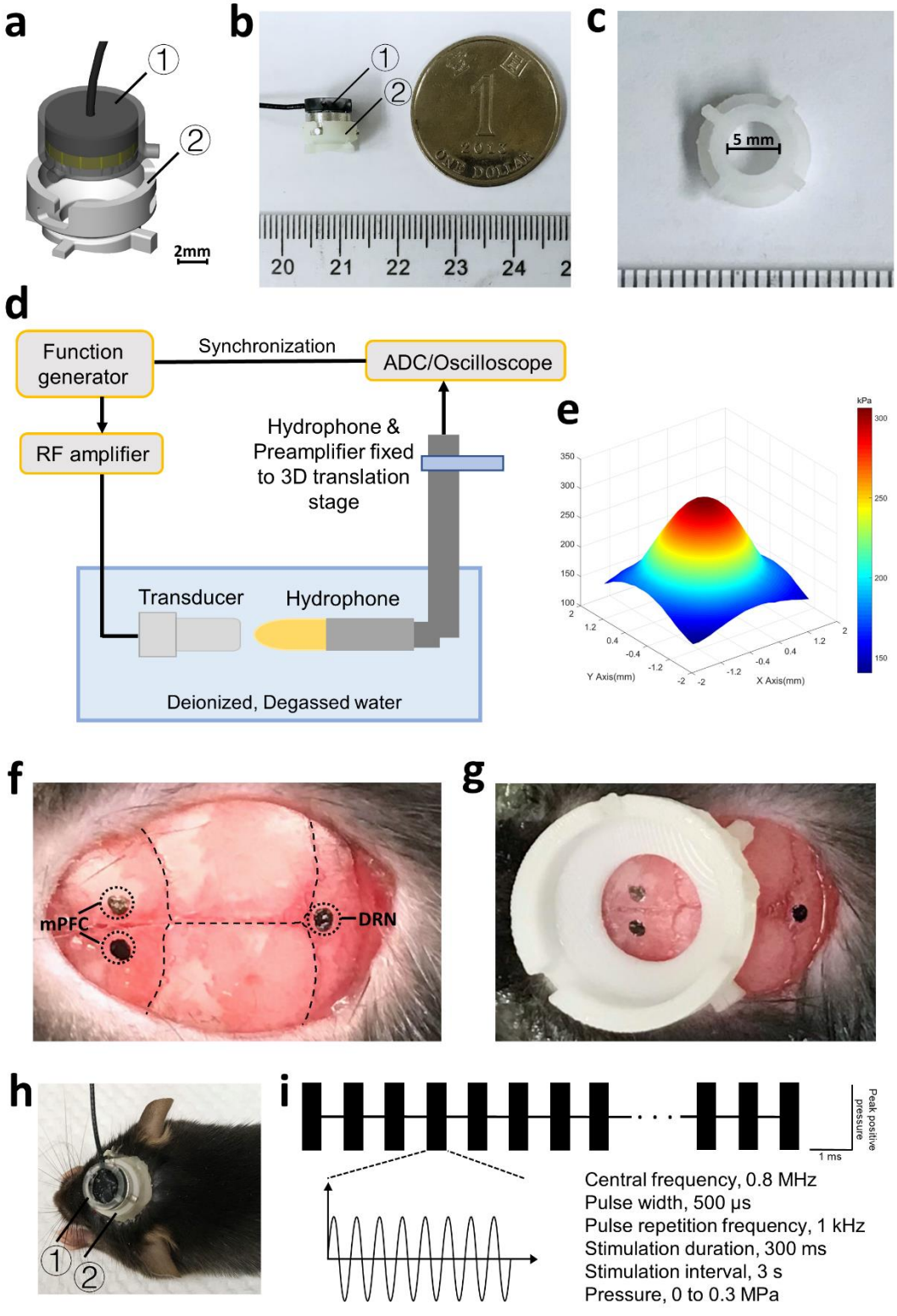

Figure 15. Millimeter-scale ultrasound setup on mouse heads to sonogenetically target region of interest. a) Schematic diagram of the ultrasonic transducer and collimator. "①" indicates the wearable customized ultrasonic transducer. "②"

indicates the ultrasonic collimator. **b)** Photograph for scale of the ultrasonic transducer and collimator. **c)** Bottom view of the ultrasonic collimator (aperture size = 5 mm). **d)** Schematic diagram of the transducer scanning platform. RF, radio frequency; ADC, analog-to-digital converter. **e)** Distribution of the acoustic field of the transducer in the XY plane (0.3 MPa). **f)** Photograph illustrates the location above the mPFC and DRN. **g)** Photograph showing the ultrasonic collimator's alignment with the mPFC without affecting the DRN. **h)** Photograph illustrating the customized wearable transducer with collimator affixed to the head of a mouse, above the mPFC. **i)** Illustration of ultrasound temporal profile applied in this study.

2.3.2 There were no obvious alterations in depression-related behaviors when sonogenetic modulation of all excitatory neurons in the mPFC

Given the fact that the mPFC is a pivotal hub for stress responses and emotional processing [194] together with previous observation of hypoactivity of the mPFC in depression [195], we aimed to utilize sonogenetic techniques to enhance the neuronal activity in the mPFC to ameliorate depression-related behaviors. We chiefly overexpressed MscL-G22S in the excitatory neurons in the mPFC under the control of the CaMKIIα promoter. Following a week of recovery, mice were subjected to CRS for consecutive 2 weeks and then ultrasonic collimators were mounted on the surface of the skull aligned with the mPFC. A week later, mice were anaesthetized by isoflurane to install the customized wearable transducer into the collimator, which was coupled with ultrasound gel, and then depression-related behaviors, including

TST, FST, and OFT, were examined when sonication of the mPFC after the mice fully awake from isoflurane. Thereinto, TST, and FST are widely employed measurements of despair-like behavioral states in rodents [184], and OFT is especially used here to distinguish between despair-like behaviors and general locomotion alterations [80]. Surprisingly, neither tendency towards the alleviation of despair-like behaviors in the FST and TST nor locomotion behavioral changes in the OFT was observed when sonication (Figure 16). One interpretation of these results is that opposed actions among different neuronal circuits projected by the excitatory neurons in the mPFC may be offset and exhibited no net effect when observation [74,79]. Previous studies demonstrated the opposite roles of optogenetic activation of axonal terminals of excitatory neurons in the mPFC projecting into the lateral habenula (LHb) (trigger) and DRN (reversal) in despair-like states [79]. These observations suggested that driving neuronal activity in a specific subclass of excitatory neurons in the mPFC may be more effective in eliciting rapid antidepressant actions.

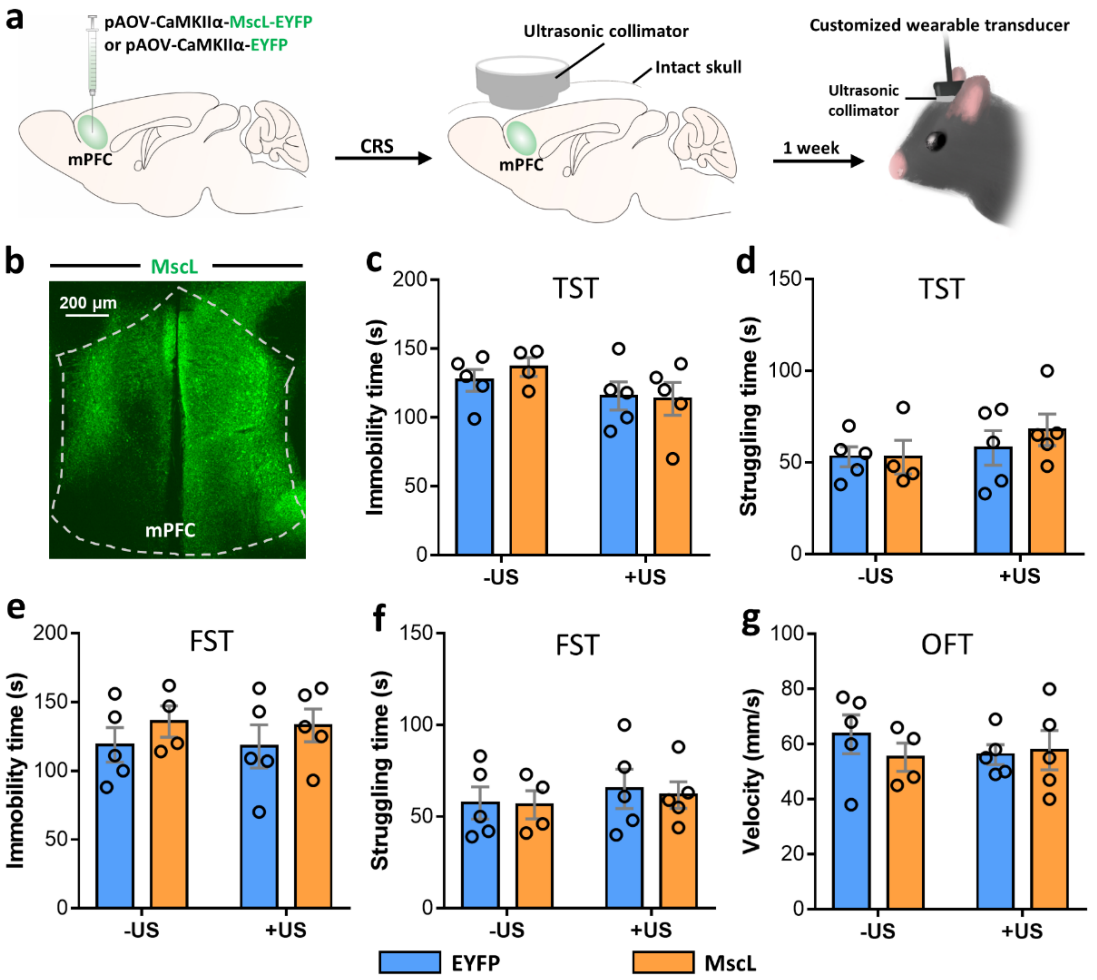

Figure 16. Depression-related behavioral performance when sonogenetic modulation of all excitatory neurons in the mPFC. a) The schematic illustration of viral transduction protocol and ultrasound stimulation. Mice were infused bilaterally in the mPFC with either AAV2/9-CaMKIIα-MscL-EYFP or AAV2/9- CaMKIIα-EYFP. Following a week of recovery, mice were subjected to the 2-week chronic restraint stress procedure. Then an ultrasonic collimator was installed and aligned with the mPFC. Another week later, the customized wearable transducer was installed into the collimator and behavioral tests were conducted when sonication of the mPFC. Ultrasound was ON from 15 minutes before behavioral tests to the end of it (a total of 21 minutes). **b)** MscL fluorescence in the mPFC. **c-f)** No obvious alteration in

despair-like states was observed when sonication. n = 4-5 mice per group. **c)** The immobile durations exhibited in the TST among Ctrl-US, MscL-US, Ctrl+US, and MscL+US groups. **d)** The struggle durations exhibited in the TST among Ctrl-US, MscL-US, Ctrl+US, and MscL+US groups. **e)** The immobile durations exhibited in the FST among Ctrl-US, MscL-US, Ctrl+US, and MscL+US groups. **f)** The struggle durations exhibited in the FST among Ctrl-US, MscL-US, Ctrl+US, and MscL+US groups. **g)** The average velocity of mice in the OFT. n = 4-5 mice per group.

2.3.3 Sonogenetic modulation of DRN-projecting excitatory neurons in the mPFC enhanced neuronal activity along this circuit

To enhance the efficacy, we targeted a more specific neuronal population and overexpressed MscL-G22S into the excitatory neurons in the mPFC only projecting to the DRN. First, monosynaptic retrograde transport virus encoding Cre recombinase (AAV2/Retro-hSyn-Cre, which permits efficient retrograde access to projection neurons [196]) was delivered into the DRN and Cre-dependent virus encoding MscL (AAV-CaMKIIα-DIO-MscL-mCherry or -mCherry, which induces overexpression in specific neuronal populations via Cre-activated “DIO” switch [197]) into the mPFC. An empty vector without MscL was used as a control, and the appropriate fluorescent reporter was chosen to avoid overlapping with the genetic sensor. The DRN was also made to express GCaMP6s (a genetically encoded calcium sensor[185]). To confirm the sonogenetic modulation of this circuit specifically, an ultrasound transducer was

assembled above the mPFC, and calcium activity in the DRN was monitored in real-time through an implanted optical fiber during the sonication of the mPFC (Fig. 17a).

The MscL-expressing neurons in the mPFC and their axon terminals surrounding the neuron overexpressed with GCaMP6s in the DRN were observed (Fig. 17b), indicating the successful expression of those viruses abovementioned. We observed that before ultrasound stimulation, MscL and Ctrl groups exhibited comparable levels of GCaMP6s baseline fluorescence (Peak ΔF/F, Ctrl-US vs. MscL-US = 0.064 ± 0.009 % vs. 0.065 ± 0.010, $p > 0.1$, Fig. 17e). When ultrasound stimulation at 0.15 MPa, there were a few tendencies that MscL group exhibited higher GCaMP6s fluorescence changes, but no statistical significance between Ctrl+US and MscL+US groups (Peak ΔF/F, Ctrl+US vs. MscL+US = 0.061 ± 0.014 vs. 0.093 ± 0.031, $p = 0.916$, Fig. 17e). Interestingly, ultrasound stimuli of 0.3 MPa repeatedly induced synchronous and repeatable elevation of GCaMP6s fluorescence intensity in the MscL group with sub-second latency, while the Ctrl group showed no obvious responses (Fig. 17c-e). The peak fluorescence change in the MscL group was significantly enhanced in contrast to the Ctrl group at 0.3 MPa stimulation (Peak ΔF/F, Ctrl+US vs. MscL+US: 0.070 ± 0.013 % vs. 0.240 ± 0.016 %, $p = 2.90 \times 10^{-5}$, Fig. 17e), indicating specific activation of the selected neurons and neural pathways.

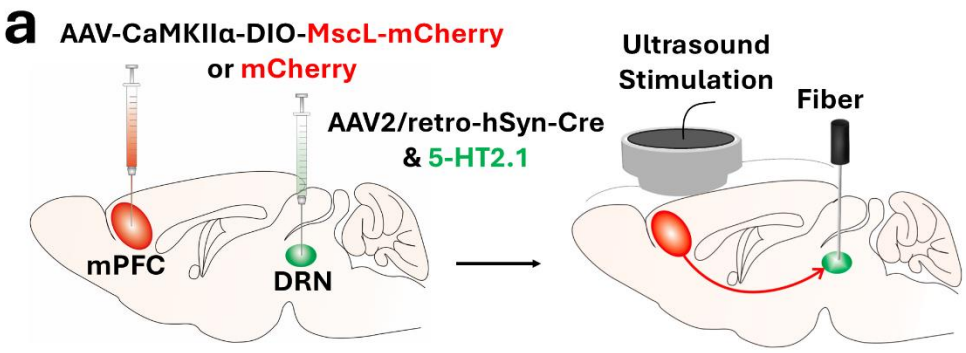
a
AAV-CaMKIIα-DIO-MscL-mCherry
or mCherry
AAV2/retro-hSyn-Cre
& 5-HT2.1
mPFC
DRN
Ultrasound
Stimulation
Fiber

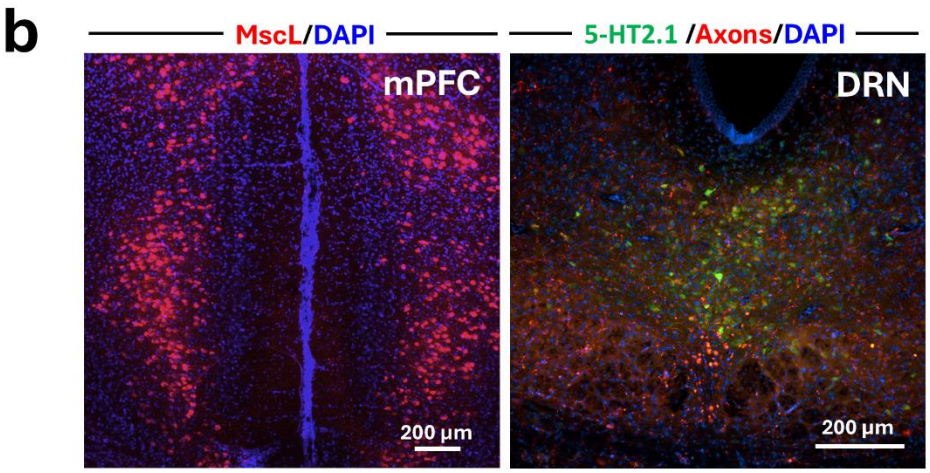
b
MscL/DAPI
5-HT2.1 /Axons/DAPI
mPFC
DRN
200 μm
200 μm

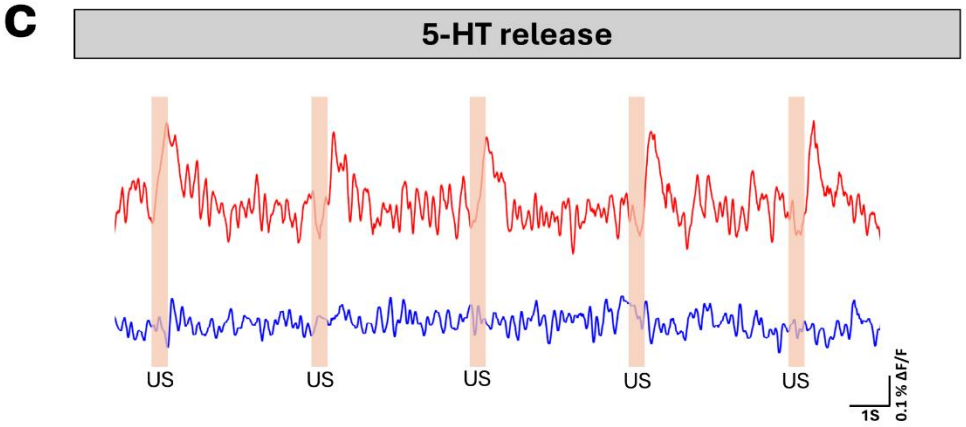
c
5-HT release
US
US
US
US
US
1S
0.1 % ΔF/F

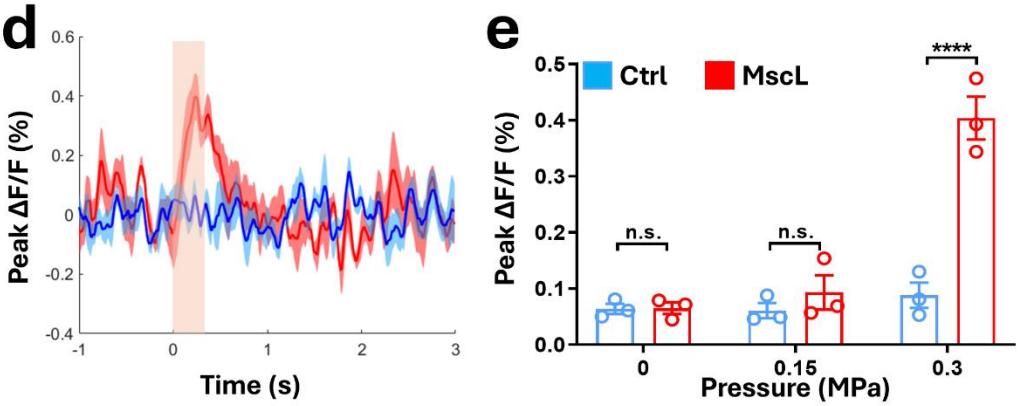
d
Peak ΔF/F (%)
Time (s)
e
Ctrl
MscL
Peak ΔF/F (%)
n.s.
n.s.
****
Pressure (MPa)

Figure 17. Sonogenetic modulation of DRN-projecting excitatory neurons in the mPFC enhanced the neuronal activity in the DRN. a) Schematic illustration of viral transduction and fiber photometry recording. **b)** Left: representative image showing MscL-expressing neurons = red fluorescence and DAPI = blue fluorescence in the mPFC; Right: representative image showing axon terminals from MscL-expressing neurons of the mPFC = red fluorescence, Ca^{2+} sensor GCaMP6s = green florescence, and DAPI = blue fluorescence in the DRN. **c)** Representative traces of GCaMP6s fluorescence changes in MscL (red) and Ctrl (blue) groups upon multiple 0.3 MPa ultrasound stimuli. **d)** The average GCaMP6s fluorescence signals from panel c. **e)** Averaged peak change of GCaMP6s fluorescence (Peak ΔF/F). n = 3 mice per group.

2.3.4 Sonogenetic modulation of DRN-projecting excitatory neurons in the mPFC increased serotonin release in the DRN

To further observe the sonogenetic effects on serotonin release, an ultrasound transducer was put aligned with the mPFC while the neuronal population in the DRN was transfected 5-HT2.1 (a genetically encoded 5-HT sensor [186]) and optical fiber was put into the DRN for recording alterations of 5-HT release when ultrasound stimulation of the mPFC (Fig. 18a). The MscL-expressing neurons in the mPFC and its axon terminals surrounding the neuron overexpressed with 5-HT2.1 in the DRN were observed (Fig. 18b). Before ultrasound stimulation, MscL and Ctrl groups exhibited comparable levels of 5-HT2.1 baseline fluorescence (Peak ΔF/F, Ctrl-US vs.

MscL-US = 0.046 ± 0.007 vs. 0.056 ± 0.006, p = 0.996, Fig. 18e). When ultrasound stimulation at 0.15 MPa, no obvious difference between Ctrl and MscL groups in 5-HT2.1 fluorescence change were observed (Fig. 18e). Similarly, 0.15 MPa ultrasound does not induce much calcium responses in the MscL group. However, 0.3 MPa-ultrasound stimuli repeatedly induced synchronous elevation of 5-HT2.1 fluorescence intensity in the MscL group, but not Ctrl group (Fig. 18c). The Peak ΔF/F of 5-HT2.1 fluorescence change (Peak ΔF/F, Ctrl vs. MscL: 0.088 ± 0.023 % vs. 0.404 ± 0.038 %, $p = 7 \times 10^{-6}$, Fig. 18e) in the MscL group were significantly enhanced in contrast to the Ctrl group when ultrasound stimulation at 0.3 MPa. Thus, we found that 0.3 MPa ultrasound stimuli delivered to the DRN-projecting excitatory neurons in the mPFC induced sub-second, repeatable and reversible activity in the downstream DRN neurons in real-time.

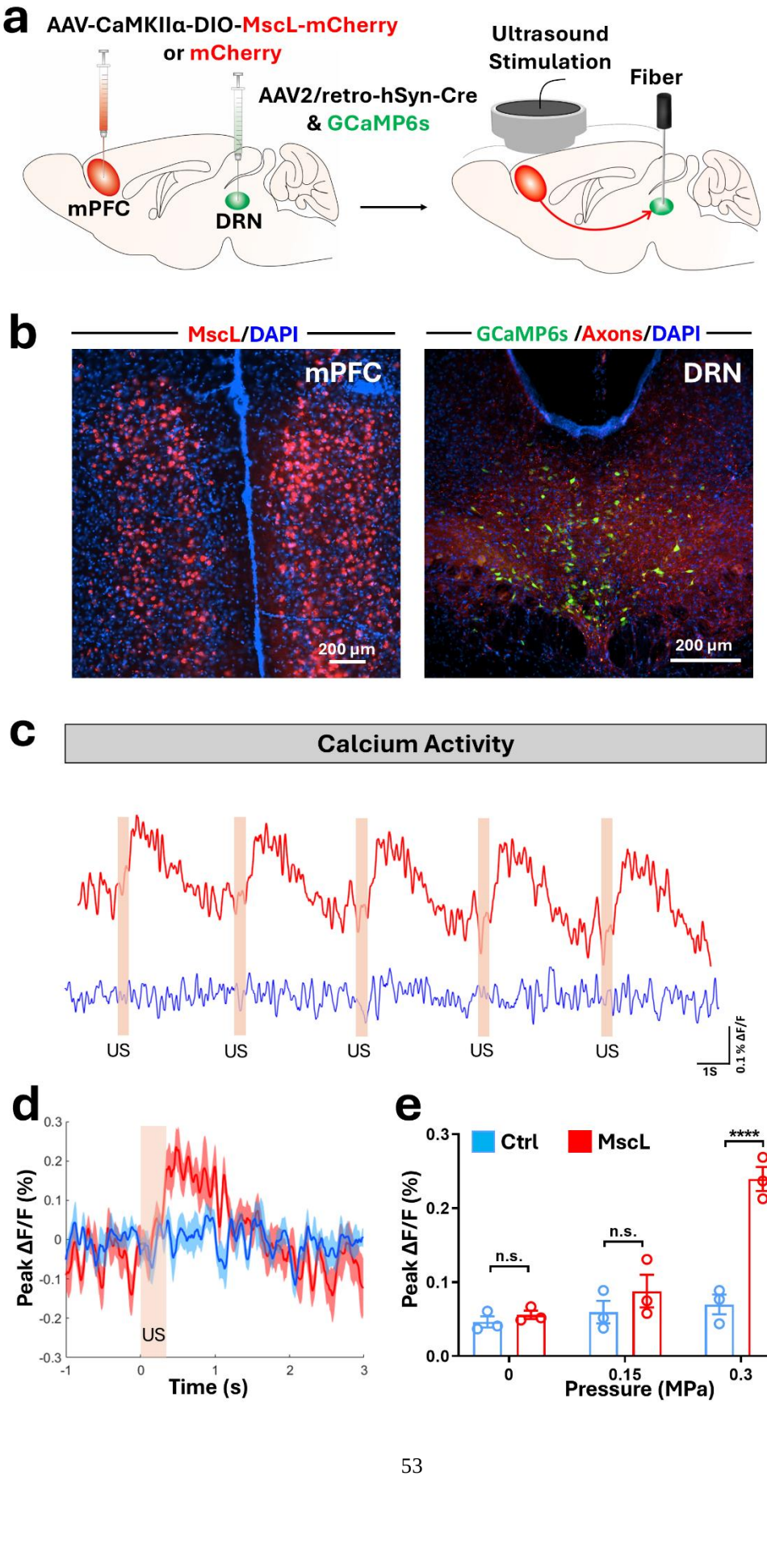
a
AAV-CaMKIIα-DIO-MscL-mCherry
or mCherry
AAV2/retro-hSyn-Cre
& GCaMP6s
mPFC
DRN
Ultrasound
Stimulation
Fiber
b
MscL/DAPI
GCaMP6s /Axons/DAPI
mPFC
DRN
200 μm
200 μm
c
Calcium Activity
US
US
US
US
US
0.1 % ΔF/F
1S
d
Peak ΔF/F (%)
US
Time (s)
e
Ctrl
MscL
Peak ΔF/F (%)
n.s.
n.s.
****
0
0.15
0.3
Pressure (MPa)

Figure 18. Sonogenetic modulation of DRN-projecting excitatory neurons in the mPFC enhanced serotonin release in the DRN. a) Schematic illustration of viral transduction and fiber photometry recording. **b)** Left: Representative image showing MscL-expressing neurons (red) and DAPI (blue) in the mPFC; Right: representative image showing axon terminals from MscL-expressing neurons of the mPFC (red), 5-HT2.1 (green), and DAPI (blue) in the DRN. **c)** Representative traces of 5-HT2.1 fluorescence change in the MscL (red line) and Ctrl (blue line) group when receiving multiple 0.3 MPa ultrasound stimuli. **d)** The averaged 5-HT2.1 fluorescence signal from panel c. **e)** The averaged peak change of 5-HT2.1 fluorescence (Peak ΔF/F). n = 3 mice in each group.

2.3.5 Sonogenetic modulation of the circuit from excitatory neurons in the mPFC to the DRN enhanced the neuronal activity of this circuit

To further verify the sonogenetic activation of neurons in the mPFC and DRN, we examined relative levels of c-Fos expression at 0.3 MPa. c-Fos is a biomarker of activated neurons, thought to interact with other genes and mediate long-term changes in neural functioning [198], in contrast to above fiber photometry experiments. Based on our previous experiences, ~20-40 min ultrasound stimulation could induce c-Fos increasement. Thus, we want to investigate the c-Fos expression in the mPFC and DRN after 20 min sonication. We found that the number of c-Fos+ neurons in the mPFC in the MscL+US group was profoundly higher than in Ctrl or -US groups (c-Fos positive cells for Ctrl-US = 17 ± 3.54, MscL-US = 21 ± 4.13, Ctrl+US = 32 ±

5.83, MscL+US = 119 ± 6.67, Fig. 2a, c). Similarly, c-Fos levels in the DRN were significantly elevated in the MscL+US group compared to all others (c-Fos positive cells for Ctrl-US = 11 ± 1.84, MscL-US = 14 ± 2.47, Ctrl+US = 22 ± 3.16, MscL+US = 76 ± 3.14, Fig. 2b, d), likely because of the excitatory axonal projections from the mPFC to this brain region. Taken together, these results show that sonogenetic modulation of DRN-projecting excitatory mPFC neurons increased neuronal activity in this circuit.

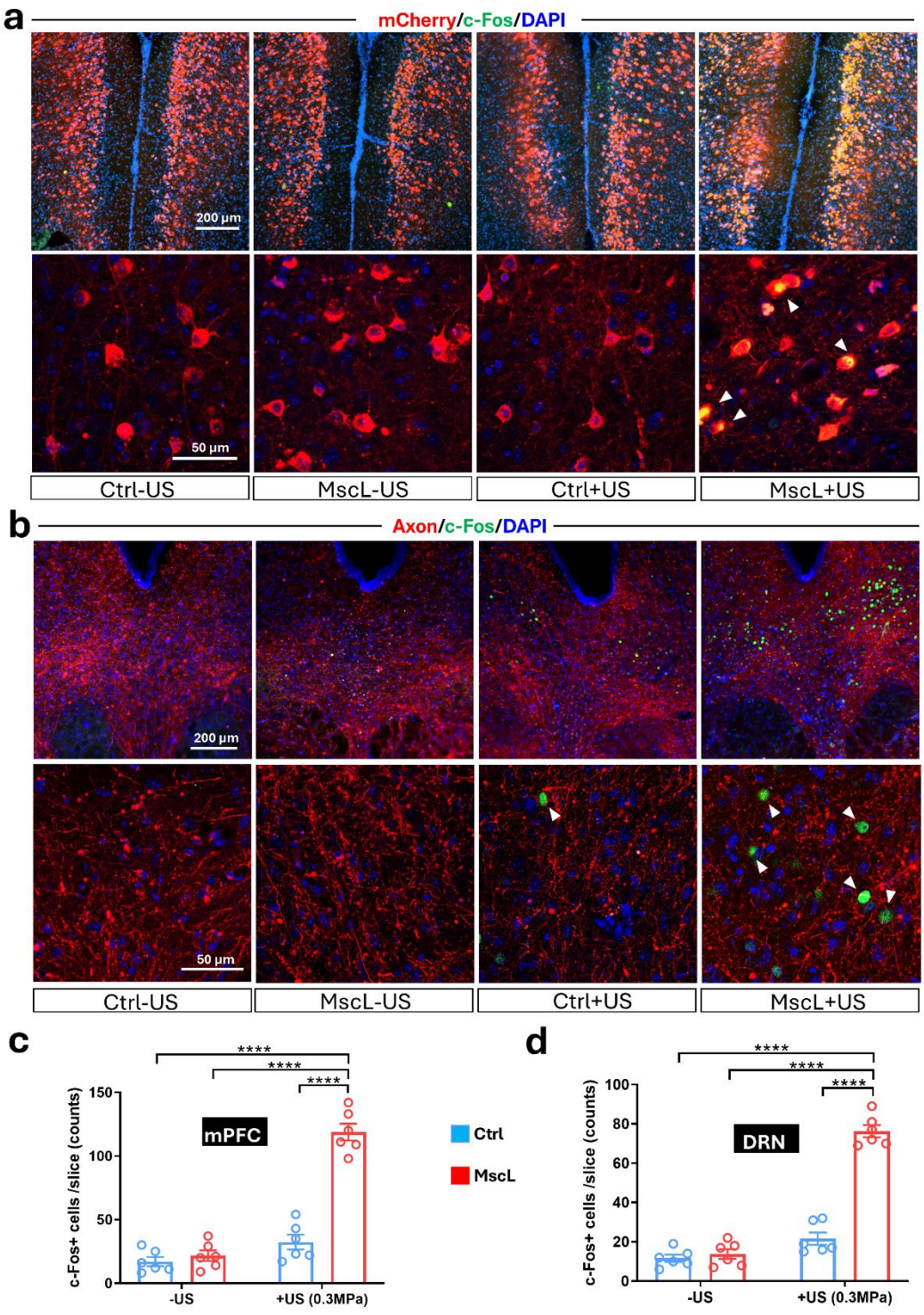

Figure 19. Sonogenetic modulation of the circuit from excitatory neurons in the mPFC to the DRN enhanced the neuronal activity of this circuit. a) The representative images show MscL-expressing neurons (red fluorescence) and c-Fos expression (green fluorescence) in the mPFC. White arrows highlight the c-Fos

positive signal within MscL-expressing neurons. **b)** The representative images depict the axonal terminals in the DRN that originate from MscL-expressing neurons in the mPFC (red fluorescence), along with c-Fos expression (green fluorescence) in the DRN. **c)** Counts of c-Fos positive neuronal populations imaged in the mPFC among Ctrl-US, MscL-US, Ctrl+US, and MscL+US groups. **d)** Counts of c-Fos positive neuronal populations imaged in the DRN among Ctrl-US, MscL-US, Ctrl+US, and MscL+US groups.

2.3.6 The successful establishment of the chronic restraint stress mouse model of depression

We observed that 0.3MPa-ultrasound modulation of the DRN-projecting excitatory neurons in the mPFC overexpressed with MscL-G22S enhanced the neuronal activity and serotonin release in the DRN. We want to further investigate whether sonogenetic modulation of this circuit can produce antidepressant actions. Before testing sonogenetic modulation, we established CRS mouse model of depression (a typical model of depression in rodents, which has been demonstrated to induce similar alterations at the molecular and behavioral levels when compared to depressive patients [199]). In this model, mice were put into a ventilated tube (many holes being manually drilled on its surface) for approximately three hours daily for 14 consecutive days as shown in the schematic illustration (Figure 20a). As a result, mice subjected to CRS exhibited more time immobile and less time struggling in both the TST and FST than the Ctrl group (Figure 20b-f) while their locomotion ability did not show obvious

difference in the OFT, suggesting CRS procedure induced obvious depression-related behaviors in mice.

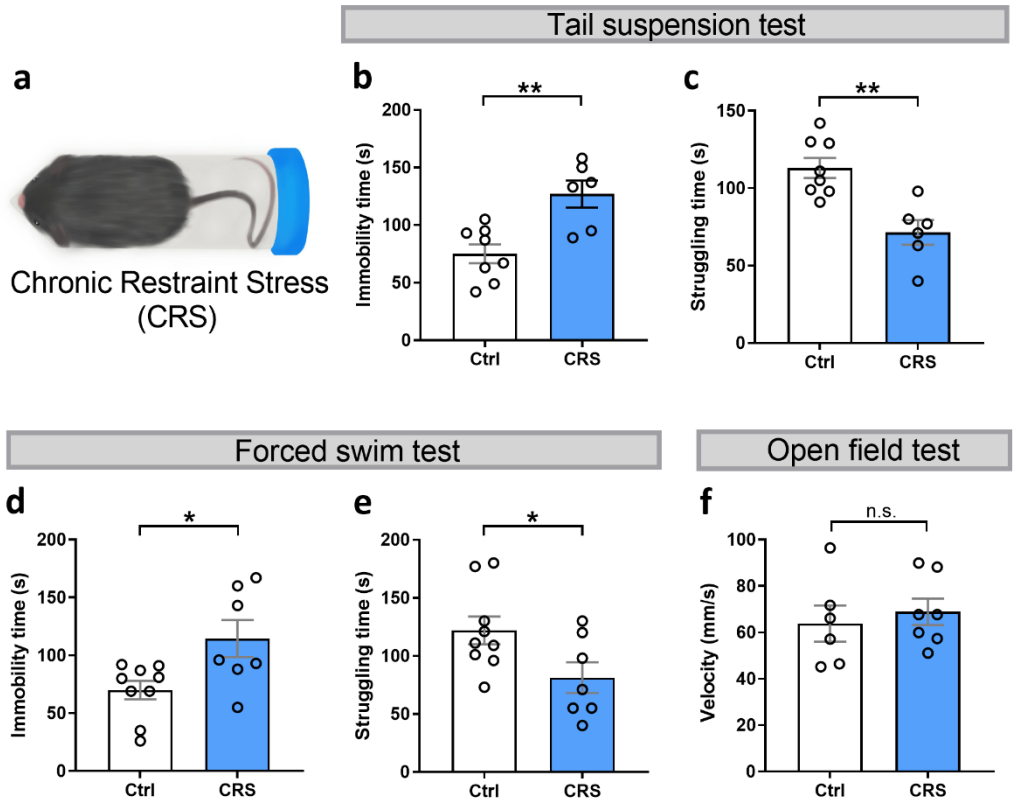

Figure 20. The establishment of the chronic restraint stress mouse model of depression. a) The schematic illustration of mice subjected to CRS (~3 h per day for 14 consecutive days). **b)** The immobile durations exhibited in the TST among Control and CRS groups (Con vs. CRS: 75.13 ± 8.17s vs. 127.00 ± 11.68 s, p = 0.0027). **c)** The struggling time in the TST (Con vs. CRS: 113.10 ± 6.49 s vs. 71.50 ± 7.89 s, p = 0.0015). **d)** The immobility time in the FST (Con vs. CRS: 70.00 ± 7.99 s vs. 114.60 ± 15.95 s, p = 0.0181). **e)** The struggling time in the FST (Con vs. CRS: 122.00 ± 11.94 s vs. 81.29 ± 13.22 s, p = 0.0389). **f)** No observed difference in the velocity in the OFT was observed between Con and CRS groups (Con vs. CRS: 63.83 ± 7.80 mm/s vs. 68.86 ± 5.66 mm/s, p = 0.6050).

2.3.7 Sonogenetic modulation of DRN-projecting excitatory neurons in the mPFC elicited rapid antidepressant effects

Having observed that 0.3 MPa ultrasound stimulation of DRN-projecting, MscL-expressing excitatory mPFC neurons enhanced neuronal activity and serotonin release in the DRN. Furthermore, 0.3 MPa ultrasound stimulation of DRN-projecting, MscL-expressing excitatory mPFC neurons induced c-Fos expression in the mPFC and DRN, activating the targeted neuronal pathway. Thus, we next wanted to investigate whether this sonogenetic approach could correspondingly change depressive-like behaviors in awake mice. Following model establishment, we observed the real-time effects of sonogenetically modulating DRN-projecting excitatory mPFC neurons on depression-related behaviors in stressed mice (Fig. 21a). Mouse mPFCs were sonicated starting 15 minutes before, and all through the administration of, behavioral tests. MscL-expressing neurons in the mPFC and their DRN-projecting axon terminals were observed (Fig. 21b), indicating successful selective overexpression of these viruses. When 0.3 MPa ultrasound stimulation, MscL+US mice spent significantly less time immobile (immobile duration for Ctrl-US = 127 ± 14.33 s, MscL-US = 131 ± 12.86 s, Ctrl+US = 122 ± 12.97 s, MscL+US = 59 ± 6.72 s, Fig. 21d) and more time struggling (struggle duration for Ctrl-US = 55 ± 6.88 s, MscL-US = 62 ± 6.80 s, Ctrl+US = 65 ± 6.03 s, MscL+US = 101 ± 7.39 s, Fig. 21e) in the TST (Fig. 21c) than the MscL-US group and both Ctrl groups. Similarly, mice in the MscL+US group also exhibited less immobility time (immobile duration for Ctrl-US = 143 ± 10.97 s, MscL-US = 132 ± 9.31 s, Ctrl+US = 138 ± 8.40 s, MscL+US = 75 ± 7.61 s, Fig. 21g)

and more struggling time (struggle duration for Ctrl-US = 51 ± 6.74 s, MscL-US = 59 ± 6.44 s, Ctrl+US = 57 ± 5.48 s, MscL+US = 93 ± 6.94 s, Fig. 21h) in the FST (Fig. 21f). In addition, an open field test (OFT) showed no obvious differences in locomotion ability among these four groups (Fig. 3i-k), excluding the potential confound of locomotor alterations when interpreting despair-like states in the TST and FST. These observations suggest sonogenetic modulation of DRN-projecting excitatory neurons in the mPFC ameliorated despair-like behaviors (a core symptom in depression) in stressed mice.

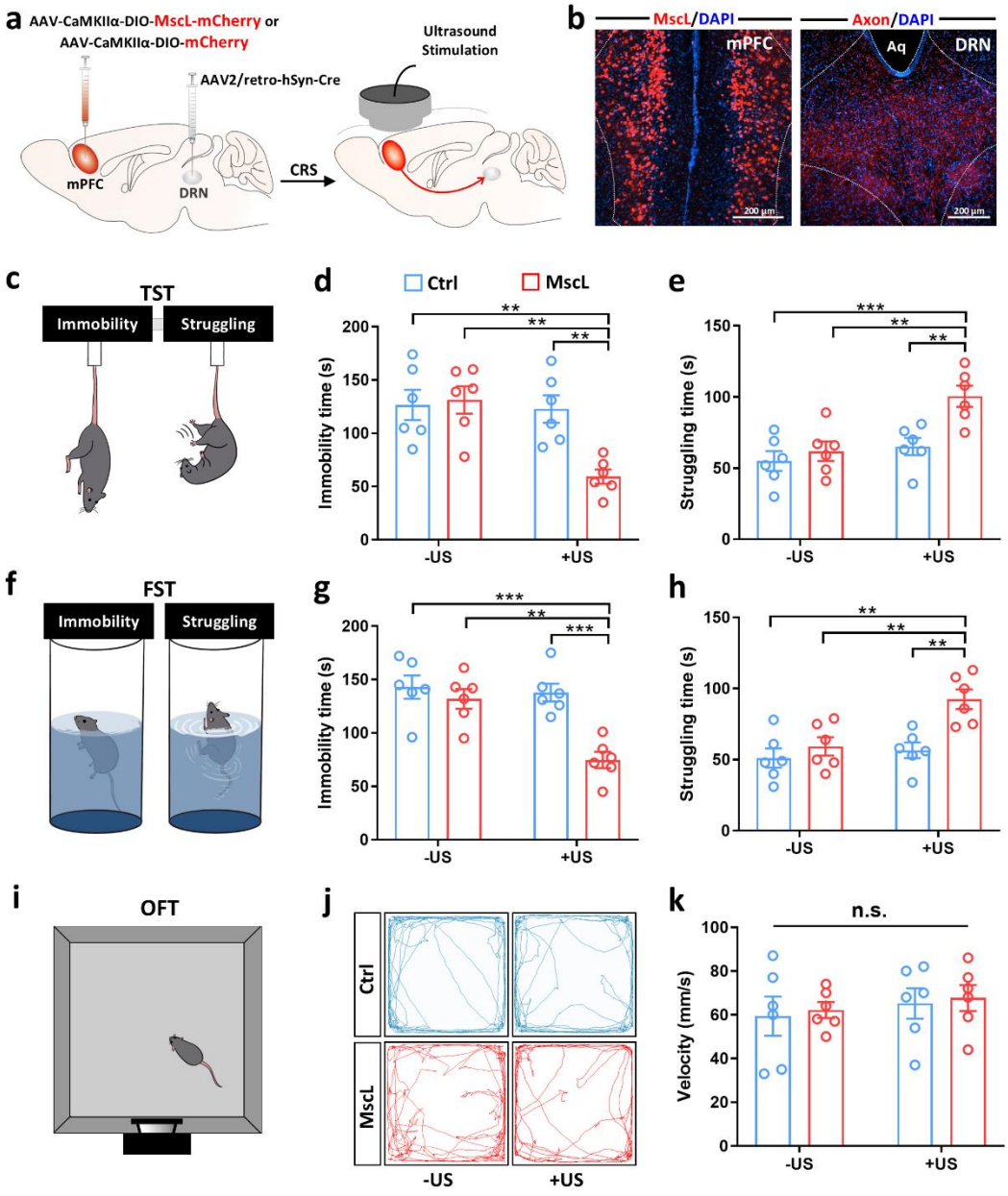

Figure 21. Sonogenetic modulation of DRN-projecting excitatory mPFC neurons elicits rapid antidepressant effects. a) Schematic illustration of viral transduction and ultrasound stimulation protocols. CRS was administered ~3 hrs/day for 14 days. 0.3 MPa ultrasound stimulation was applied starting 15 minutes before behavioral tests until the end of 6-minute test sessions in awake mice. **b)** MscL-expressing neurons (red) in the mPFC and their axon terminals in the DRN. **c-e)** Tail suspension test (TST) with/without ultrasound. **c)** Illustration of struggling and immobility

behaviors exhibited in the TST. **d)** Mean TST immobility time displayed by mice in each group. **e)** Mean TST struggling times displayed by mice in each group. **f-h)** Forced swim test (FST) with/without ultrasound. **f)** Illustration of struggling and immobility behaviors exhibited in the FST. **g)** Mean FST immobility time displayed by mice in each group. **h)** Mean FST struggling time displayed by mice in each group. **i-k)** Open field tests (OFTs) showing groups' roughly similar locomotion ability. **i**) Schematic illustration of OFT box setup (50 x 50 x 50 cm). **j)** Representative locomotion traces of mice from each group. **k**) Mean calculated velocity of mice in each group.

2.3.8 Activation of DRN neurons is necessary to elicit antidepressant effects through sonogenetic stimulation of the mPFC-DRN circuit

We observed that sonogenetic modulation of DRN-projecting excitatory neurons in the mPFC increased neuronal activity along the circuit and reversed despair-like behaviors in real-time. To further ascertain the role of DRN neurons in mediating the antidepressant action, the circuit was blocked downstream of the site of stimulation by chemogenetically inhibiting the activity of DRN neurons. Briefly, DRN-projecting mPFC excitatory neurons were transduced with MscL, and the activity of DRN neurons was controlled via a chemogenetic approach. AAVs encoding engineered Gi-coupled hM4D receptor (AAV-hSyn-hM4D-mCherry) were delivered into the DRN (Fig. 22a) and clozapine-N-oxide (CNO) was injected intraperitoneally to activate the hM4D receptor, thereby engaging the Gi signaling pathway and inhibiting neuronal

activity [200]. The presence of MscL-expressing mPFC neurons and their axon terminals surrounding hM4D-overexpressing DRN neurons were observed via fluorescent microscopy (Fig. 22b), indicating successful expression of these viruses. The efficacy of hM4D(Gi)-mediated inhibition was further confirmed via *ex vivo* electrophysiological patch clamp (Fig. 22c-d). Firstly, we choose neurons with red fluorescence in the DRN, which represented the successful expression of hM4D(Gi) protein. When stable recording it for several minutes, CNO was given to the perfusion solutions and arrived at the recording chamber. We found that CNO bath dramatically reduced the frequency of action potentials (APs) in the recorded neuron. After washing out, it recovered and elicited more APs which were quite similar to the state before CNO bath. These results exhibited obvious and reversible inhibition effects of this chemogenetic system.

Following this, depression-related behaviors during sonogenetic modulation of the mPFC-to-DRN pathway when chemogenetic inhibition of DRN neurons were examined in stressed mice. In behavioral tests *in vivo*, no significant differences were found in baseline despair-like behaviors between Ctrl and hM4D (with CNO) without ultrasound stimulation (Ctrl-US and hM4D-US) (Fig. 22e-h). However, upon ultrasound stimulation following 30 min of CNO administration, hM4D mice exhibited significantly more immobility time in the TST (hM4D+US (30 min post CNO) vs. Ctrl+US (30 min post CNO): 131 ± 8.11 s vs. 60.33 ± 6.91 s, $p = 0.0001$, Fig. 22e) and less struggling time (hM4D+US (30 min post CNO) vs. Ctrl+US (30 min post CNO): 55.83 ± 7.01 s vs. 98.67 ± 7.58 s, $p = 0.01$ Fig. 22f). Similarly, in the

FST, the hM4D+US (30 min post CNO) group spent significantly more time immobile (hM4D+US (30 min post CNO) vs. Ctrl+US (30 min post CNO): 125.3 ± 8.40 s vs. 64.17 ± 7.11 s, p = 0.0003, Fig. 22g) and less time struggling (hM4D+US (30 min post CNO) vs. Ctrl+US (30 min post CNO): 58.17 ± 5.59 s vs. 106.70 ± 5.70 s, p = 0.0002, Fig. 22h). These results indicate that artificially silencing DRN neurons blocked the antidepressant actions of sonogenetic stimulation along the mPFC-DRN circuit. Furthermore, when neurons were allowed 3 days to metabolize the CNO and then stimulated with ultrasound, hM4D and Ctrl groups showed comparable immobility and struggling times in both tests, suggesting the observed phenomenon in the hM4D group was not due to damage from chemogenetic treatment (Fig. 22e-h). This point was emphasized by post-experiment OFTs, which showed no significant differences in the general locomotion ability among these groups (Fig. 22i).

Taken together, these data show that inhibiting DRN neurons abrogated the antidepressant effects of sonogenetically modulating the mPFC-DRN circuit. This finding indicates that the observed effects of the MscL-mediated sonogenetic stimulation in the present study were effectuated through the specific activation of the mPFC-DRN circuit.

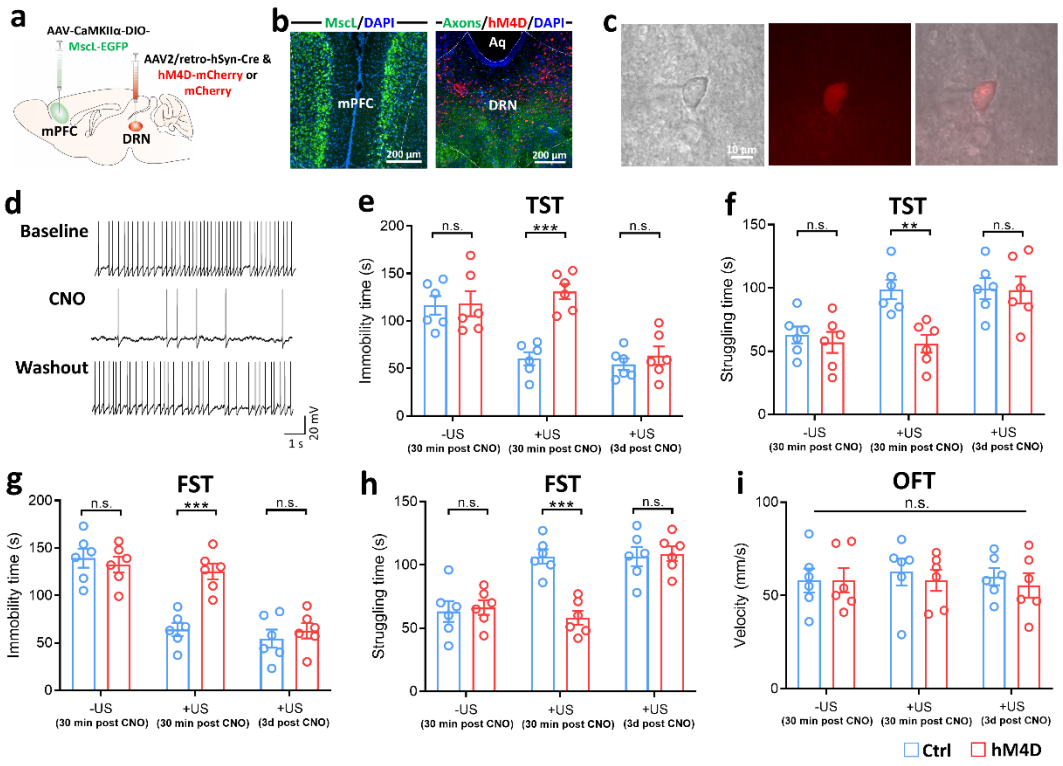

Figure 22. Activating DRN neurons is necessary for the antidepressant action of sonogenetically modulating the mPFC-DRN circuit. a) Schematic illustration of the viral transduction scheme. **b)** Representative images in the mPFC (left, MscL-expressing neurons = green, scale bar = 200 μm) and the DRN (right, hM4D-expressing DRN neurons = red; axon terminals from MscL-expressing DRN-projecting mPFC neurons = green, scale bar = 200 μm). **c)** DIC, fluorescent, and merged images of recorded hM4D-expressing DRN neurons (scale bar = 10 μm) in *ex vivo* patch clamp experiments. **d)** Representative traces showing the inhibitory effects of CNO on hM4D-expressing DRN neurons. **e)** Mean TST immobility time of different groups. **f)** Mean TST struggling time of different groups. **g)** Mean FST immobility time of different groups. **h)** Mean TST struggling time of different groups. **i)** Mean OFT velocities of different groups. n = 6 mice per group.

2.3.9 Functional silencing of 5-HT^{DRN} neurons blocked the antidepressant effects when sonogenetic modulation of DRN-projecting excitatory neurons in the mPFC

DRN houses many serotoninergic neurons abovementioned, and we found that activation of DRN neurons is essential to elicit antidepressant-like actions via sonogenetic modulation of DRN-projecting excitatory mPFC neurons. Going even further, we also studied the effect of sonogenetically modulating the circuit upon depression-related behaviors when 5-HT^{DRN} neurons were synaptically inactivated with tetanus toxin [201]. To be specific, we inactivated them by injecting AAV carrying tetanus toxin light chain, which was used to inhibit neurotransmitter release, into the DRN and examined depression-related behaviors when sonogenetic modulation of the DRN-projecting excitatory neurons in the mPFC in stressed mice. After viral expression, the MscL-expressing neurons in the mPFC and its axon terminals surrounding the neurons overexpressed with TetTox in the DRN were observed with fluorescent microscope (Fig. 24a). We did not observe any difference in baseline despair-like behavioral performance, either the immobility time and struggling time in the TST (Fig. 24b, c) or FST (Fig. 24d, e), between the mCherry- and TetTox-expressing stressed mice without ultrasound stimulation (Ctrl-US and TetTox-US). Interestingly, mCherry-expressing mice exhibited less immobility time (Fig. 24b) and more time struggling (Fig. 24c) in the TST than TetTox-expressing mice when sonication. The Ctrl+US group also spent less time immobile (Fig. 24d) and more time struggling (Fig. 24e) in the FST than TetTox+US group. Following

experimentation, we examined the general locomotion activity and found no observed difference in the velocity in the OFT among these four groups (Fig. 24f).

Collectively, these observaions show that inhibiting the synaptic function of 5-HT^{DRN} neurons abrogated the antidepressant effects of sonogenetically modulating the mPFC-DRN circuit. These observations indicate that the observed effects of the MscL-mediated sonogenetic stimulation in the present study were effectuated through the specific activation of the mPFC-DRN circuit. This finding underlines the ability of this approach to stimulate the targeted neuronal population, activate specific mesoscale neuronal circuits, and elicit changes in behavior patterns, which may be beneficial in the disease context.

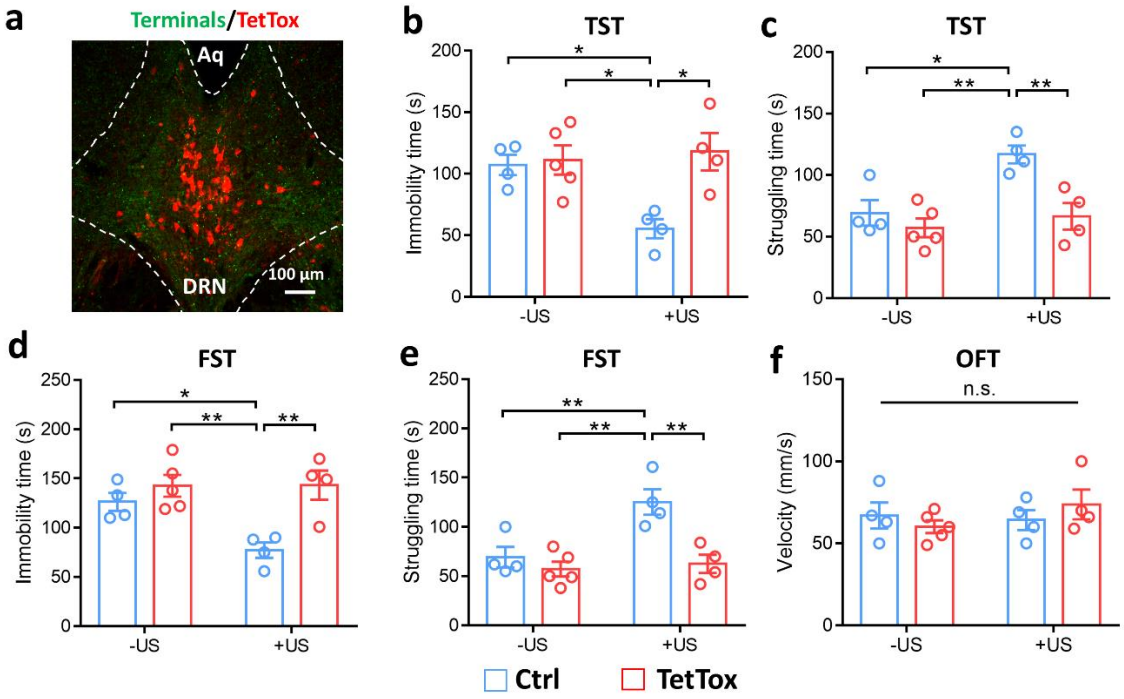

Figure 23. Functional silencing of 5-HTDRN neurons blocked the antidepressant effects when sonogenetic modulation of DRN-projecting excitatory neurons in the mPFC. AAV-CaMKIIα-DIO-MscL-EGFP and AAV2/retro-hSyn-Cre were

delivered into the mPFC and DRN, respectively. Following one week of recovery, mice were exposed to CRS and then AAV-TPH2-TetTox-mCherry or controlled AAV-TPH2-mCherry was injected into the DRN in CRS mice. Ultrasonic collimator and transducer were installed and aligned with the mPFC. Ultrasound was applied 15 minutes before, and all through the duration of, the 6-minute tests. **a)** Representative image of viral expression the DRN (TetTox-expressing neurons = red, axon terminals from MscL-expressing neurons of the mPFC = green. **b)** Mean TST immobility time (Ctrl+US vs. TetTox+US, Ctrl-US, TetTox-US: 55.50 ± 7.79 s vs. 118.00 ± 15.29 s, 107.30 ± 8.38 s, 111.20 ± 11.86 s; $p = 0.0112$, $p = 0.0364$, $p = 0.0170$). **c)** Mean TST struggling time (Ctrl+US vs. TetTox+US, Ctrl-US, TetTox-US: 116.80 ± 7.22 s vs. 66.50 ± 10.68 s, 69.25 ± 10.36 s, 57.52 ± 7.57 s). **d)** Mean FST immobility time (Ctrl+US vs. TetTox+US, Ctrl-US, TetTox-US: 77.25 ± 7.83 s vs. 143.30 ± 14.80 s, 126.30 ± 9.14 s, 142.60 ± 11.14 s). **e)** Mean FST struggling time (Ctrl+US vs. TetTox+US, Ctrl-US, TetTox-US: 125.30 ± 12.89 s vs. 62.50 ± 9.18 s, 69.25 ± 10.36 s, 57.20 ± 7.57 s). **f)** Mean velocities measured from OFT.

2.3.10 Sonogenetic modulation is safe at the cellular and tissue level

To examine the safety of sonogenetic modulation at the cellular level, we stained glial fibrillary acidic protein (GFAP) and ionized calcium-binding adapter molecule 1 (Iba1), which are typical biomarkers of microglia [202] and astrocytes [203]. The abnormal activation of these cell types has been widely identified as an early indicator of adverse inflammatory responses [204]. As shown in Fig. 23a-c, there was no observed

difference in morphology or cellular numbers of astrocytes and microglia among MscL+US, Ctrl+US, MscL-US, and Ctrl-US groups, indicating there are no severe inflammatory responses after sonogenetic modulation.

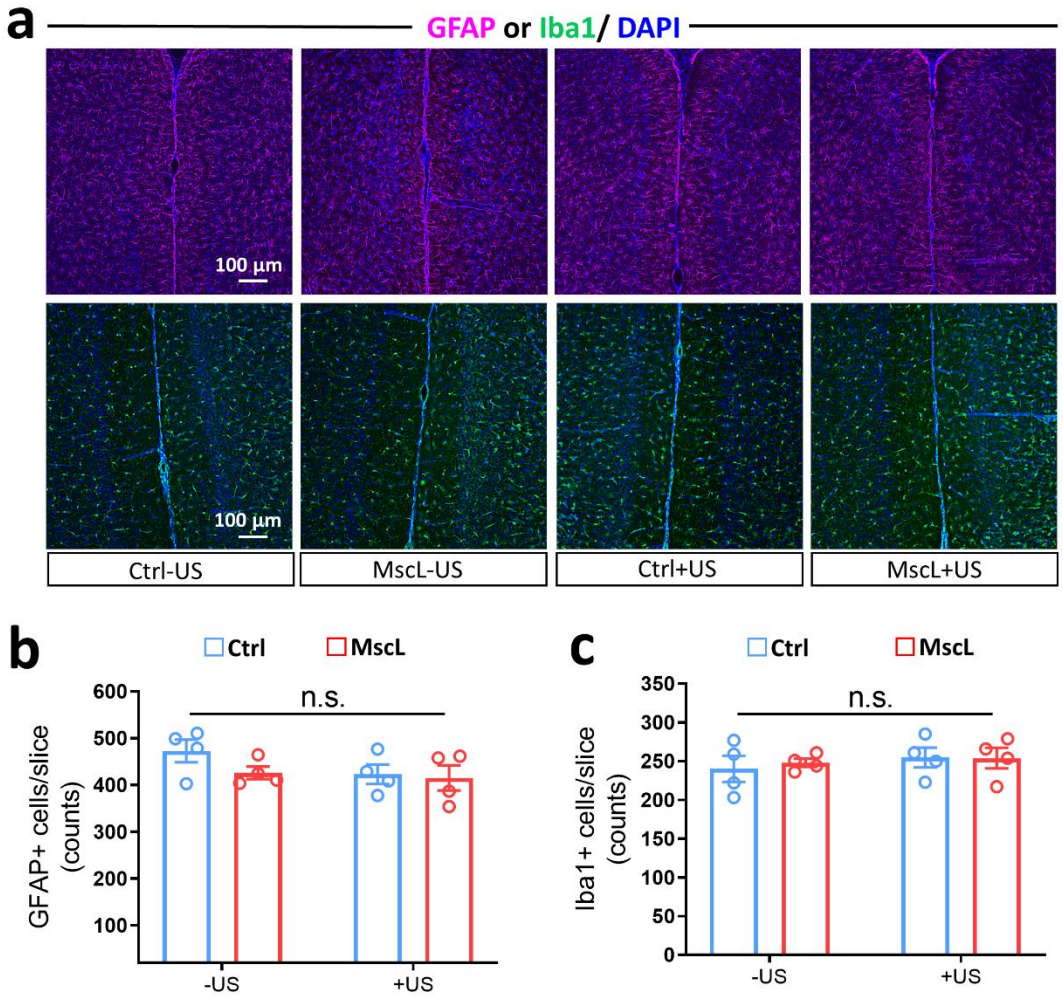

Figure 24. Sonogenetic modulation of the mPFC-DRN circuit did not influence the activity of astrocytes or microglia. a) Representative images of GFAP (upper panel, red fluorescence) and Iba1 (lower panel, green fluorescence) in the mPFC among Ctrl-US, MscL-US, Ctrl+US, and MscL+US groups. **b)** Counts of GFAP-positive cells in the mPFC among Ctrl-US, MscL-US, Ctrl+US, and MscL+US groups. **c)** Counts of Iba1-positive cells in the mPFC among Ctrl-US, MscL-US, Ctrl+US, and MscL+US groups.

In addition, the mPFC sections were procured and stained with H&E to examine the safety of our sonogenetic approach at a tissue level. Neuronal axons were found to be clear without signs of loss or damage after sonogenetic modulation (Figure 24). No abnormal alterations in the morphology of neurons were observed. There's no detectable tissue damage after sonogenetic modulation. Taken together, these observations suggest that the outlined sonogenetic approach was capable of activating the targeted neuronal populations without inducing obvious microglia/astrocytes activation or tissue damage.

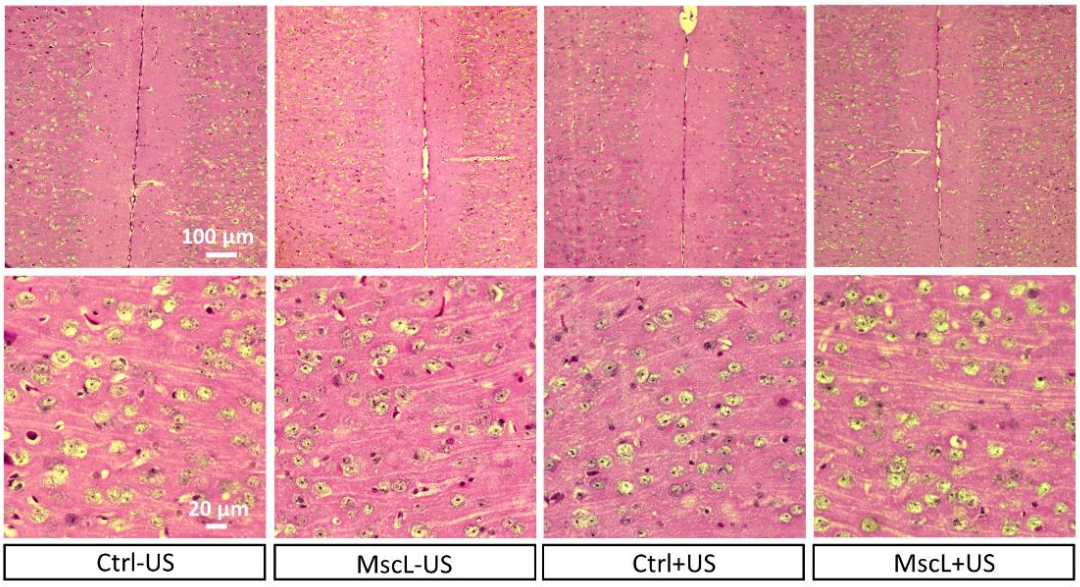

Figure 25. No detectable tissue damage in the mPFC after sonogenetic modulation. H&E representative images in the mPFC among Ctrl-US, MscL-US, Ctrl+US, and MscL+US groups.

CHAPTER 3: Sonogenetic modulation of serotonergic neurons in the DRN elicited rapid antidepressant actions

3.1 Introduction

Our observations indicate that sonogenetic modulation of the circuit from excitatory neurons in the mPFC to the DRN enhanced the neuronal activity within this circuit and resulted in rapid antidepressant effects. Moreover, we discovered that chemogenetic inhibition of DRN neurons counteracted these antidepressant effects when modulating the circuit, suggesting activating DRN neurons is essential to elicit antidepressant-like effects. The DRN, which houses the largest serotonergic neuronal populations in CNS, has been strongly associated with depression [83-85,205]. Previous studies also suggested DBS of the mPFC produced a significant amelioration in despair-like behaviors, and this improvement was entirely abrogated when depleted the serotonin [206]. Thus, we wanted to further investigate whether direct sonogenetic modulation of serotoninergic neurons in the DRN ($5\text{-}HT^{DRN}$) can produce antidepressant actions.

3.2 Materials and methods

3.2.1 Mice

The animals used here were the same as previously described in **Part 2.2.1**.

3.2.2 Viral Vectors

AAV2/9-TPH2-Mscl-G22S-F2A-EGFP, AAV2/9-TPH2-Mscl-G22S-F2A-mCherry, AAV2/9-TPH2-EGFP, AAV2/9-TPH2-mCherry, AAV2/9-hSyn-NES-jRGECO1a, AAV2/9-hSyn-5HT2.1 were diluted into 1×10^{12} vg/ml for using.

Company	Virus	Experimental Purpose
BrainVTA	AAV2/9-TPH2-Mscl-G22S-F2A-EGFP or AAV2/9-TPH2-EGFP	Overexpress MscL-EGFP into serotoninergic neurons in the DRN
BrainVTA	AAV2/9-TPH2-Mscl-G22S-F2A-mCherry or AAV2/9-TPH2-mCherry	Overexpress MscL-mCherry into serotoninergic neurons in the DRN
BrainVTA	AAV2/9-hSyn-NES-jRGECO1a	Record calcium activity in the DRN
BrainVTA	AAV2/9-hSyn-5HT2.1	Record serotonin release in the DRN

Table 3. The usage of the virus in Chapter 3.

3.2.3 Stereotaxic surgery

Mice were fixed on apparatus and their scalp was removed by a sterile surgical blade to expose bregma and lambda. After cleaning and leveling the skull, we injected the virus into the DRN and implanted optical fibers or installed ultrasonic collimators as depicted in **Part 2.2.3**. Fiber photometry or behavioral tests were conducted on mice at least 7 days after surgery.

3.2.4 Ultrasound system and stimulation

The customized wearable transducer was installed into the collimator coupled with ultrasound gel for all awake behavioral tests. The commercial ultrasonic transducer was mounted upon the skull above the DRN when conducted fiber photometry recording in the DRN under anesthesia. The parameters of ultrasound stimulation were shown as follows (central frequency, 0.8 MHz; intensity, 0.11 or 0.25 MPa; pulse width, 500 μs; pulse repetition frequency, 1 kHz; stimulation duration, 300 ms; stimulation interval, 3 s).

3.2.5 Fiber photometry recording

A wire was used to connect the implanted fiber and the recording system, and the excitation wavelength for jRGECO1a and 5-HT2.1 was 570 nm and 480 nm, respectively. Another fiber-optic patch cord was used to connect the recording system and ultrasound stimulation system to synchronize signals. The ultrasound transducer was put upon the DRN while recording the alteration of florescent intensities in the DRN. Data was collected and analyzed as previously described in **Part. 2.2.5**.

3.2.6 Chronic restraint stress and behavioral test

The CRS mouse model of depression and behavioral tests conducted here were the same as previously described in **Part 2.2.7 & 2.2.8**.

3.2.7 Immunofluorescence staining

After anesthesia, mice were perfused with PBS (Cat. no., 70011044; Thermo Fisher Scientific Inc., Waltham, USA) followed by a 4% paraformaldehyde (PFA) solution (Cat. no., sc-281692; Santa Cruz Biotechnology Inc., California, USA), and brain was exacted and put inro a 4% PFA solution overnight in a 4 ℃ refrigerator. Coronal sections containing the DRN with a thickness of 40 μm were attained from the fixed brain by the vibrating microtome (VT1200S; Leica Biosystems GmbH, Wetzlar, Germany). Slices were blocked with prepared blocking for 90 min at RT and covered by prepared primary antibody solution (TPH2, 1:1000, Cat. no., 51124, CST, Massachusetts, USA; c-Fos, 1:1000, Cat. no., 2250, CST, Massachusetts, USA; Iba-1, 1:1000; Cat. no., 17198, CST, Massachusetts, USA; GFAP, 1:500, Cat. no., 12389, CST, Massachusetts, USA) overnight in a 4 ℃ refrigerator. After washing, slices were incubated with anti-rabbit Alexa Fluor 555 plus or 633 secondary antibodies (1:1000; Thermo Fisher Scientific Inc., Waltham, USA) for 90 min at RT. Then, sectioned were dried and mounted as previously descripted in **Part. 2.2.9**.

Primary antibody	Secondary antibody	Brain region
TPH2	Alexa Fluor 555	The DRN
c-Fos	Alexa Fluor 633	The DRN
Iba1	Alexa Fluor 555	The DRN
GFAP	Alexa Fluor 633	The DRN
c-Fos	Alexa Fluor 488	The AC

Table 4. The usage of antibodies in Chapter 3.

3.2.8 Hematoxylin and eosin staining

The method of HE staining conducted here was the same as previously described in **Part 2.2.10**.

3.2.9 Data analysis

Data analysis principles applied in this chapter were the same as **Part 2.2.11.**

3.3 Results and discussion

3.3.1 Verification of the efficacy of virus with mouse Tph2 promoter

The largest present site of serotonergic neurons is the DRN, consisting of around one-third of all serotonergic neurons in CNS [81]. In the DRN, serotonergic neurons approximately account for 30%-50% of all neurons, and there are non-serotonergic neurons as well, such as glutamatergic, dopaminergic, and GABAergic neurons [207]. It was reported that optogenetic stimulation of non 5-HT^{DRN} neurons instead of 5-HT^{DRN} neurons, induced reward-related behavior (drug-seeking behavior) [208]. Apart from neurons, the DRN contains non-neuronal cells, like astrocytes, oligodendrocytes, microglia, and other non-neuronal cells [81]. Both animal and clinical studies found abnormal activation of microglia in the DRN contributed to the development of depression [47], suggesting that cellular populations in the DRN are anatomically and neurochemically diverse, relating to different behavioral paradigms.

Regarding depression treatment, we aim to specifically activate 5-HT^{DRN} neurons with sonogenetic modulation and observe depressive-like behaviors in mice. To

achieve it, we first exogenously overexpressed MscL-G22S into serotoninergic neurons in the DRN via injecting adeno-associated virus (AVV) bearing MscL-G22S into the DRN (rAAV-TPH2-Mscl-G22S-F2A-EGFP-WPRE-pA or rAAV-TPH2-EGFP-WPRE-pA). The TPH serves as the rate-limiting enzyme in serotonin's synthesis and includes two isozymes, i.e., TPH1 and TPH2 [209]. TPH1 is rich in the gut, while TPH2 is only expressed within brain and its gene *Tph2* is commonly used as a specific promoter for investigating the function of serotoninergic neurons [84,209]. After injecting the virus, the expression of MscL-expressing neurons with green fluorescence was observed in the DRN (Figure 25), suggesting the virus was successfully infused into the DRN. To further verify *Tph2* promoter's efficacy, we stained TPH2 with an antibody and observed the co-expression of TPH2 and EGPF in the DRN by confocal microscope. The green, red, and orange fluorescence represented the EGPF, TPH2, and co-expression of EGPF and TPH2, respectively (Figure 25). The percentage of TPH2 and GFP co-positive neurons in GFP+ neurons in EGFP control and MscL group are 91.9±1.8% and 89.3±2.5%, respectively (Figure 25), suggesting the majority of neuronal population expressed green fluorescence are serotoninergic neurons.

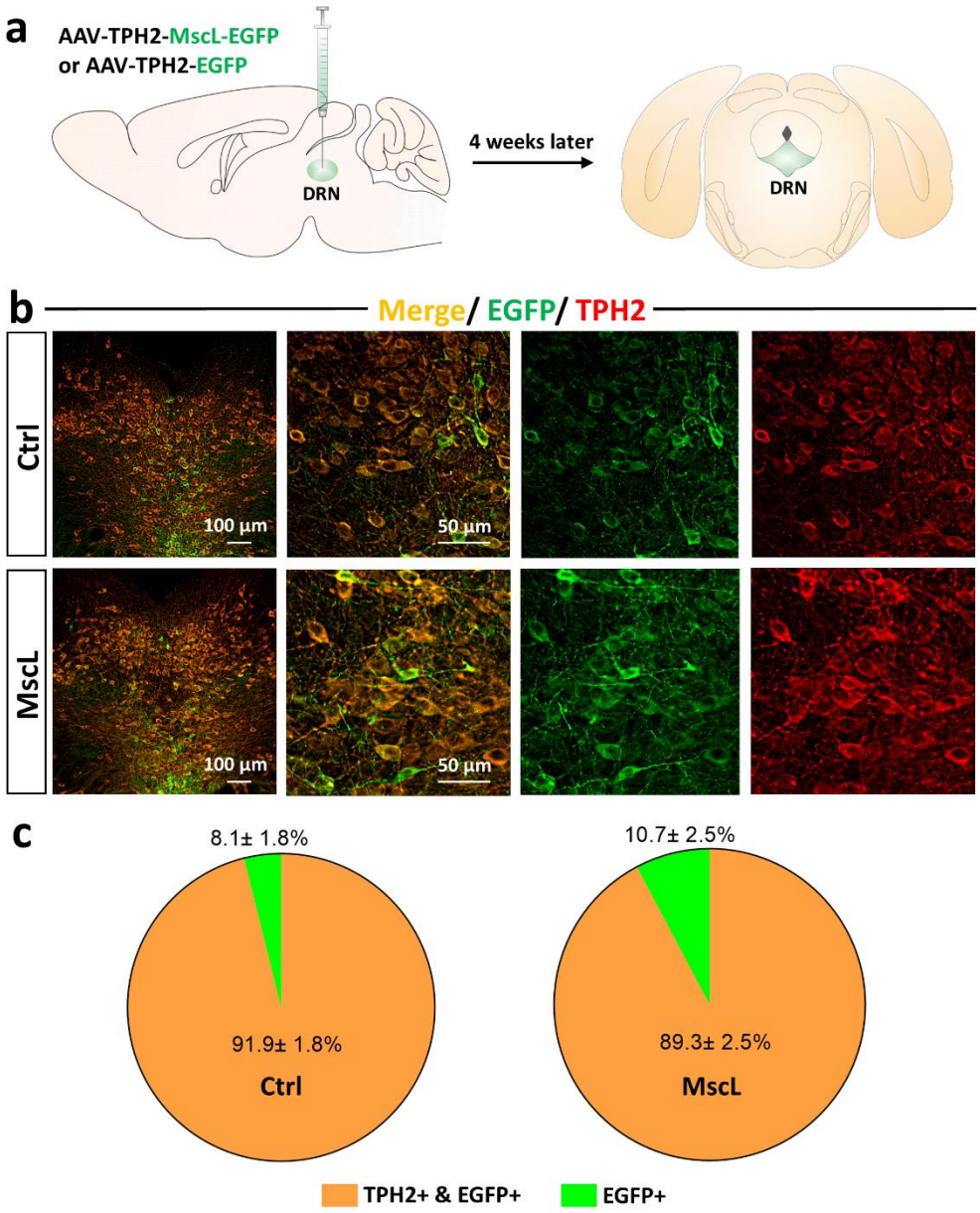

Figure 26. AAVs carrying the *Tph2* promoter efficiently transduced serotonergic neurons in the DRN. a) The schematic illustration of viral transfection. AAV-TPH2-MscL-EGFP or AAV-TPH2-EGFP were delivered into the DRN, and DRN-containing coronal sections were attained for staining by anti-TPH2 antibodies after one month. After staining, the colocalization of TPH2 and MscL-EGFP or EGFP was observed with confocal microscopy. **b)** Representative images expressed EGFP fluorescence and stained TPH2 in the DRN. **c)** The percentage of TPH2 and EGFP double-positive

cells in EGFP-positive cells (left: EGFP group; right: MscL-EGFP group). n = 3 mice per group.

3.3.2 Sonogenetic modulation of 5-HT^{DRN} enhanced the neuronal activity in the DRN

To investigate whether ultrasound stimulation can induce real-time neuronal activation, we co-injected AAVs for expressing jRGECO1a (a genetically encoded calcium sensor with red fluorescence [210]; rAAV-hSyn-NES-jRGECO1a-WPRE-hGH-pA) with AAVs for expressing MscL or EGFP (the same as the above virus) in the DRN and then implanted the optical fiber over the DRN. Four weeks later, the red fluorescence signal was measured *in vivo* when sonication (shown in the schematic illustration, Fig. 26a). The massive colocalization between red fluorescence signals representing neurons overexpressed jRGECO1a and green fluorescence signals representing neurons overexpressed with MscL or EGFP was observed (Fig. 26b). Before ultrasound stimulation, both Ctrl and MscL mice exhibited similar baseline fluorescence (Peak ΔF/F, MscL vs. EGFP: 0.093 ± 0.022 % vs. 0.075 ± 0.015 %, p = 0.5142, Fig. 26d). When sonication at 0.11 MPa, there are no obvious changes of the jRGECO1a fluorescence intensity between MscL and Ctrl groups (Peak ΔF/F, MscL vs. EGFP: 0.115 ± 0.019 % vs. 0.082 ± 0.012 %, p = 0.1577, Fig. 26d). But 0.25 MPa-ultrasound stimuli repeatedly induced synchronous elevation of jRGECO1a fluorescence intensity in MscL group, but not EGFP group (Fig. 26c). And the Peak ΔF/F in MscL+US group was significantly increased when compared with EGFP+US

group at 0.25 MPa ultrasound stimulation (Peak ΔF/F, MscL vs. EGFP: 0.365 ± 0.029 % vs. 0.072 ± 0.020 %, $p = 2.4 \times 10^{-5}$, Fig. 28d). These observations collectively suggest sonogenetic stimulation was capable of real-timely increasing the calcium activity in the DRN.

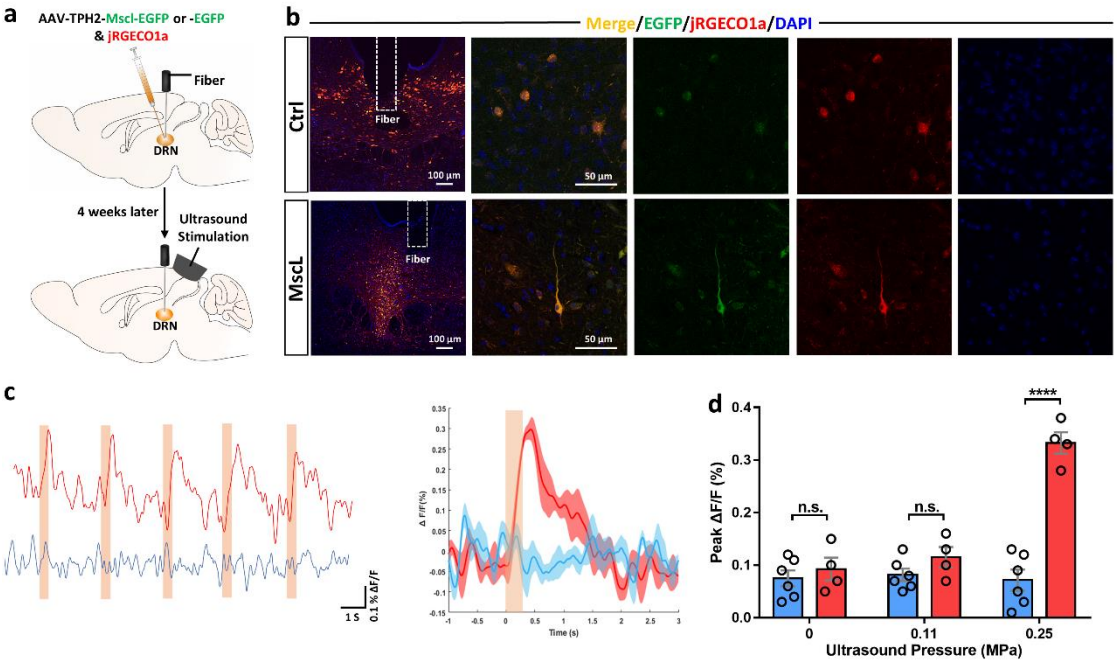

Figure 27. The neuronal activity in the DRN when sonogenetic modulation of 5-HT^{DRN} neurons. a) The schematic illustration of viral transduction and fiber photometry. Four virus expressions, the alteration of red fluorescence intensity was measured *in vivo* when ultrasound stimulation. **b)** Representative images of the DRN overexpressed with jRGECO1a and MscL or EGFP. Green, red, and blue fluorescence indicate MscL- or EGFP-expressing neurons, jRGECO1a signal, and DAPI, respectively. The dashed rectangle indicates the location of the fiber. **c, d)** Ultrasound stimulation increased neuronal activity in the DRN. Blue and red colors indicated EGFP (n = 6 mice) and MscL (n = 4 mice) groups, respectively. **c)** Representative jRGECO1a fluorescence traces of MscL- and EGFP-expressing mice when received 5

pulses of 0.25 MPa ultrasound stimulation (left) and averaged jRGECO1a fluorescence signal from the left panel (right). **d)** The averaged peak change of jRGECO1a fluorescence (Peak ΔF/F) in response to 0, 0.11, 0.25 MPa ultrasound stimulation.

3.3.3 Sonogenetic modulation of 5-HT^{DRN} enhanced the serotonin release in the DRN

Given previous observation that 5-HT neurons extend richly branching axon collaterals to the DRN [211] and the well-known biological phenomenon that increased neuronal activities lead to enhanced neurotransmitter release [212], we further observed serotonin release in the DRN when ultrasound stimulation. We co-injected a 5-HT sensor and AAVs for expressing MscL into the DRN and then installed the fiber (shown in the following schematic illustration, Fig. 27a). The massive colocalization between green fluorescence signals representing neurons overexpressed 5-HT2.1 and red fluorescence signals representing neurons overexpressed with MscL or mCherry was observed (Fig. 27b). Following experiments, the change of green fluorescence intensity was measured *in vivo* when sonication. There is no obvious difference in the baseline fluorescence before ultrasound stimulation between MscL and mCherry groups (Peak ΔF/F, MscL vs. mCherry: 0.054 ± 0.020 % vs. 0.048 ± 0.009 %, p = 0.7947, Fig. 27d). In addition, no significant change of the 5-HT fluorescence intensity between MscL and mCherry groups was detected when ultrasound stimulation at 0.11 MPa (Peak ΔF/F, MscL vs. mCherry: 0.114 ± 0.022 % vs. 0.063 ±

0.015, p = 0.1085, Fig. 27d). But 0.25 MPa-ultrasound stimuli synchronously induced the enhancement of the 5-HT fluorescence intensity in MscL group, but not mCherry group (Fig. 27c). And 5-HT fluorescence intensity was elevated in the MscL group, instead of mCherry, when ultrasound stimulation at 0.25 MPa (Peak ΔF/F, MscL vs. mCherry: 0.482 ± 0.028 % vs. 0.078 ± 0.026, %, $p = 1.7 \times 10^{-5}$, Fig. 27d). Collectively, sonogenetic modulation of the 5-HT^{DRN} neurons increased the neuronal activity and serotonin release in the DRN in a real-time manner.

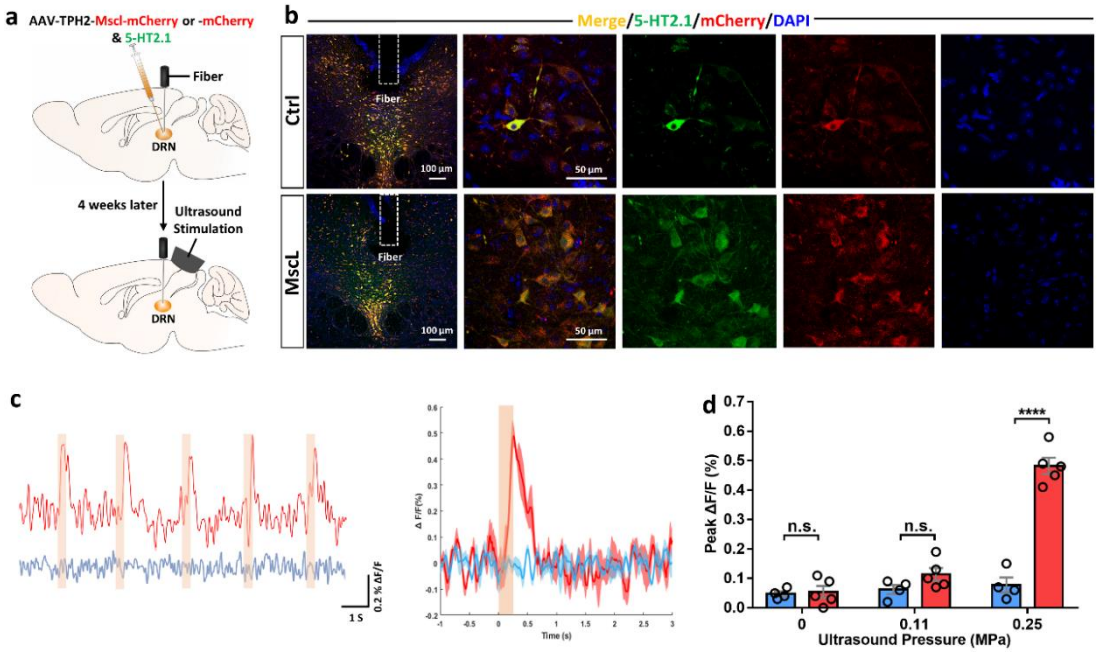

Figure 28. The real-time serotonin release in the DRN when sonogenetic modulation. a) The schematic illustration of viral transduction and fiber photometry. AAV-hSyn-5-HT2.1 and AAV-TPH2-MscL-mCherry or AAV-TPH2-mCherry were delivered to the DRN and then fibers were installed. Four weeks later, the alteration of green fluorescence intensity was measured *in vivo* when ultrasound stimulation. **b)** Representative images of the DRN overexpressed with a 5-HT sensor and MscL or mCherry. Green, red, and blue fluorescence indicate the signal of the 5-HT sensor,

MscL- or EGFP-expressing neurons, and DAPI, respectively. The dashed rectangle indicates the location of the fiber. **c, d)** Ultrasound stimulation induced the release of serotonin in the DRN. Blue and red colors indicated the mCherry (n = 4 mice) and MscL (n = 5 mice) groups, respectively. **c)** Representative 5-HT fluorescence traces of MscL- and mCherry-groups when receiving multiple pulses of 0.25 MPa ultrasound stimulation (left) and averaged 5-HT fluorescence signal from the left panel (right). **d)** The average peak change of 5-HT fluorescence (Peak ΔF/F) in response to 0, 0.11, 0.25 MPa ultrasound stimulation.

3.2.4 Sonogenetic modulation of the 5-HT^{DRN} neurons rapidly reversed despair-like behaviors

We have observed that sonogenetic modulation of the 5-HT^{DRN} neurons increased neuronal activity and enhanced serotonin release in the DRN in a real-time manner. Following experiments, we want to further investigate whether sonogenetic modulation of them can rapidly ameliorate depression-related behaviors. To target 5-HT^{DRN} neurons, we infused AAVs carrying either MscL-EGFP or EGFP with *Tph2* promoter into the DRN. Following recovery, mice were subjected to CRS for 14 successive days. Then an ultrasonic collimator was installed above the DRN. Another week later, the customized wearable transducer was installed into the collimator coupled with ultrasound gel, and depression-related behaviors were observed when sonication. When comparing MscL-US with the Ctrl-US group, we didn't observe obvious behavioral changes either in TST or FST (Fig. 28c-f), indicating our

sonogenetic tool MscL didn't affect the baseline of despair-like states in our setup. Importantly, when applying ultrasound stimulation, MscL-expressing mice spent significantly less time immobile (MscL+US vs. Ctrl+US: 53.29 ± 13.74 s vs. 134.60 ± 14.51 s, p = 0.0009, Fig. 28c) and more time struggling (MscL+US vs. Ctrl+US: 141.40 ± 12.11 s vs. 58.14 ± 10.82 s, $p = 2.1 \times 10^{-5}$, Fig. 28d) in the TST than EGFP-expressing mice. Mice in the MscL+US group also exhibited less immobility time (MscL+US vs. Ctrl+US: 58.50 ± 10.28 s vs. 121.40 ± 18.02 s, p = 0.0373, Fig. 28e) and more struggling time (MscL+US vs. Ctrl+US: 129.10 ± 15.17 s vs. 76.00 ± 13.23 s, p = 0.0367, Fig. 28f) in the FST than mice in Ctrl+US group. But the velocity of movement in the OFT among these groups showed no obvious difference (Fig. 28g). These observations suggest that sonogenetic modulation of 5-HT^{DRN} neurons can rapidly reverse despair-like behaviors in stressed mice.

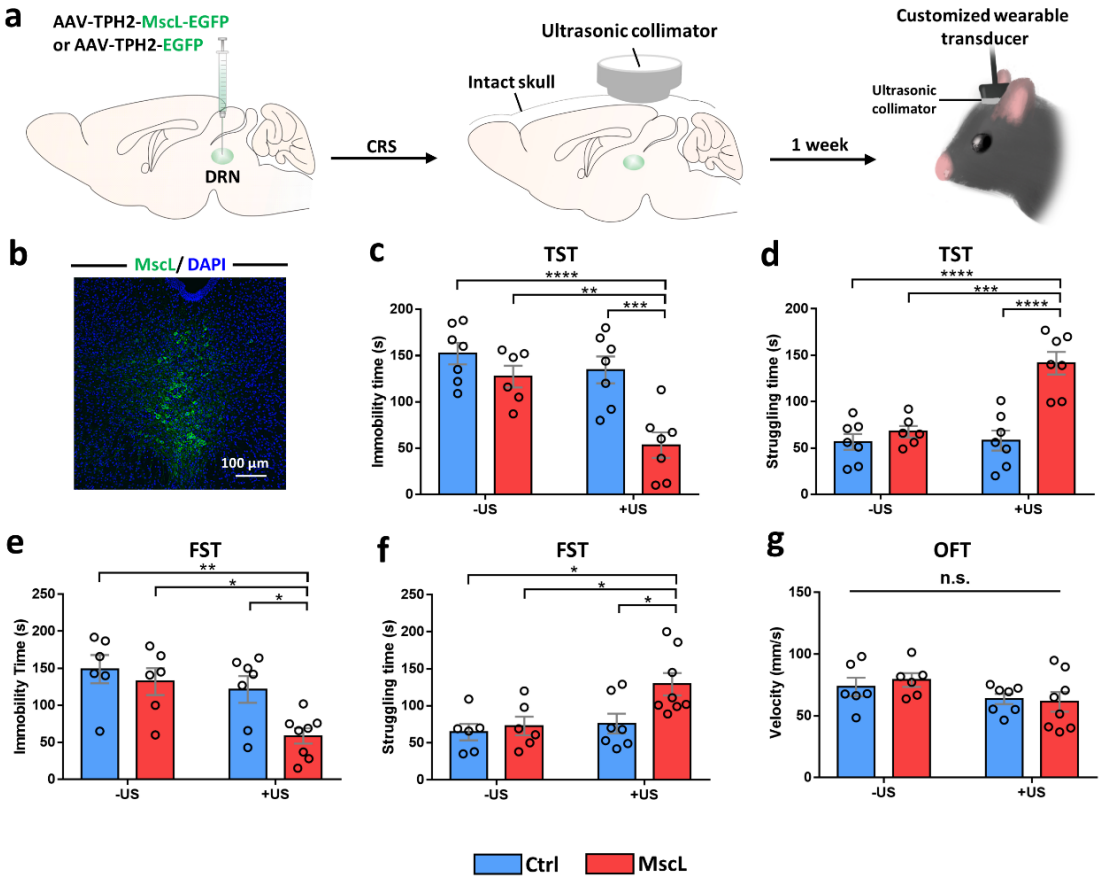

Figure 29. Sonogenetic modulation of 5-HT^{DRN} neurons rapidly reversed despair-like behaviors. a) The schematic illustration of viral transduction and ultrasound stimulation. AAV-TPH2-MscL-EGFP or AAV-TPH2-EGFP were delivered into the DRN. Following recovery, mice were subjected to CRS for 14 days. Then an ultrasonic collimator was installed above the DRN. Another week later, the customized wearable transducer was installed into the collimator and depression-related behavioral tests were conducted when sonication. **b)** MscL fluorescence with DAPI in the DRN. **c-f)** Sonogenetic modulation of 5-HT^{DRN} neurons reversed despair-like behaviors. **c)** The immobility time in the TST among Ctrl-US, MscL-US, Ctrl+US, and MscL+US groups. **d)** The struggling time in the TST among Ctrl-US, MscL-US, Ctrl+US, and MscL+US groups. **e)** The immobility time in the FST among

Ctrl-US, MscL-US, Ctrl+US, and MscL+US groups. **f)** The struggling time in the FST among Ctrl-US, MscL-US, Ctrl+US, and MscL+US groups. **g)** The speed in the OFT among Ctrl-US, MscL-US, Ctrl+US, and MscL+US groups.

3.3.5 Sonogenetic modulation of 5-HT^{DRN} neurons enhanced the neuronal activity in the DRN in stressed mice

To further confirm the select specificity of sonogenetic modulation targeting 5-HT^{DRN} neurons, we examined whether the activated neurons are MscL-expressing neurons. We found that sonogenetic modulation significantly elevated c-Fos protein in the DRN (MscL+US vs. Ctrl+US, MscL-US, Ctrl-US: 81.50 ± 5.92 vs. 32.33 ± 5.40, 28.20 ± 5.21, 22.60 ± 4.76, $p = 1.6 \times 10^{-5}$, 1.0×10^{-5}, 2.6×10^{-6}, Fig. 29a, b). Importantly, the colocalization between c-Fos positive and green EGFP fluorescence signals in the MscL+US group (67.78 ± 3.60%) was significantly higher than the Ctrl+US group (21.39 ± 3.74%, $p = 2.1 \times 10^{-8}$), MscL-US group (17.60 ± 2.85%, $p = 1.3 \times 10^{-8}$), and Ctrl-US group (18.55 ± 1.86%, $p = 1.8 \times 10^{-8}$) (Fig. 29a, c), indicating the activated neurons by sonogenetic modulation are mainly MscL-expressing neurons. In addition, MscL-transfected neurons are chief serotonergic neurons as verified by staining TPH2 as described in part 3.3.1. These results indicate that sonogenetic neuromodulation of 5-HT^{DRN} neurons specifically enhanced the activity of 5-HT^{DRN} neurons.

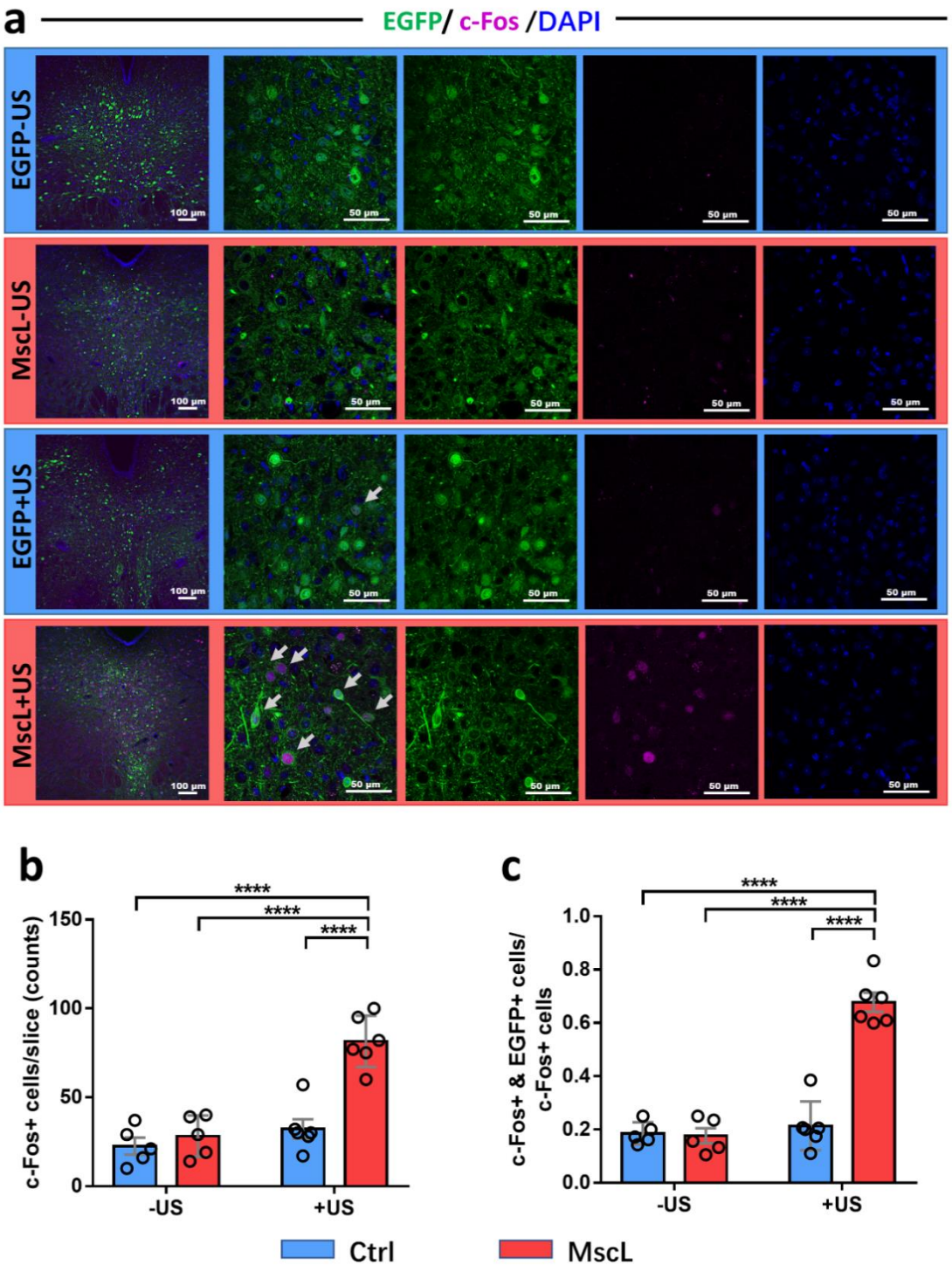

Figure 30. Sonogenetic modulation of 5-HT^{DRN} neurons elevated their neuronal activity. a) The images which showed c-Fos protein in the DRN among Ctrl-US, MscL-US, Ctrl+US, and MscL+US groups. Green, red, and blue fluorescence indicated MscL- or EGFP-expressing neurons, c-Fos positive signal, and DAPI,

respectively. **b)** Counted numbers of c-Fos+ cells in the DRN among Ctrl-US, MscL+US, Ctrl+US, and MscL+US groups. **c)** The ratio of c-Fos & EGFP positive cells to c-Fos positive neurons in the DRN among Ctrl-US, MscL+US, Ctrl+US, and MscL+US groups.

3.3.6. Biosafety assessments after sonogenetic modulation of the DRN

As described previously, Iba1 and GFAP are typical biomarkers of activated microglia [202] and astrocytes [203], respectively. Their activation has been identified as early indicator of adverse tissue responses [204]. In this study, no difference in the expression of either Iba1 or GFAP was observed among MscL+US, Ctrl+US, MscL-US, and Ctrl-US groups (Figure 30).

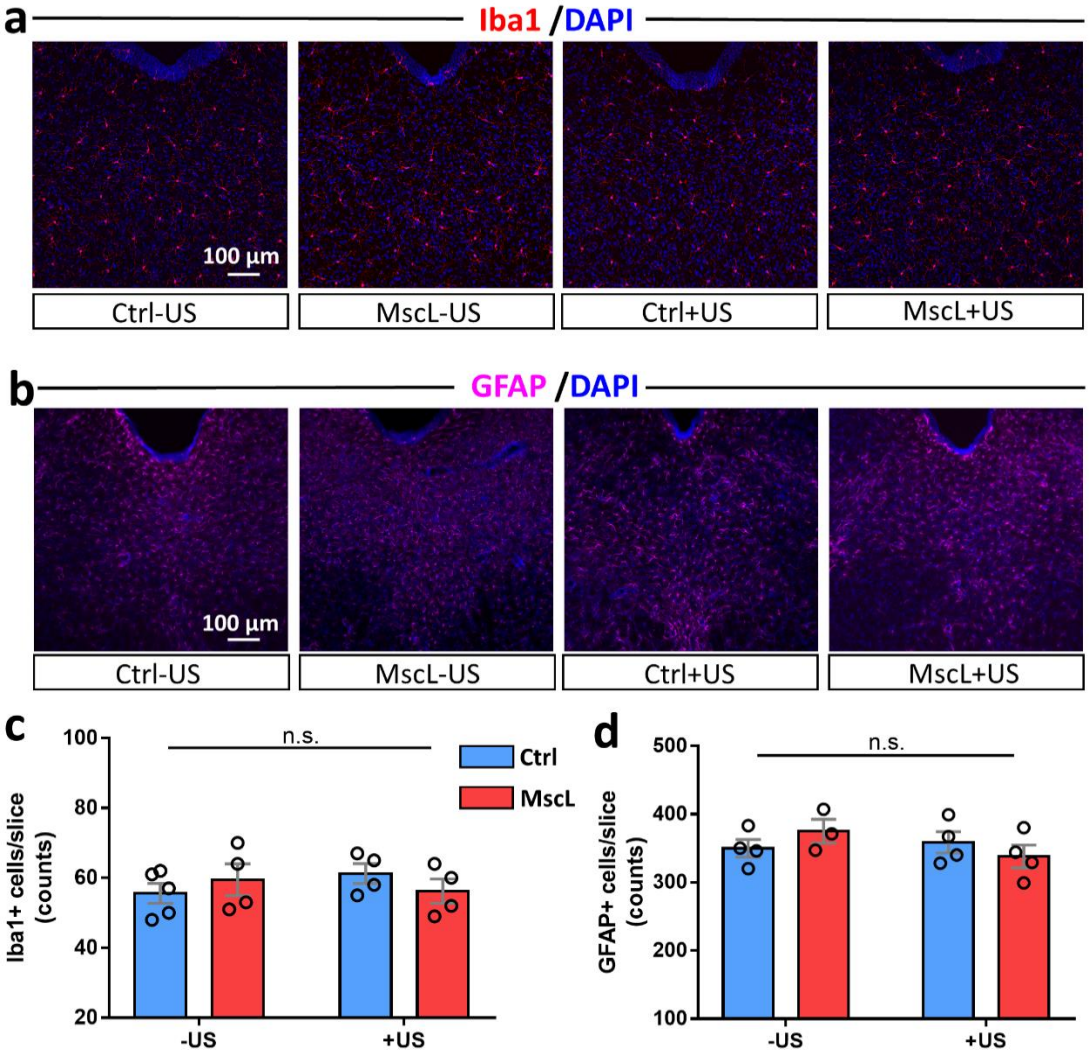

Figure 31. Sonogenetic modulation of serotoninergic neurons in the DRN did not influence the activity of astrocytes or microglia. **a)** Representative images of Iba1 in the DRN among Ctrl-US, MscL-US, Ctrl+US, and MscL+US groups. **b)** Representative images of GFAP in the DRN among Ctrl-US, MscL-US, Ctrl+US, and MscL+US groups. **c)** Counts of Iba1-positive cells in the DRN among Ctrl-US, MscL-US, Ctrl+US, and MscL+US groups. Blue and red bars in the histogram indicated EGFP and MscL groups, respectively. **d)** Counts of GFAP-positive cells per slice imaged in the DRN. n = 3-4 mice per group. Blue and red bars in the histogram indicated EGFP and MscL group, respectively.

In addition, there was no detected neuronal loss or changes in tissue responses in the DRN after sonogenetic modulation (Figure 31). Taking together, these results suggest that sonogenetic modulation was capable of selectively activating 5-HT^{DRN} neurons without activating the sign of microglia/astrocytes activation or tissue damage.

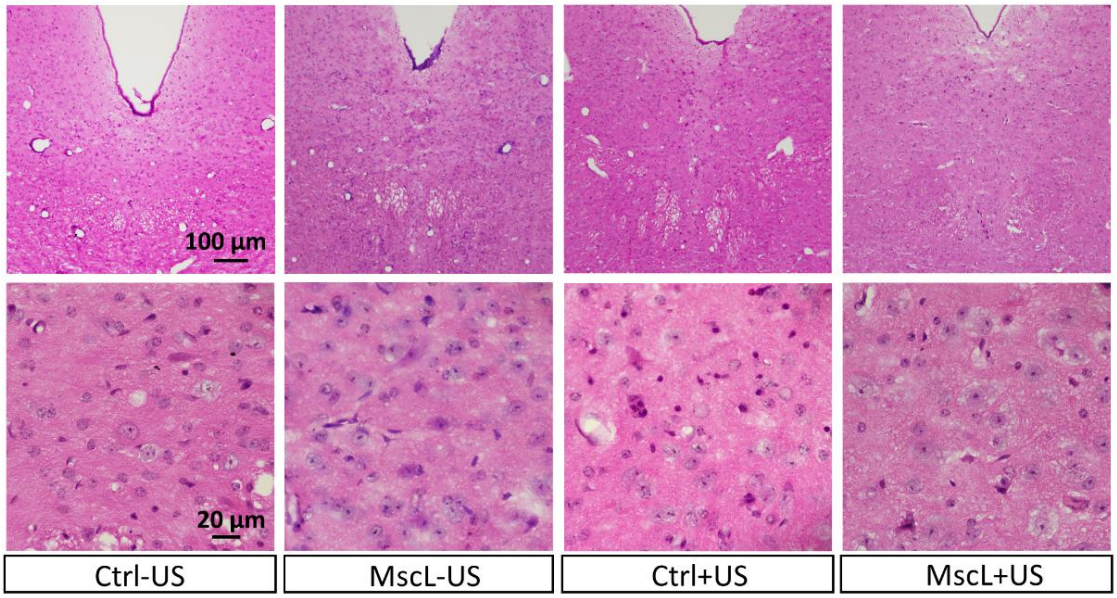

Figure 32. No detectable tissue response in the DRN after sonogenetic modulation. H&E representative images in the DRN among Ctrl-US, MscL-US, Ctrl+US, and MscL+US groups.

3.3.7 The activity of neurons in the auditory cortex

Several studies indicated that ultrasound could activate the auditory pathways which may contribute to the bioeffects of ultrasonic neuromodulation [117,118]. We assessed c-Fos levels in the auditory cortex (AC) following sonogenetic modulation. Interestingly, c-Fos levels in the AC increased after ultrasound stimulation in awake

mice (Fig. 32). However, there was no difference in c-Fos levels between the Ctrl+US and MscL+US groups (Fig. 32). These findings suggest that while ultrasound stimulation activates the AC in awake mice, the antidepressant effects are not due to auditory activation. Therefore, the observed antidepressant-like effects of sonogenetic modulation are most likely to result from the specific activation of targeted neuronal circuits or populations.

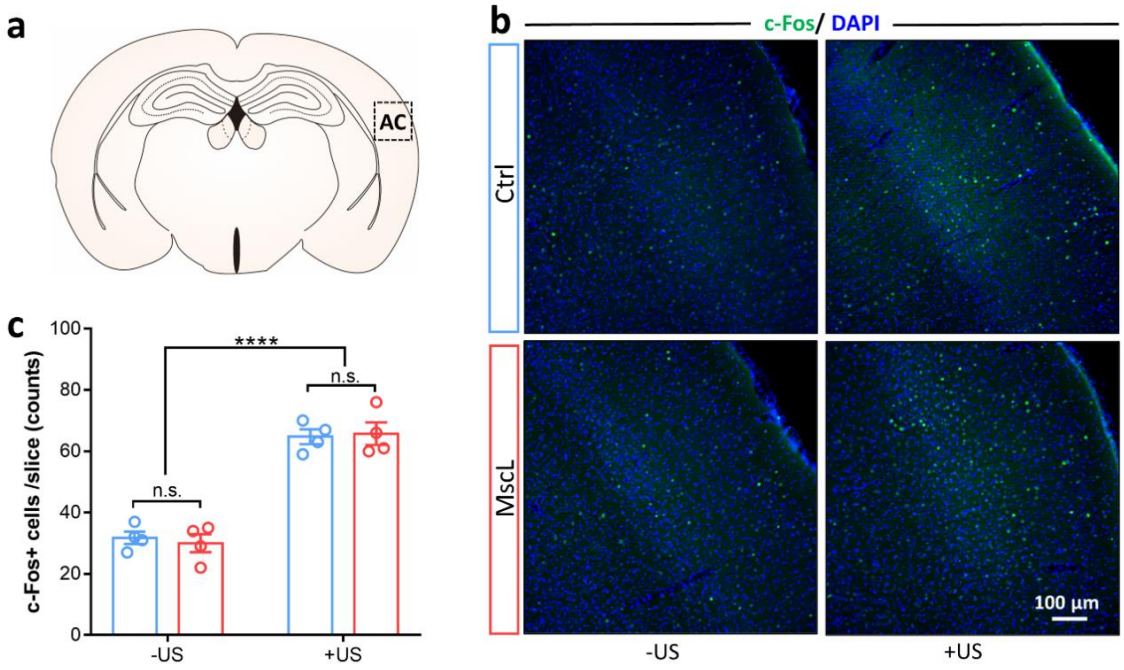

Figure 33. The c-Fos expression in the auditory cortex. a) The schematic illustration of the AC. b**)** The representative images of the c-Fos protein in the AC after sonogenetic modulation among Ctrl-US, MscL-US, Ctrl+US, and MscL+US groups. **c)** Counts of c-Fos positive cells imaged in the AC among Ctrl-US, MscL-US, Ctrl+US, and MscL+US groups.

CHAPTER 4. Conclusions and future work

This study first attempts to utilize sonogenetic modulation as a novel therapeutic modality in the context of depression. As shown in the graphic summary (Figure 33), We found that non-invasive ultrasound stimulation of DRN-projecting excitatory mPFC neurons, heterologously made to express MscL-G22S, enhanced real-time neuronal activity and serotonin release in the DRN. We observed calcium and serotonin responses in the DRN closely synchronous with ultrasound stimuli (sub-second responses), and these responses were repeatable and reversible. Crucially, we also demonstrated that sonogenetic modulation of DRN-projecting excitatory neurons in the mPFC specifically enhanced the activity of this neuronal circuit and elicited rapid antidepressant actions in stressed mice, without any sign of tissue damage or abnormal activation of microglia or astrocytes. Functionally silencing downstream DRN neurons abrogated the antidepressant effects during sonogenetic stimulation of the mPFC, suggesting DRN neurons were necessary to elicit antidepressant effects through sonogenetic stimulation of the mPFC-DRN circuit. Furthermore, we used sonogenetic modulation to directly activate serotoninergic neurons in the DRN (5-HT^{DRN}) and observed the real-time secretion of 5-HT and rapid antidepressant actions. Taken together, we lay the groundwork and show that sonogenetic modulation shows potential to be a new therapeutic method for depression and, possibly, other brain diseases.

Sonogenetic neuromodulation integrates the merits of ultrasound stimulation and

genetic modification to achieve non-invasive and selective control of specific neuronal populations with fine spatiotemporal resolution [213]. Several studies suggest that ultrasound stimulation alone (over 2 weeks) without genetic modification has a positive effect on depressive-like behaviors in rodents [142-145]. However, mechanosensitive ion channels and receptors are endogenously expressed on all major cell types in the brain, such as neurons, microglia, and astrocytes [214]. Moreover, these endogenous mechanosensitive ion channels, including TRP family channels, Piezo1/2, TREK1/2, and TRAAK channels, exhibit different sensitivity in response to ultrasound stimulation [214]. Given the mixed and ambiguous spatial profile of endogenous ultrasound-responsive ion channels in the brain, at the current stage, it would be challenging to achieve specific, targeted bioeffects or to interpret complex experimental data – such as behaviors – through ultrasound stimulation alone [214]. This problem also exists in other non-specific stimulation neuromodulation therapies, such as whole-brain electrical or magnetic stimulation due to mixed cellular populations. By contrast, in sonogenetic modulation, exogenous overexpression of mechanosensitive ion channels into targeted neuronal populations could sensitize them to low-intensity ultrasound stimulation to achieve cell-type selective stimulation. Indeed, in the present study, our low-intensity sonogenetic stimulation method could activate a targeted mesoscale circuit and rapidly rescue despair-like behaviors, without obvious activation of other brain areas or glial cells. Importantly, due to the profile of endogenous expression of mechanosensitive ion channels, even when using ultrasound neuromodulation and focusing on the same circuit as optogenetics, it is

still a challenge instead of straightforwardly replicating the results observed in optogenetic research.

In the clinic, TMS is a widely available neuromodulation treatment for depression, in which magnetic fields are used to stimulate the brain to relieve depressive symptoms [100]. Studies have reported that TMS of the mPFC as monotherapy for three consecutive weeks ameliorated depressive symptoms [215], but the remission rate was lower than 50%, and they lack a specific neuronal target for identifying subjects most likely to respond to TMS or the implicated mechanism(s) [216]. By contrast, in sonogenetic modulation, exogenous overexpression of mechanosensitive ion channels into targeted neuronal populations could sensitize them to low-intensity ultrasound stimulation to achieve cell-type selective stimulation. The accuracy and selectivity of sonogenetic modulation can help make both therapeutic effects and side effects more predictable and controllable, thereby enabling improved treatments. As we mentioned above, depression is multifactorial, and many brain circuits and areas manipulate depressive behaviors. Here, we focused on the mesoscale mPFC-DRN circuit, showing huge potential to treat depression. More depression-related circuits and areas that aforementioned in the Part. 1.1.6 need to be further investigated with sonogenetic modulation, such as mPFC-NAc, DRN-LHb, and LHb-RMTg. Meanwhile, sonogenetic modulation should be applied to more animal models of depression to cover more facets of depression as far as possible. The present study only focused on a chronic restraint stress mouse model of depression and primarily assessed despair-like behaviors which, while useful experimental indicators, do not generalize perfectly

to other forms of stress or capture the gamut of human symptoms, such as feelings of sadness and anhedonia [217]. To pave the way for applying sonogenetic neuromodulation in depressive patients in the future, further research is needed to explore various ultrasound parameters, examine different depression-related behaviors across multiple strains and models, as well as extending the scope of experimentation to include large animals and humans [217]. In addition, sonogenetic modulation could further be utilized with other techniques, such as fMRI, to identify personalized, symptom-specific brain areas and provide tailored treatments. It is also amenable to being developed into a closed-loop stimulation technique in which adjustable ultrasound is output based on monitoring patients' clinical conditions. The flexibility of sonogenetics and its ability to be combined with other modalities, thus, can make it possible for researchers to investigate many different strategies for further study and eventual clinical transition.

A significant hurdle in the present approach is that it involves surgical invasion into the brain to deliver viral particles that induce expression of the heterologous channel. To further realize full noninvasiveness and pave the way for clinical translation, developing safe ways to deliver sonogenetic tools (e.g., ultrasound-sensitive channels like MscL-G22S) is needed, instead of transcranial injection. Early evidence is present for minimally invasive approaches such as tail-vein [218] or intranasal [219] administration, and ultrasound-facilitated gene delivery via transiently opening the blood-brain barrier [158]. However, these will still require significant work before they can replace local administration and should be the subject of study in the future.

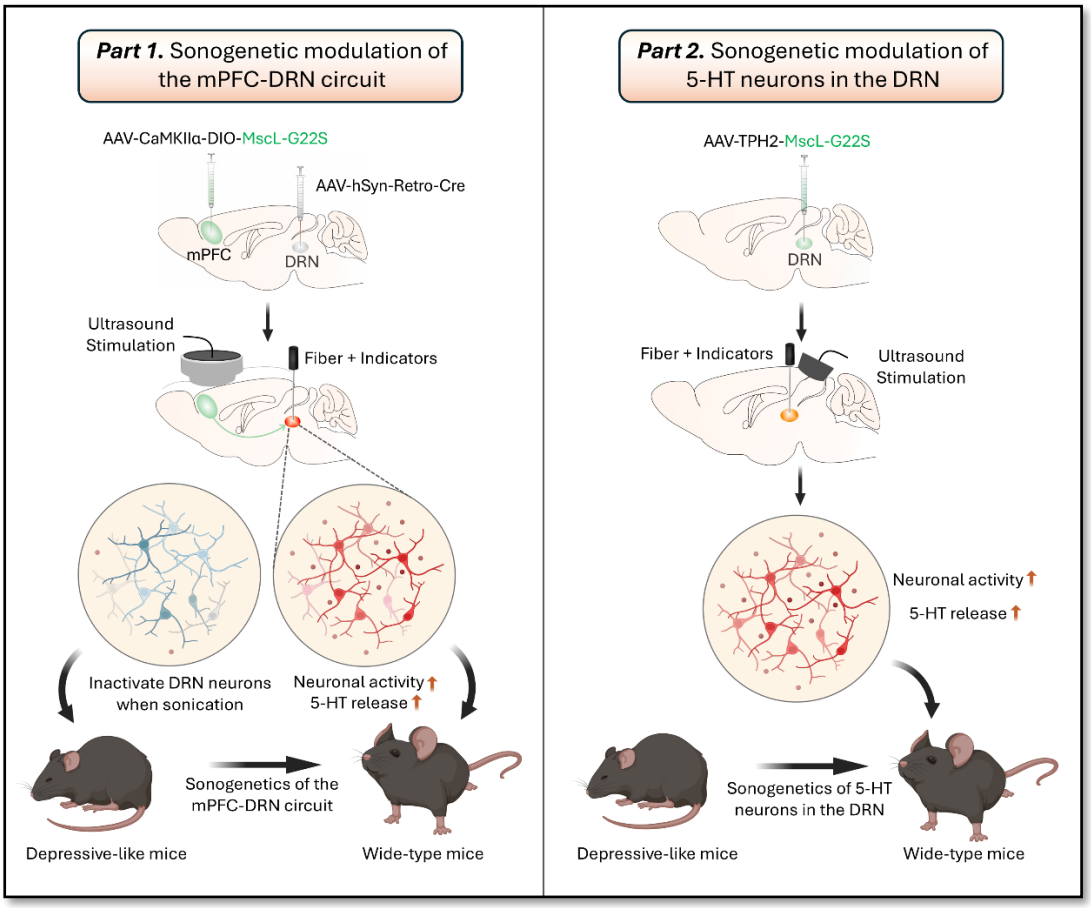

Figure 34. The graphical summary of sonogenetic modulation for depression. This study is divided into two main parts: the first part focuses on sonogenetic modulation of the circuit from excitatory neurons in the mPFC to the DRN, while the second part examines sonogenetic modulation of 5-HT^{DRN} neurons. As shown in the left panel, sonogenetic modulation of DRN-projecting excitatory mPFC neurons induced the activation of DRN neurons and antidepressant effects. Conversely, inactivating DRN neurons abrogated this antidepressant effect produced by sonogenetic modulation of the mPFC-DRN circuit. Therefore, as depicted in the right panel, 5-HT^{DRN} neurons were targeted in part 2. Sonogenetic modulation of 5-HT^{DRN} neurons enhanced their neuronal activity and resulted in antidepressant effects. These discoveries highlight the capability of the novel technique - sonogenetic modulation -

to activate targeted neuronal populations, engage specific mesoscale neuronal circuits, and induce changes in behavior patterns, potentially offering therapeutic benefits in depression contexts.

LIST OF TABLES

LIST OF FIGURES

calcium influx (D1). The accumulation of calcium calcium-sensitive sodium channels such as TRPM4 (D2), then T-type calcium channels (D3), which further activated voltage-gated calcium and sodium channels (D4), and finally excited neurons.

Figure 13. The current applications of ultrasound neuromodulation (adapted from [156]).

Figure 14. The crystal structure of MscL which visualized from the plane of membrane (left) and cytoplasm (right) (adapted from [169]).

Figure 15. Millimeter-scale ultrasound setup on mouse heads to sonogenetically target region of interest. a) Schematic diagram of the ultrasonic transducer and collimator. "①" indicates the wearable customized ultrasonic transducer. "②" indicates the ultrasonic collimator. **b)** Photograph for scale of the ultrasonic transducer and collimator. **c)** Bottom view of the ultrasonic collimator (aperture size = 5 mm). **d)** Schematic diagram of the transducer scanning platform. RF, radio frequency; ADC, analog-to-digital converter. **e)** Distribution of the acoustic field of the transducer in the XY plane (0.3 MPa). **f)** Photograph to illustrate the location above the mPFC and DRN. **g)** Photograph showing the ultrasonic collimator's alignment with the mPFC without affecting the DRN. **h)** Photograph illustrating the customized wearable transducer with collimator affixed to the head of a mouse, above the mPFC. **i)** Illustration of the ultrasound temporal profile applied in this study.

Figure 16. Depression-related behavioral performance when sonogenetic modulation of all excitatory neurons in the mPFC. a) The schematic illustration of viral transduction protocol and ultrasound stimulation. Mice were infused bilaterally

in the mPFC with either AAV2/9-CaMKIIα-MscL-EYFP or AAV2/9- CaMKIIα-EYFP. Following a week of recovery, mice were subjected to the 2-week chronic restraint stress procedure. Then an ultrasonic collimator was installed and aligned with the mPFC. Another week later, the customized wearable transducer was installed into the collimator and behavioral tests were conducted when sonication of the mPFC. Ultrasound was ON from 15 minutes before behavioral tests to the end of it (a total of 21 minutes). **b)** MscL fluorescence in the mPFC. **c-f)** No obvious alteration in despair-like states was observed when sonication. n = 4-5 mice per group. **c)** The immobile durations exhibited in the TST among Ctrl-US, MscL-US, Ctrl+US, and MscL+US groups. **d)** The struggle durations exhibited in the TST among Ctrl-US, MscL-US, Ctrl+US, and MscL+US groups. **e)** The immobile durations exhibited in the FST among Ctrl-US, MscL-US, Ctrl+US, and MscL+US groups. **f)** The struggle durations exhibited in the FST among Ctrl-US, MscL-US, Ctrl+US, and MscL+US groups. **g)** The average velocity of mice in the OFT. n = 4-5 mice per group.

Figure 17. Sonogenetic modulation of DRN-projecting excitatory neurons in the mPFC enhanced the neuronal activity in the DRN. a) Schematic illustration of viral transduction and fiber photometry recording. **b)** Left: representative image showing MscL-expressing neurons = red fluorescence and DAPI = blue fluorescence in the mPFC; Right: representative image showing axon terminals from MscL-expressing neurons of the mPFC = red fluorescence, Ca^{2+} sensor GCaMP6s = green florescence, and DAPI = blue fluorescence in the DRN. **c)** Representative traces of GCaMP6s fluorescence changes in MscL (red) and Ctrl (blue) groups upon multiple

0.3 MPa ultrasound stimuli. **d)** The average GCaMP6s fluorescence signals from panel c. **e)** Averaged peak change of GCaMP6s fluorescence (Peak ΔF/F). n = 3 mice per group.

Figure 18. Sonogenetic modulation of DRN-projecting excitatory neurons in the mPFC enhanced serotonin release in the DRN. a) Schematic illustration of viral transduction and fiber photometry recording. **b)** Left: Representative image showing MscL-expressing neurons (red) and DAPI (blue) in the mPFC; Right: representative image showing axon terminals from MscL-expressing neurons of the mPFC (red), 5-HT2.1 (green), and DAPI (blue) in the DRN. **c)** Representative traces of 5-HT2.1 fluorescence change in the MscL (red line) and Ctrl (blue line) group when receiving multiple 0.3 MPa ultrasound stimuli. **d)** The averaged 5-HT2.1 fluorescence signal from panel c. **e)** The averaged peak change of 5-HT2.1 fluorescence (Peak ΔF/F). n = 3 mice in each group.

Figure 19. Sonogenetic modulation of the circuit from excitatory neurons in the mPFC to the DRN enhanced the neuronal activity of this circuit. a) The representative images show MscL-expressing neurons (red fluorescence) and c-Fos expression (green fluorescence) in the mPFC. White arrows highlight the c-Fos positive signal within MscL-expressing neurons. **b)** The representative images depict the axonal terminals in the DRN that originate from MscL-expressing neurons in the mPFC (red fluorescence), along with c-Fos expression (green fluorescence) in the DRN. **c)** Counts of c-Fos positive neuronal populations imaged in the mPFC among Ctrl-US, MscL-US, Ctrl+US, and MscL+US groups. **d)** Counts of c-Fos positive

neuronal populations imaged in the DRN among Ctrl-US, MscL-US, Ctrl+US, and MscL+US groups.

Figure 20. The establishment of the chronic restraint stress mouse model of depression. a) The schematic illustration of mice subjected to CRS (~3 h per day for 14 consecutive days). **b)** The immobile durations exhibited in the TST among Control and CRS groups (Con vs. CRS: 75.13 ± 8.17s vs. 127.00 ± 11.68 s, p = 0.0027). **c)** The struggling time in the TST (Con vs. CRS: 113.10 ± 6.49 s vs. 71.50 ± 7.89 s, p = 0.0015). **d)** The immobility time in the FST (Con vs. CRS: 70.00 ± 7.99 s vs. 114.60 ± 15.95 s, p = 0.0181). **e)** The struggling time in the FST (Con vs. CRS: 122.00 ± 11.94 s vs. 81.29 ± 13.22 s, p = 0.0389). **f)** No observed difference in the velocity in the OFT was observed between Con and CRS groups (Con vs. CRS: 63.83 ± 7.80 mm/s vs. 68.86 ± 5.66 mm/s, p = 0.6050).

Figure 21. Sonogenetic modulation of DRN-projecting excitatory mPFC neurons elicits rapid antidepressant effects. a) Schematic illustration of viral transduction and ultrasound stimulation protocols. CRS was administered ~3 hrs/day for 14 days. 0.3 MPa ultrasound stimulation was applied starting 15 minutes before behavioral tests until the end of 6-minute test sessions in awake mice. **b)** MscL-expressing neurons (red) in the mPFC and their axon terminals in the DRN. **c-e)** Tail suspension test (TST) with/without ultrasound. **c)** Illustration of struggling and immobility behaviors exhibited in the TST. **d)** Mean TST immobility time displayed by mice in each group. **e)** Mean TST struggling times displayed by mice in each group. **f-h)** Forced swim test (FST) with/without ultrasound. **f)** Illustration of struggling and

immobility behaviors exhibited in the FST. **g)** Mean FST immobility time displayed by mice in each group. **h)** Mean FST struggling time displayed by mice in each group. **i-k)** Open field tests (OFTs) showing groups' roughly similar locomotion ability. **i**) Schematic illustration of OFT box setup (50 x 50 x 50 cm). **j)** Representative locomotion traces of mice from each group. **k**) Mean calculated velocity of mice in each group.

Figure 22. Activating DRN neurons is necessary for the antidepressant action of sonogenetically modulating the mPFC-DRN circuit. a) Schematic illustration of the viral transduction scheme. **b)** Representative images in the mPFC (left, MscL-expressing neurons = green, scale bar = 200 μm) and the DRN (right, hM4D-expressing DRN neurons = red; axon terminals from MscL-expressing DRN-projecting mPFC neurons = green, scale bar = 200 μm). **c)** DIC, fluorescent, and merged images of recorded hM4D-expressing DRN neurons (scale bar = 10 μm) in *ex vivo* patch clamp experiments. **d)** Representative traces showing the inhibitory effects of CNO on hM4D-expressing DRN neurons. **e)** Mean TST immobility time of different groups. **f)** Mean TST struggling time of different groups. **g)** Mean FST immobility time of different groups. **h)** Mean TST struggling time of different groups. **i)** Mean OFT velocities of different groups. n = 6 mice per group.

Figure 23. Functional silencing of 5-HTDRN neurons blocked the antidepressant effects when sonogenetic modulation of DRN-projecting excitatory neurons in the mPFC. AAV-CaMKIIα-DIO-MscL-EGFP and AAV2/retro-hSyn-Cre were delivered into the mPFC and DRN, respectively. Following one week of recovery,

mice were exposed to CRS and then AAV-TPH2-TetTox-mCherry or controlled AAV-TPH2-mCherry was injected into the DRN in CRS mice. Ultrasonic collimator and transducer were installed and aligned with the mPFC. Ultrasound was applied 15 minutes before, and all through the duration of, the 6-minute tests. **a)** Representative image of viral expression the DRN (TetTox-expressing neurons = red, axon terminals from MscL-expressing neurons of the mPFC = green. **b)** Mean TST immobility time (Ctrl+US vs. TetTox+US, Ctrl-US, TetTox-US: 55.50 ± 7.79 s vs. 118.00 ± 15.29 s, 107.30 ± 8.38 s, 111.20 ± 11.86 s; $p = 0.0112$, $p = 0.0364$, $p = 0.0170$). **c)** Mean TST struggling time (Ctrl+US vs. TetTox+US, Ctrl-US, TetTox-US: 116.80 ± 7.22 s vs. 66.50 ± 10.68 s, 69.25 ± 10.36 s, 57.52 ± 7.57 s). **d)** Mean FST immobility time (Ctrl+US vs. TetTox+US, Ctrl-US, TetTox-US: 77.25 ± 7.83 s vs. 143.30 ± 14.80 s, 126.30 ± 9.14 s, 142.60 ± 11.14 s). **e)** Mean FST struggling time (Ctrl+US vs. TetTox+US, Ctrl-US, TetTox-US: 125.30 ± 12.89 s vs. 62.50 ± 9.18 s, 69.25 ± 10.36 s, 57.20 ± 7.57 s). **f)** Mean velocities measured from OFT.

Figure 24. Sonogenetic modulation of the mPFC-DRN circuit did not influence the activity of astrocytes or microglia. a) Representative images of GFAP (upper panel, red fluorescence) and Iba1 (lower panel, green fluorescence) in the mPFC among Ctrl-US, MscL-US, Ctrl+US, and MscL+US groups. **b)** Counts of GFAP-positive cells in the mPFC among Ctrl-US, MscL-US, Ctrl+US, and MscL+US groups. **c)** Counts of Iba1-positive cells in the mPFC among Ctrl-US, MscL-US, Ctrl+US, and MscL+US groups.

Figure 25. No detectable tissue damage in the mPFC after sonogenetic modulation. H&E representative images in the mPFC among Ctrl-US, MscL-US, Ctrl+US, and MscL+US groups.

Figure 26. AAVs carrying the *Tph2* promoter efficiently transduced serotonergic neurons in the DRN. a) The schematic illustration of viral transfection. AAV-TPH2-MscL-EGFP or AAV-TPH2-EGFP were delivered into the DRN, and DRN-containing coronal sections were attained for staining by anti-TPH2 antibodies after one month. After staining, the colocalization of TPH2 and MscL-EGFP or EGFP was observed with confocal microscopy. **b)** Representative images expressed EGFP fluorescence and stained TPH2 in the DRN. **c)** The percentage of TPH2 and EGFP double-positive cells in EGFP-positive cells (left: EGFP group; right: MscL-EGFP group). n = 3 mice per group.

Figure 27. The neuronal activity in the DRN when sonogenetic modulation of 5-HT^{DRN} neurons. a) The schematic illustration of viral transduction and fiber photometry. Four virus expressions, the alteration of red fluorescence intensity was measured *in vivo* when ultrasound stimulation. **b)** Representative images of the DRN overexpressed with jRGECO1a and MscL or EGFP. Green, red, and blue fluorescence indicate MscL- or EGFP-expressing neurons, jRGECO1a signal, and DAPI, respectively. The dashed rectangle indicates the location of the fiber. **c, d)** Ultrasound stimulation increased neuronal activity in the DRN. Blue and red colors indicated EGFP (n = 6 mice) and MscL (n = 4 mice) groups, respectively. **c)** Representative jRGECO1a fluorescence traces of MscL- and EGFP-expressing mice when received 5

pulses of 0.25 MPa ultrasound stimulation (left) and averaged jRGECO1a fluorescence signal from the left panel (right). **d)** The averaged peak change of jRGECO1a fluorescence (Peak ΔF/F) in response to 0, 0.11, 0.25 MPa ultrasound stimulation.

Figure 28. The real-time serotonin release in the DRN when sonogenetic modulation. a) The schematic illustration of viral transduction and fiber photometry. AAV-hSyn-5-HT2.1 and AAV-TPH2-MscL-mCherry or AAV-TPH2-mCherry were delivered to the DRN and then fibers were installed. Four weeks later, the alteration of green fluorescence intensity was measured *in vivo* when ultrasound stimulation. **b)** Representative images of the DRN overexpressed with a 5-HT sensor and MscL or mCherry. Green, red, and blue fluorescence indicate the signal of the 5-HT sensor, MscL- or EGFP-expressing neurons, and DAPI, respectively. The dashed rectangle indicates the location of the fiber. **c, d)** Ultrasound stimulation induced the release of serotonin in the DRN. Blue and red colors indicated the mCherry (n = 4 mice) and MscL (n = 5 mice) groups, respectively. **c)** Representative 5-HT fluorescence traces of MscL- and mCherry-groups when receiving multiple pulses of 0.25 MPa ultrasound stimulation (left) and averaged 5-HT fluorescence signal from the left panel (right). **d)** The average peak change of 5-HT fluorescence (Peak ΔF/F) in response to 0, 0.11, 0.25 MPa ultrasound stimulation.

Figure 29. Sonogenetic modulation of 5-HT^{DRN} neurons rapidly reversed despair-like behaviors. a) The schematic illustration of viral transduction and ultrasound stimulation. AAV-TPH2-MscL-EGFP or AAV-TPH2-EGFP were delivered into the

DRN. Following recovery, mice were subjected to CRS for 14 days. Then an ultrasonic collimator was installed above the DRN. Another week later, the customized wearable transducer was installed into the collimator and depression-related behavioral tests were conducted when sonication. **b)** MscL fluorescence with DAPI in the DRN. **c-f)** Sonogenetic modulation of 5-HT^{DRN} neurons reversed despair-like behaviors. **c)** The immobility time in the TST among Ctrl-US, MscL-US, Ctrl+US, and MscL+US groups. **d)** The struggling time in the TST among Ctrl-US, MscL-US, Ctrl+US, and MscL+US groups. **e)** The immobility time in the FST among Ctrl-US, MscL-US, Ctrl+US, and MscL+US groups. **f)** The struggling time in the FST among Ctrl-US, MscL-US, Ctrl+US, and MscL+US groups. **g)** The speed in the OFT among Ctrl-US, MscL-US, Ctrl+US, and MscL+US groups.

Figure 30. Sonogenetic modulation of 5-HT^{DRN} neurons elevated their neuronal activity. a) The images which showed c-Fos protein in the DRN among Ctrl-US, MscL-US, Ctrl+US, and MscL+US groups. Green, red, and blue fluorescence indicated MscL- or EGFP-expressing neurons, c-Fos positive signal, and DAPI, respectively. **b)** Counted numbers of c-Fos+ cells in the DRN among Ctrl-US, MscL+US, Ctrl+US, and MscL+US groups. **c)** The ratio of c-Fos & EGFP positive cells to c-Fos positive neurons in the DRN among Ctrl-US, MscL+US, Ctrl+US, and MscL+US groups.

Figure 31. Sonogenetic modulation of serotoninergic neurons in the DRN did not influence the activity of astrocytes or microglia. a) Representative images of Iba1 in the DRN among Ctrl-US, MscL-US, Ctrl+US, and MscL+US groups. **b)**

Representative images of GFAP in the DRN among Ctrl-US, MscL-US, Ctrl+US, and MscL+US groups. **c)** Counts of Iba1-positive cells in the DRN among Ctrl-US, MscL-US, Ctrl+US, and MscL+US groups. Blue and red bars in the histogram indicated EGFP and MscL groups, respectively. **d)** Counts of GFAP-positive cells per slice imaged in the DRN. n = 3-4 mice per group. Blue and red bars in the histogram indicated EGFP and MscL group, respectively.

Figure 32. No detectable tissue response in the DRN after sonogenetic modulation. H&E representative images in the DRN among Ctrl-US, MscL-US, Ctrl+US, and MscL+US groups.

Figure 33. The c-Fos expression in the auditory cortex. a) The schematic illustration of the AC. b**)** The representative images of the c-Fos protein in the AC after sonogenetic modulation among Ctrl-US, MscL-US, Ctrl+US, and MscL+US groups. **c)** Counts of c-Fos positive cells imaged in the AC among Ctrl-US, MscL-US, Ctrl+US, and MscL+US groups.

Figure 34. The graphical summary of sonogenetic modulation for depression. This study is divided into two main parts: the first part focuses on sonogenetic modulation of the circuit from excitatory neurons in the mPFC to the DRN, while the second part examines sonogenetic modulation of 5-HT^{DRN} neurons. As shown in the left panel, sonogenetic modulation of DRN-projecting excitatory mPFC neurons induced the activation of DRN neurons and antidepressant effects. Conversely, inactivating DRN neurons abrogated this antidepressant effect produced by sonogenetic modulation of the mPFC-DRN circuit. Therefore, as depicted in the right

panel, 5-HT^{DRN} neurons were targeted in part 2. Sonogenetic modulation of 5-HT^{DRN} neurons enhanced their neuronal activity and resulted in antidepressant effects. These discoveries highlight the capability of the novel technique - sonogenetic modulation - to activate targeted neuronal populations, engage specific mesoscale neuronal circuits, and induce changes in behavior patterns, potentially offering therapeutic benefits in depression contexts.

REFERENCES

1 Organization, W. H. *Depression*, <https://www.who.int/news-room/fact-sheets/detail/depression> (2022).

2 Global Burden of Disease Study, C. Global, regional, and national incidence, prevalence, and years lived with disability for 301 acute and chronic diseases and injuries in 188 countries, 1990-2013: a systematic analysis for the Global Burden of Disease Study 2013. *Lancet* **386**, 743-800 (2015). https://doi.org:10.1016/S0140-6736(15)60692-4

3 Bachmann, S. Epidemiology of Suicide and the Psychiatric Perspective. *Int J Environ Res Public Health* **15** (2018). https://doi.org:10.3390/ijerph15071425

4 Caraci, F. *et al.* International Union of Basic and Clinical Pharmacology CIV: The Neurobiology of Treatment-resistant Depression: From Antidepressant Classifications to Novel Pharmacological Targets. *Pharmacol Rev* **70**, 475-504 (2018). https://doi.org:10.1124/pr.117.014977

5 Oxford, U. o. *Prevalence of depressive disorders worldwide*, <https://ourworldindata.org/grapher/share-with-depression> (2019).

6 Otte, C. *et al.* Major depressive disorder. *Nat Rev Dis Primers* **2**, 16065 (2016). https://doi.org:10.1038/nrdp.2016.65

7 Geschwind, D. H. & Flint, J. Genetics and genomics of psychiatric disease. *Science* **349**, 1489-1494 (2015). https://doi.org:10.1126/science.aaa8954

8 Sullivan, P. F., Neale, M. C. & Kendler, K. S. Genetic epidemiology of major depression: review and meta-analysis. *Am J Psychiatry* **157**, 1552-1562 (2000). https://doi.org:10.1176/appi.ajp.157.10.1552

9 Shadrina, M., Bondarenko, E. A. & Slominsky, P. A. Genetics Factors in Major Depression Disease. *Front Psychiatry* **9**, 334 (2018). https://doi.org:10.3389/fpsyt.2018.00334

10 Nugent, N. R., Tyrka, A. R., Carpenter, L. L. & Price, L. H. Gene-environment interactions: early life stress and risk for depressive and anxiety disorders. *Psychopharmacology (Berl)* **214**, 175-196 (2011). https://doi.org:10.1007/s00213-010-2151-x

11 McCann, K. E. *et al.* Histone deacetylase and acetyltransferase inhibitors modulate behavioral responses to social stress. *Psychoneuroendocrinology* **75**, 100-109 (2017). https://doi.org:10.1016/j.psyneuen.2016.10.022

12 Oberlander, T. F. *et al.* Prenatal exposure to maternal depression, neonatal methylation of human glucocorticoid receptor gene (NR3C1) and infant cortisol stress responses. *Epigenetics* **3**, 97-106 (2008). https://doi.org:10.4161/epi.3.2.6034

13 Sabunciyan, S. *et al.* Genome-wide DNA methylation scan in major depressive disorder. *PLoS One* **7**, e34451 (2012). https://doi.org:10.1371/journal.pone.0034451

14 Hirschfeld, R. M. History and evolution of the monoamine hypothesis of depression. *J Clin Psychiatry* **61 Suppl 6**, 4-6 (2000).

15 Muller, J. C., Pryor, W. W., Gibbons, J. E. & Orgain, E. S. Depression and anxiety occurring during Rauwolfia therapy. *J Am Med Assoc* **159**, 836-839 (1955). https://doi.org:10.1001/jama.1955.02960260006002

16 Carlsson, A., Lindqvist, M. & Magnusson, T. 3,4-Dihydroxyphenylalanine and 5-hydroxytryptophan as reserpine antagonists. *Nature* **180**, 1200 (1957).

https://doi.org:10.1038/1801200a0

17 Crane, G. E. The psychiatric side-effects of iproniazid. *Am J Psychiatry* **112**, 494-501 (1956). https://doi.org:10.1176/ajp.112.7.494

18 Loomer, H. P., Saunders, J. C. & Kline, N. S. A clinical and pharmacodynamic evaluation of iproniazid as a psychic energizer. *Psychiatr Res Rep Am Psychiatr Assoc* **8**, 129-141 (1957).

19 Zeller, E., Barsky, J., Fouts, J., Kirchheimer, W. & Van Orden, L. Influence of isonicotinic acid hydrazide (INH) and 1-isonicotinyl-2-isopropyl hydrazide (IIH) on bacterial and mammalian enzymes. *Experientia* **8**, 349-350 (1952).

20 Ban, T. A. Fifty years chlorpromazine: a historical perspective. *Neuropsychiatr Dis Treat* **3**, 495-500 (2007).

21 Kuhn, R. The treatment of depressive states with G 22355 (imipramine hydrochloride). *American Journal of Psychiatry* **115**, 459-464 (1958).

22 Hillhouse, T. M. & Porter, J. H. A brief history of the development of antidepressant drugs: from monoamines to glutamate. *Exp Clin Psychopharmacol* **23**, 1-21 (2015). https://doi.org:10.1037/a0038550

23 Pereira, V. S. & Hiroaki-Sato, V. A. A brief history of antidepressant drug development: from tricyclics to beyond ketamine. *Acta Neuropsychiatr* **30**, 307-322 (2018). https://doi.org:10.1017/neu.2017.39

24 Chong, P. S., Fung, M. L., Wong, K. H. & Lim, L. W. Therapeutic Potential of Hericium erinaceus for Depressive Disorder. *Int J Mol Sci* **21** (2019). https://doi.org:10.3390/ijms21010163

25 Brigitta, B. Pathophysiology of depression and mechanisms of treatment. *Dialogues Clin Neurosci* **4**, 7-20 (2002). https://doi.org:10.31887/DCNS.2002.4.1/bbondy

26 Stetler, C. & Miller, G. E. Depression and hypothalamic-pituitary-adrenal activation: a quantitative summary of four decades of research. *Psychosom Med* **73**, 114-126 (2011). https://doi.org:10.1097/PSY.0b013e31820ad12b

27 Knorr, U., Vinberg, M., Kessing, L. V. & Wetterslev, J. Salivary cortisol in depressed patients versus control persons: a systematic review and meta-analysis. *Psychoneuroendocrinology* **35**, 1275-1286 (2010). https://doi.org:10.1016/j.psyneuen.2010.04.001

28 Nemeroff, C. B. *et al.* Elevated concentrations of CSF corticotropin-releasing factor-like immunoreactivity in depressed patients. *Science* **226**, 1342-1344 (1984). https://doi.org:10.1126/science.6334362

29 *The structure of hypothalamus-pituitary-adrenal axis*, <https://www.medindia.net/patients/lifestyleandwellness/link-between-maternal-stress-and-preterm-delivery.htm#what-is-preterm-delivery> (2021).

30 Amsterdam, A., Tajima, K. & Sasson, R. Cell-specific regulation of apoptosis by glucocorticoids: implication to their anti-inflammatory action. *Biochem Pharmacol* **64**, 843-850 (2002). https://doi.org:10.1016/s0006-2952(02)01147-4

31 Bellavance, M. A. & Rivest, S. The HPA - Immune Axis and the Immunomodulatory Actions of Glucocorticoids in the Brain. *Front Immunol* **5**, 136 (2014). https://doi.org:10.3389/fimmu.2014.00136

32 Dowlati, Y. *et al.* A meta-analysis of cytokines in major depression. *Biol Psychiatry* **67**,

446-457 (2010). https://doi.org:10.1016/j.biopsych.2009.09.033

33 Maes, M. *et al.* Increased serum IL-6 and IL-1 receptor antagonist concentrations in major depression and treatment resistant depression. *Cytokine* **9**, 853-858 (1997). https://doi.org:10.1006/cyto.1997.0238

34 Maes, M. *et al.* Increased plasma concentrations of interleukin-6, soluble interleukin-6, soluble interleukin-2 and transferrin receptor in major depression. *J Affect Disord* **34**, 301-309 (1995). https://doi.org:10.1016/0165-0327(95)00028-l

35 Hodes, G. E., Kana, V., Menard, C., Merad, M. & Russo, S. J. Neuroimmune mechanisms of depression. *Nat Neurosci* **18**, 1386-1393 (2015). https://doi.org:10.1038/nn.4113

36 Koo, J. W. & Duman, R. S. IL-1beta is an essential mediator of the antineurogenic and anhedonic effects of stress. *Proc Natl Acad Sci U S A* **105**, 751-756 (2008). https://doi.org:10.1073/pnas.0708092105

37 Meagher, M. W. *et al.* Interleukin-6 as a mechanism for the adverse effects of social stress on acute Theiler's virus infection. *Brain Behav Immun* **21**, 1083-1095 (2007). https://doi.org:10.1016/j.bbi.2007.05.001

38 Maes, M. *et al.* Leukocytosis, monocytosis and neutrophilia: hallmarks of severe depression. *J Psychiatr Res* **26**, 125-134 (1992). https://doi.org:10.1016/0022-3956(92)90004-8

39 James, S. J., Swendseid, M. & Makinodan, T. Macrophage-mediated depression of T-cell proliferation in zinc-deficient mice. *J Nutr* **117**, 1982-1988 (1987). https://doi.org:10.1093/jn/117.11.1982

40 Caldwell, C. L., Irwin, M. & Lohr, J. Reduced natural killer cell cytotoxicity in depression but not in schizophrenia. *Biol Psychiatry* **30**, 1131-1138 (1991). https://doi.org:10.1016/0006-3223(91)90183-m

41 Miller, G. E. *et al.* Greater inflammatory activity and blunted glucocorticoid signaling in monocytes of chronically stressed caregivers. *Brain Behav Immun* **41**, 191-199 (2014). https://doi.org:10.1016/j.bbi.2014.05.016

42 Jin, Y., Sun, L. H., Yang, W., Cui, R. J. & Xu, S. B. The Role of BDNF in the Neuroimmune Axis Regulation of Mood Disorders. *Front Neurol* **10**, 515 (2019). https://doi.org:10.3389/fneur.2019.00515

43 Wohleb, E. S., Powell, N. D., Godbout, J. P. & Sheridan, J. F. Stress-induced recruitment of bone marrow-derived monocytes to the brain promotes anxiety-like behavior. *J Neurosci* **33**, 13820-13833 (2013). https://doi.org:10.1523/JNEUROSCI.1671-13.2013

44 Frank, M. G., Baratta, M. V., Sprunger, D. B., Watkins, L. R. & Maier, S. F. Microglia serve as a neuroimmune substrate for stress-induced potentiation of CNS pro-inflammatory cytokine responses. *Brain Behav Immun* **21**, 47-59 (2007). https://doi.org:10.1016/j.bbi.2006.03.005

45 Torres-Platas, S. G., Cruceanu, C., Chen, G. G., Turecki, G. & Mechawar, N. Evidence for increased microglial priming and macrophage recruitment in the dorsal anterior cingulate white matter of depressed suicides. *Brain Behav Immun* **42**, 50-59 (2014). https://doi.org:10.1016/j.bbi.2014.05.007

46 Setiawan, E. *et al.* Role of translocator protein density, a marker of neuroinflammation, in the brain during major depressive episodes. *JAMA Psychiatry* **72**, 268-275 (2015). https://doi.org:10.1001/jamapsychiatry.2014.2427

47 Brisch, R. *et al.* Microglia in the dorsal raphe nucleus plays a potential role in both suicide facilitation and prevention in affective disorders. *Eur Arch Psychiatry Clin Neurosci* **267**, 403-415 (2017). https://doi.org:10.1007/s00406-017-0774-1

48 Steiner, J. *et al.* Immunological aspects in the neurobiology of suicide: elevated microglial density in schizophrenia and depression is associated with suicide. *J Psychiatr Res* **42**, 151-157 (2008). https://doi.org:10.1016/j.jpsychires.2006.10.013

49 Garcia-Gutierrez, E., Mayer, M. J., Cotter, P. D. & Narbad, A. Gut microbiota as a source of novel antimicrobials. *Gut Microbes* **10**, 1-21 (2019). https://doi.org:10.1080/19490976.2018.1455790

50 Simpson, C. A., Mu, A., Haslam, N., Schwartz, O. S. & Simmons, J. G. Feeling down? A systematic review of the gut microbiota in anxiety/depression and irritable bowel syndrome. *J Affect Disord* **266**, 429-446 (2020). https://doi.org:10.1016/j.jad.2020.01.124

51 Banerjee, A., Sarkhel, S., Sarkar, R. & Dhali, G. K. Anxiety and Depression in Irritable Bowel Syndrome. *Indian J Psychol Med* **39**, 741-745 (2017). https://doi.org:10.4103/IJPSYM.IJPSYM_46_17

52 Varesi, A. *et al.* The brain-gut-microbiota interplay in depression: A key to design innovative therapeutic approaches. *Pharmacol Res* **192**, 106799 (2023). https://doi.org:10.1016/j.phrs.2023.106799

53 Wu, M. *et al.* Associations between disordered gut microbiota and changes of neurotransmitters and short-chain fatty acids in depressed mice. *Transl Psychiatry* **10**, 350 (2020). https://doi.org:10.1038/s41398-020-01038-3

54 Fang, M. *et al.* Scutellarin promotes microglia-mediated astrogliosis coupled with improved behavioral function in cerebral ischemia. *Neurochemistry International* **97**, 154-171 (2016).

55 Kowianski, P. *et al.* BDNF: A Key Factor with Multipotent Impact on Brain Signaling and Synaptic Plasticity. *Cell Mol Neurobiol* **38**, 579-593 (2018). https://doi.org:10.1007/s10571-017-0510-4

56 Filho, C. B. *et al.* Chronic unpredictable mild stress decreases BDNF and NGF levels and Na(+),K(+)-ATPase activity in the hippocampus and prefrontal cortex of mice: antidepressant effect of chrysin. *Neuroscience* **289**, 367-380 (2015). https://doi.org:10.1016/j.neuroscience.2014.12.048

57 Kubera, M., Obuchowicz, E., Goehler, L., Brzeszcz, J. & Maes, M. In animal models, psychosocial stress-induced (neuro)inflammation, apoptosis and reduced neurogenesis are associated to the onset of depression. *Prog Neuropsychopharmacol Biol Psychiatry* **35**, 744-759 (2011). https://doi.org:10.1016/j.pnpbp.2010.08.026

58 Siuciak, J. A., Lewis, D. R., Wiegand, S. J. & Lindsay, R. M. Antidepressant-like effect of brain-derived neurotrophic factor (BDNF). *Pharmacol Biochem Behav* **56**, 131-137 (1997). https://doi.org:10.1016/S0091-3057(96)00169-4

59 Duman, R. S., Heninger, G. R. & Nestler, E. J. A molecular and cellular theory of depression. *Arch Gen Psychiatry* **54**, 597-606 (1997). https://doi.org:10.1001/archpsyc.1997.01830190015002

60 Altar, C. A. Neurotrophins and depression. *Trends Pharmacol Sci* **20**, 59-61 (1999). https://doi.org:10.1016/s0165-6147(99)01309-7

61 Molendijk, M. L. *et al.* Serum BDNF concentrations as peripheral manifestations of

depression: evidence from a systematic review and meta-analyses on 179 associations (N=9484). *Mol Psychiatry* **19**, 791-800 (2014). https://doi.org:10.1038/mp.2013.105

62 Zhang, F. F., Peng, W., Sweeney, J. A., Jia, Z. Y. & Gong, Q. Y. Brain structure alterations in depression: Psychoradiological evidence. *CNS Neurosci Ther* **24**, 994-1003 (2018). https://doi.org:10.1111/cns.12835

63 Yang, Y. & Raine, A. Prefrontal structural and functional brain imaging findings in antisocial, violent, and psychopathic individuals: a meta-analysis. *Psychiatry Res* **174**, 81-88 (2009). https://doi.org:10.1016/j.pscychresns.2009.03.012

64 Zhao, K. *et al.* Altered patterns of association between cortical thickness and subcortical volume in patients with first episode major depressive disorder: A structural MRI study. *Psychiatry Res Neuroimaging* **260**, 16-22 (2017). https://doi.org:10.1016/j.pscychresns.2016.12.001

65 Kong, L. *et al.* Frontal-subcortical volumetric deficits in single episode, medication-naive depressed patients and the effects of 8 weeks fluoxetine treatment: a VBM-DARTEL study. *PLoS One* **9**, e79055 (2014). https://doi.org:10.1371/journal.pone.0079055

66 Shen, Z. *et al.* Changes of grey matter volume in first-episode drug-naive adult major depressive disorder patients with different age-onset. *Neuroimage Clin* **12**, 492-498 (2016). https://doi.org:10.1016/j.nicl.2016.08.016

67 Lu, Y. *et al.* The volumetric and shape changes of the putamen and thalamus in first episode, untreated major depressive disorder. *Neuroimage Clin* **11**, 658-666 (2016). https://doi.org:10.1016/j.nicl.2016.04.008

68 Dombrovski, A. Y. *et al.* The temptation of suicide: striatal gray matter, discounting of delayed rewards, and suicide attempts in late-life depression. *Psychol Med* **42**, 1203-1215 (2012). https://doi.org:10.1017/S0033291711002133

69 Forbes, E. E. *et al.* Altered striatal activation predicting real-world positive affect in adolescent major depressive disorder. *Am J Psychiatry* **166**, 64-73 (2009). https://doi.org:10.1176/appi.ajp.2008.07081336

70 Satterthwaite, T. D. *et al.* Common and Dissociable Dysfunction of the Reward System in Bipolar and Unipolar Depression. *Neuropsychopharmacology* **40**, 2258-2268 (2015). https://doi.org:10.1038/npp.2015.75

71 Geerlings, M. I. & Gerritsen, L. Late-Life Depression, Hippocampal Volumes, and Hypothalamic-Pituitary-Adrenal Axis Regulation: A Systematic Review and Meta-analysis. *Biol Psychiatry* **82**, 339-350 (2017). https://doi.org:10.1016/j.biopsych.2016.12.032

72 Campbell, S., Marriott, M., Nahmias, C. & MacQueen, G. M. Lower hippocampal volume in patients suffering from depression: a meta-analysis. *Am J Psychiatry* **161**, 598-607 (2004). https://doi.org:10.1176/appi.ajp.161.4.598

73 Tendolkar, I. *et al.* Electroconvulsive therapy increases hippocampal and amygdala volume in therapy refractory depression: a longitudinal pilot study. *Psychiatry Res* **214**, 197-203 (2013). https://doi.org:10.1016/j.pscychresns.2013.09.004

74 Hare, B. D. & Duman, R. S. Prefrontal cortex circuits in depression and anxiety: contribution of discrete neuronal populations and target regions. *Mol Psychiatry* **25**, 2742-2758 (2020). https://doi.org:10.1038/s41380-020-0685-9

75 Fakhoury, M. Optogenetics: A revolutionary approach for the study of depression. *Prog*

Neuropsychopharmacol Biol Psychiatry **106**, 110094 (2021). https://doi.org:10.1016/j.pnpbp.2020.110094

76 Cheng, Z., Cui, R., Ge, T., Yang, W. & Li, B. Optogenetics: What it has uncovered in potential pathways of depression. *Pharmacol Res* **152**, 104596 (2020). https://doi.org:10.1016/j.phrs.2019.104596

77 Riga, D. *et al.* Optogenetic dissection of medial prefrontal cortex circuitry. *Front Syst Neurosci* **8**, 230 (2014). https://doi.org:10.3389/fnsys.2014.00230

78 Bagot, R. C. *et al.* Ventral hippocampal afferents to the nucleus accumbens regulate susceptibility to depression. *Nat Commun* **6**, 7062 (2015). https://doi.org:10.1038/ncomms8062

79 Warden, M. R. *et al.* A prefrontal cortex-brainstem neuronal projection that controls response to behavioural challenge. *Nature* **492**, 428-432 (2012). https://doi.org:10.1038/nature11617

80 Biselli, T., Lange, S. S., Sablottny, L., Steffen, J. & Walther, A. Optogenetic and chemogenetic insights into the neurocircuitry of depression-like behaviour: A systematic review. *Eur J Neurosci* **53**, 9-38 (2021). https://doi.org:10.1111/ejn.14603

81 Huang, K. W. *et al.* Molecular and anatomical organization of the dorsal raphe nucleus. *Elife* **8** (2019). https://doi.org:10.7554/eLife.46464

82 Monti, J. M. The structure of the dorsal raphe nucleus and its relevance to the regulation of sleep and wakefulness. *Sleep Med Rev* **14**, 307-317 (2010). https://doi.org:10.1016/j.smrv.2009.11.004

83 Ohmura, Y. *et al.* Different roles of distinct serotonergic pathways in anxiety-like behavior, antidepressant-like, and anti-impulsive effects. *Neuropharmacology* **167**, 107703 (2020). https://doi.org:10.1016/j.neuropharm.2019.107703

84 Nishitani, N. *et al.* Manipulation of dorsal raphe serotonergic neurons modulates active coping to inescapable stress and anxiety-related behaviors in mice and rats. *Neuropsychopharmacology* **44**, 721-732 (2019). https://doi.org:10.1038/s41386-018-0254-y

85 Challis, C. *et al.* Raphe GABAergic neurons mediate the acquisition of avoidance after social defeat. *J Neurosci* **33**, 13978-13988, 13988a (2013). https://doi.org:10.1523/JNEUROSCI.2383-13.2013

86 Zhang, H. *et al.* Dorsal raphe projection inhibits the excitatory inputs on lateral habenula and alleviates depressive behaviors in rats. *Brain Struct Funct* **223**, 2243-2258 (2018). https://doi.org:10.1007/s00429-018-1623-3

87 Yang, Y., Wang, H., Hu, J. & Hu, H. Lateral habenula in the pathophysiology of depression. *Curr Opin Neurobiol* **48**, 90-96 (2018). https://doi.org:10.1016/j.conb.2017.10.024

88 Proulx, C. D. *et al.* A neural pathway controlling motivation to exert effort. *Proc Natl Acad Sci U S A* **115**, 5792-5797 (2018). https://doi.org:10.1073/pnas.1801837115

89 Carreno, F. R. *et al.* Activation of a ventral hippocampus-medial prefrontal cortex pathway is both necessary and sufficient for an antidepressant response to ketamine. *Mol Psychiatry* **21**, 1298-1308 (2016). https://doi.org:10.1038/mp.2015.176

90 Calder, A. J., Lawrence, A. D. & Young, A. W. Neuropsychology of fear and loathing. *Nat Rev Neurosci* **2**, 352-363 (2001). https://doi.org:10.1038/35072584

91 Ramirez, S. *et al.* Activating positive memory engrams suppresses depression-like behaviour. *Nature* **522**, 335-339 (2015). https://doi.org:10.1038/nature14514

92 Clinic, M. *Antidepressants: Selecting one that's right for you*, <https://www.mayoclinic.org/diseases-conditions/depression/in-depth/antidepressants/art-20046273> (

93 *Major classes of antidepressants*, <https://www.compoundchem.com/2015/01/20/antidepressants/> (2015).

94 Cuijpers, P., van Straten, A., Warmerdam, L. & Andersson, G. Psychotherapy versus the combination of psychotherapy and pharmacotherapy in the treatment of depression: a meta-analysis. *Depress Anxiety* **26**, 279-288 (2009). https://doi.org:10.1002/da.20519

95 Schatzberg, A. F. *et al.* Chronic depression: medication (nefazodone) or psychotherapy (CBASP) is effective when the other is not. *Arch Gen Psychiatry* **62**, 513-520 (2005). https://doi.org:10.1001/archpsyc.62.5.513

96 Fava, M. Diagnosis and definition of treatment-resistant depression. *Biol Psychiatry* **53**, 649-659 (2003). https://doi.org:10.1016/s0006-3223(03)00231-2

97 Zugliani, M. M. *et al.* Clinical effectiveness of non-TMS neurostimulation in depression: Clinical trials from 2010 to 2020. *Prog Neuropsychopharmacol Biol Psychiatry* **110**, 110287 (2021). https://doi.org:10.1016/j.pnpbp.2021.110287

98 Medda, P., Perugi, G., Zanello, S., Ciuffa, M. & Cassano, G. B. Response to ECT in bipolar I, bipolar II and unipolar depression. *J Affect Disord* **118**, 55-59 (2009). https://doi.org:10.1016/j.jad.2009.01.014

99 Ben-Menachem, E. Vagus nerve stimulation, side effects, and long-term safety. *J Clin Neurophysiol* **18**, 415-418 (2001). https://doi.org:10.1097/00004691-200109000-00005

100 Hallett, M. Transcranial magnetic stimulation: a primer. *Neuron* **55**, 187-199 (2007). https://doi.org:10.1016/j.neuron.2007.06.026

101 Eranti, S. *et al.* A randomized, controlled trial with 6-month follow-up of repetitive transcranial magnetic stimulation and electroconvulsive therapy for severe depression. *Am J Psychiatry* **164**, 73-81 (2007). https://doi.org:10.1176/ajp.2007.164.1.73

102 Junao Wang, A. S. W. *Neuromodulation Approaches to Mood Disorders*, <https://www.psychiatrictimes.com/view/neuromodulation-approaches-mood-disorders> (2020).

103 Daskalakis, Z. J. *et al.* Magnetic seizure therapy (MST) for major depressive disorder. *Neuropsychopharmacology* **45**, 276-282 (2020). https://doi.org:10.1038/s41386-019-0515-4

104 Kong, J., Fang, J., Park, J., Li, S. & Rong, P. Treating Depression with Transcutaneous Auricular Vagus Nerve Stimulation: State of the Art and Future Perspectives. *Front Psychiatry* **9**, 20 (2018). https://doi.org:10.3389/fpsyt.2018.00020

105 Holtzheimer, P. E. *et al.* Subcallosal cingulate deep brain stimulation for treatment-resistant depression: a multisite, randomised, sham-controlled trial. *Lancet Psychiatry* **4**, 839-849 (2017). https://doi.org:10.1016/S2215-0366(17)30371-1

106 Scangos, K. W. *et al.* Closed-loop neuromodulation in an individual with treatment-resistant depression. *Nat Med* **27**, 1696-1700 (2021). https://doi.org:10.1038/s41591-021-01480-w

107 Generoso, M. B. *et al.* Effect of a 10-day transcutaneous trigeminal nerve stimulation

(TNS) protocol for depression amelioration: A randomized, double blind, and sham-controlled phase II clinical trial. *Epilepsy Behav* **95**, 39-42 (2019). https://doi.org:10.1016/j.yebeh.2019.03.025

108 Askalsky, P. & Iosifescu, D. V. Transcranial Photobiomodulation For The Management Of Depression: Current Perspectives. *Neuropsychiatr Dis Treat* **15**, 3255-3272 (2019). https://doi.org:10.2147/NDT.S188906

109 *Clinical trails*, <https://clinicaltrials.gov/ct2/results?cond=depression&term=photobiomodulation&country=&state=&city=&dist=> (

110 Wang, S. *et al.* Ultrasonic Neuromodulation and Sonogenetics: A New Era for Neural Modulation. *Front Physiol* **11**, 787 (2020). https://doi.org:10.3389/fphys.2020.00787

111 Kamimura, H. A. S., Conti, A., Toschi, N. & Konofagou, E. E. Ultrasound neuromodulation: mechanisms and the potential of multimodal stimulation for neuronal function assessment. *Front Phys* **8** (2020). https://doi.org:10.3389/fphy.2020.00150

112 O'Brien, W. D., Jr. Ultrasound-biophysics mechanisms. *Prog Biophys Mol Biol* **93**, 212-255 (2007). https://doi.org:10.1016/j.pbiomolbio.2006.07.010

113 Wang, P., Zhang, J., Yu, J., Smith, C. & Feng, W. Brain Modulatory Effects by Low-Intensity Transcranial Ultrasound Stimulation (TUS): A Systematic Review on Both Animal and Human Studies. *Front Neurosci* **13**, 696 (2019). https://doi.org:10.3389/fnins.2019.00696

114 Tufail, Y. *et al.* Transcranial pulsed ultrasound stimulates intact brain circuits. *Neuron* **66**, 681-694 (2010). https://doi.org:10.1016/j.neuron.2010.05.008

115 Yoo, S. S. *et al.* Focused ultrasound modulates region-specific brain activity. *Neuroimage* **56**, 1267-1275 (2011). https://doi.org:10.1016/j.neuroimage.2011.02.058

116 Guo, M., Xu, Y. & Gruebele, M. Temperature dependence of protein folding kinetics in living cells. *Proc Natl Acad Sci U S A* **109**, 17863-17867 (2012). https://doi.org:10.1073/pnas.1201797109

117 Sato, T., Shapiro, M. G. & Tsao, D. Y. Ultrasonic Neuromodulation Causes Widespread Cortical Activation via an Indirect Auditory Mechanism. *Neuron* **98**, 1031-1041 e1035 (2018). https://doi.org:10.1016/j.neuron.2018.05.009

118 Guo, H. *et al.* Ultrasound Produces Extensive Brain Activation via a Cochlear Pathway. *Neuron* **98**, 1020-1030.e1024 (2018). https://doi.org:10.1016/j.neuron.2018.04.036

119 Qiu, Z. *et al.* The Mechanosensitive Ion Channel Piezo1 Significantly Mediates In Vitro Ultrasonic Stimulation of Neurons. *iScience* **21**, 448-457 (2019). https://doi.org:10.1016/j.isci.2019.10.037

120 Mohammadjavadi, M. *et al.* Elimination of peripheral auditory pathway activation does not affect motor responses from ultrasound neuromodulation. *Brain Stimul* **12**, 901-910 (2019). https://doi.org:10.1016/j.brs.2019.03.005

121 Niu, X., Yu, K. & He, B. On the Neuromodulatory Pathways of the In Vivo Brain by Means of Transcranial Focused Ultrasound. *Curr Opin Biomed Eng* **8**, 61-69 (2018). https://doi.org:10.1016/j.cobme.2018.10.004

122 Airan, R. D. & Butts Pauly, K. Hearing out Ultrasound Neuromodulation. *Neuron* **98**, 875-877 (2018). https://doi.org:10.1016/j.neuron.2018.05.031

123 Krasovitski, B., Frenkel, V., Shoham, S. & Kimmel, E. Intramembrane cavitation as a

unifying mechanism for ultrasound-induced bioeffects. *Proc Natl Acad Sci U S A* **108**, 3258-3263 (2011). https://doi.org:10.1073/pnas.1015771108

124 Plaksin, M., Kimmel, E. & Shoham, S. Cell-Type-Selective Effects of Intramembrane Cavitation as a Unifying Theoretical Framework for Ultrasonic Neuromodulation. *eNeuro* **3** (2016). https://doi.org:10.1523/ENEURO.0136-15.2016

125 Heureaux, J., Chen, D., Murray, V. L., Deng, C. X. & Liu, A. P. Activation of a bacterial mechanosensitive channel in mammalian cells by cytoskeletal stress. *Cell Mol Bioeng* **7**, 307-319 (2014). https://doi.org:10.1007/s12195-014-0337-8

126 Chesler, A. T. *et al.* The Role of PIEZO2 in Human Mechanosensation. *N Engl J Med* **375**, 1355-1364 (2016). https://doi.org:10.1056/NEJMoa1602812

127 Beurg, M. & Fettiplace, R. PIEZO2 as the anomalous mechanotransducer channel in auditory hair cells. *J Physiol* **595**, 7039-7048 (2017). https://doi.org:10.1113/JP274996

128 Ridone, P., Vassalli, M. & Martinac, B. Piezo1 mechanosensitive channels: what are they and why are they important. *Biophys Rev* **11**, 795-805 (2019). https://doi.org:10.1007/s12551-019-00584-5

129 Ibsen, S., Tong, A., Schutt, C., Esener, S. & Chalasani, S. H. Sonogenetics is a non-invasive approach to activating neurons in Caenorhabditis elegans. *Nat Commun* **6**, 8264 (2015). https://doi.org:10.1038/ncomms9264

130 Burks, S. R., Lorsung, R. M., Nagle, M. E., Tu, T. W. & Frank, J. A. Focused ultrasound activates voltage-gated calcium channels through depolarizing TRPC1 sodium currents in kidney and skeletal muscle. *Theranostics* **9**, 5517-5531 (2019). https://doi.org:10.7150/thno.33876

131 Oh, S.-J. *et al.* Ultrasonic Neuromodulation via Astrocytic TRPA1. *Current Biology* **29**, 3386-3401.e3388 (2019). https://doi.org:10.1016/j.cub.2019.08.021

132 Kubanek, J. *et al.* Ultrasound modulates ion channel currents. *Sci Rep* **6**, 24170 (2016). https://doi.org:10.1038/srep24170

133 Sorum, B., Rietmeijer, R. A., Gopakumar, K., Adesnik, H. & Brohawn, S. G. Ultrasound activates mechanosensitive TRAAK K(+) channels through the lipid membrane. *Proc Natl Acad Sci U S A* **118** (2021). https://doi.org:10.1073/pnas.2006980118

134 Tyler, W. J. *et al.* Remote excitation of neuronal circuits using low-intensity, low-frequency ultrasound. *PLoS One* **3**, e3511 (2008). https://doi.org:10.1371/journal.pone.0003511

135 Yoo, S., Mittelstein, D. R., Hurt, R. C., Lacroix, J. & Shapiro, M. G. Focused ultrasound excites cortical neurons via mechanosensitive calcium accumulation and ion channel amplification. *Nat Commun* **13**, 493 (2022). https://doi.org:10.1038/s41467-022-28040-1

136 Nourse, J. L. & Pathak, M. M. How cells channel their stress: Interplay between Piezo1 and the cytoskeleton. *Semin Cell Dev Biol* **71**, 3-12 (2017). https://doi.org:10.1016/j.semcdb.2017.06.018

137 Tyler, W. J. The mechanobiology of brain function. *Nat Rev Neurosci* **13**, 867-878 (2012). https://doi.org:10.1038/nrn3383

138 Niu, X., Yu, K. & He, B. Transcranial focused ultrasound induces sustained synaptic plasticity in rat hippocampus. *Brain Stimul* **15**, 352-359 (2022). https://doi.org:10.1016/j.brs.2022.01.015

139 Yoo, S., Mittelstein, D. R., Hurt, R., Lacroix, J. & Shapiro, M. G. (2020). https://doi.org:10.1101/2020.05.19.101196

140 Hameroff, S. *et al.* Transcranial ultrasound (TUS) effects on mental states: a pilot study. *Brain Stimul* **6**, 409-415 (2013). https://doi.org:10.1016/j.brs.2012.05.002

141 Sanguinetti, J. L. *et al.* Transcranial Focused Ultrasound to the Right Prefrontal Cortex Improves Mood and Alters Functional Connectivity in Humans. *Front Hum Neurosci* **14**, 52 (2020). https://doi.org:10.3389/fnhum.2020.00052

142 Zhang, D. *et al.* Antidepressant-Like Effect of Low-Intensity Transcranial Ultrasound Stimulation. *IEEE Trans Biomed Eng* **66**, 411-420 (2019). https://doi.org:10.1109/TBME.2018.2845689

143 Zhang, J. *et al.* Low-intensity pulsed ultrasound ameliorates depression-like behaviors in a rat model of chronic unpredictable stress. *CNS Neurosci Ther* **27**, 233-243 (2021). https://doi.org:10.1111/cns.13463

144 Wang, F. *et al.* Low-intensity focused ultrasound ameliorates depression-like behaviors associated with improving the synaptic plasticity in the vCA1-mPFC pathway. *Cereb Cortex* (2023). https://doi.org:10.1093/cercor/bhad095

145 Zhu, Y. *et al.* Transcranial ultrasound stimulation relieves depression in mice with chronic restraint stress. *J Neural Eng* (2022). https://doi.org:10.1088/1741-2552/ac8bfd

146 Wang, Z., Yan, J., Wang, X., Yuan, Y. & Li, X. Transcranial Ultrasound Stimulation Directly Influences the Cortical Excitability of the Motor Cortex in Parkinsonian Mice. *Mov Disord* **35**, 693-698 (2020). https://doi.org:10.1002/mds.27952

147 Xu, T. *et al.* Ultrasonic stimulation of the brain to enhance the release of dopamine - A potential novel treatment for Parkinson's disease. *Ultrason Sonochem* **63**, 104955 (2020). https://doi.org:10.1016/j.ultsonch.2019.104955

148 Lin, W. T., Chen, R. C., Lu, W. W., Liu, S. H. & Yang, F. Y. Protective effects of low-intensity pulsed ultrasound on aluminum-induced cerebral damage in Alzheimer's disease rat model. *Sci Rep* **5**, 9671 (2015). https://doi.org:10.1038/srep09671

149 Li, X. *et al.* Low-Intensity Pulsed Ultrasound Stimulation Modulates the Nonlinear Dynamics of Local Field Potentials in Temporal Lobe Epilepsy. *Front Neurosci* **13**, 287 (2019). https://doi.org:10.3389/fnins.2019.00287

150 Hakimova, H. *et al.* Ultrasound stimulation inhibits recurrent seizures and improves behavioral outcome in an experimental model of mesial temporal lobe epilepsy. *Epilepsy Behav* **49**, 26-32 (2015). https://doi.org:10.1016/j.yebeh.2015.04.008

151 Min, B. K. *et al.* Focused ultrasound-mediated suppression of chemically-induced acute epileptic EEG activity. *BMC Neurosci* **12**, 23 (2011). https://doi.org:10.1186/1471-2202-12-23

152 Chen, S. G. *et al.* Transcranial focused ultrasound pulsation suppresses pentylenetetrazol induced epilepsy in vivo. *Brain Stimul* **13**, 35-46 (2020). https://doi.org:10.1016/j.brs.2019.09.011

153 Leinenga, G. & Gotz, J. Scanning ultrasound removes amyloid-beta and restores memory in an Alzheimer's disease mouse model. *Sci Transl Med* **7**, 278ra233 (2015). https://doi.org:10.1126/scitranslmed.aaa2512

154 Todd, N. *et al.* Modulation of brain function by targeted delivery of GABA through the disrupted blood-brain barrier. *Neuroimage* **189**, 267-275 (2019).

https://doi.org:10.1016/j.neuroimage.2019.01.037

155 Huang, Y. S. *et al.* Sonogenetic Modulation of Cellular Activities Using an Engineered Auditory-Sensing Protein. *Nano Lett* **20**, 1089-1100 (2020). https://doi.org:10.1021/acs.nanolett.9b04373

156 Zhang, M., Rodrigues, A., Zhou, Q. & Li, G. Focused ultrasound: growth potential and future directions in neurosurgery. *J Neurooncol* **156**, 23-32 (2022). https://doi.org:10.1007/s11060-021-03820-9

157 Duque, M. *et al.* Sonogenetic control of mammalian cells using exogenous Transient Receptor Potential A1 channels. *Nat Commun* **13**, 600 (2022). https://doi.org:10.1038/s41467-022-28205-y

158 Wu, C. Y. *et al.* Targeted delivery of engineered auditory sensing protein for ultrasound neuromodulation in the brain. *Theranostics* **10**, 3546-3561 (2020). https://doi.org:10.7150/thno.39786

159 Fan, C. H. *et al.* Sonogenetic-Based Neuromodulation for the Amelioration of Parkinson's Disease. *Nano Lett* **21**, 5967-5976 (2021). https://doi.org:10.1021/acs.nanolett.1c00886

160 Walton, T. A., Idigo, C. A., Herrera, N. & Rees, D. C. MscL: channeling membrane tension. *Pflugers Arch* **467**, 15-25 (2015). https://doi.org:10.1007/s00424-014-1535-x

161 Perozo, E., Cortes, D. M., Sompornpisut, P., Kloda, A. & Martinac, B. Open channel structure of MscL and the gating mechanism of mechanosensitive channels. *Nature* **418**, 942-948 (2002). https://doi.org:10.1038/nature00992

162 Birkner, J. P., Poolman, B. & Kocer, A. Hydrophobic gating of mechanosensitive channel of large conductance evidenced by single-subunit resolution. *Proc Natl Acad Sci U S A* **109**, 12944-12949 (2012). https://doi.org:10.1073/pnas.1205270109

163 Maurer, J. A. & Dougherty, D. A. A high-throughput screen for MscL channel activity and mutational phenotyping. *Biochim Biophys Acta* **1514**, 165-169 (2001). https://doi.org:10.1016/s0005-2736(01)00390-x

164 Shan, F. *et al.* Mechanosensitive channel of large conductance enhances the mechanical stretching-induced upregulation of glycolysis and oxidative metabolism in Schwann cells. *Cell Commun Signal* **22**, 93 (2024). https://doi.org:10.1186/s12964-024-01497-x

165 Heureaux-Torres, J. *et al.* The effect of mechanosensitive channel MscL expression in cancer cells on 3D confined migration. *APL Bioeng* **2**, 032001 (2018). https://doi.org:10.1063/1.5019770

166 Rosholm, K. R. *et al.* Activation of the mechanosensitive ion channel MscL by mechanical stimulation of supported Droplet-Hydrogel bilayers. *Sci Rep* **7**, 45180 (2017). https://doi.org:10.1038/srep45180

167 Soloperto, A. *et al.* Mechano-sensitization of mammalian neuronal networks through expression of the bacterial large-conductance mechanosensitive ion channel. *J Cell Sci* **131** (2018). https://doi.org:10.1242/jcs.210393

168 Ye, J. *et al.* Ultrasonic Control of Neural Activity through Activation of the Mechanosensitive Channel MscL. *Nano Lett* **18**, 4148-4155 (2018). https://doi.org:10.1021/acs.nanolett.8b00935

169 Romantsov, T., Guan, Z. & Wood, J. M. Cardiolipin and the osmotic stress responses of bacteria. *Biochim Biophys Acta* **1788**, 2092-2100 (2009).

https://doi.org:10.1016/j.bbamem.2009.06.010

170 Qiu, Z. *et al.* Targeted Neurostimulation in Mouse Brains with Non-invasive Ultrasound. *Cell Rep* **32**, 108033 (2020). https://doi.org:10.1016/j.celrep.2020.108033

171 Xian, Q. *et al.* Modulation of deep neural circuits with sonogenetics. *Proc Natl Acad Sci U S A* **120**, e2220575120 (2023). https://doi.org:10.1073/pnas.2220575120

172 Cadoni, S. *et al.* Ectopic expression of a mechanosensitive channel confers spatiotemporal resolution to ultrasound stimulations of neurons for visual restoration. *Nat Nanotechnol* (2023). https://doi.org:10.1038/s41565-023-01359-6

173 Hahmann, J., Ishaqat, A., Lammers, T. & Herrmann, A. Sonogenetics for Monitoring and Modulating Biomolecular Function by Ultrasound. *Angew Chem Int Ed Engl* **63**, e202317112 (2024). https://doi.org:10.1002/anie.202317112

174 Shapiro, M. G. *et al.* Biogenic gas nanostructures as ultrasonic molecular reporters. *Nat Nanotechnol* **9**, 311-316 (2014). https://doi.org:10.1038/nnano.2014.32

175 Bar-Zion, A. *et al.* Acoustically triggered mechanotherapy using genetically encoded gas vesicles. *Nat Nanotechnol* **16**, 1403-1412 (2021). https://doi.org:10.1038/s41565-021-00971-8

176 Guilhon, E. *et al.* Spatial and temporal control of transgene expression in vivo using a heat-sensitive promoter and MRI-guided focused ultrasound. *J Gene Med* **5**, 333-342 (2003). https://doi.org:10.1002/jgm.345

177 Wu, Y. *et al.* Control of the activity of CAR-T cells within tumours via focused ultrasound. *Nat Biomed Eng* **5**, 1336-1347 (2021). https://doi.org:10.1038/s41551-021-00779-w

178 Yang, Y. *et al.* Sonothermogenetics for noninvasive and cell-type specific deep brain neuromodulation. *Brain Stimul* **14**, 790-800 (2021). https://doi.org:10.1016/j.brs.2021.04.021

179 Organization, W. H. *Suicide prevention*, <https://www.who.int/health-topics/suicide#tab=tab_1> (2023).

180 Cipriani, A. *et al.* Comparative efficacy and acceptability of 21 antidepressant drugs for the acute treatment of adults with major depressive disorder: a systematic review and network meta-analysis. *Lancet* **391**, 1357-1366 (2018). https://doi.org:10.1016/S0140-6736(17)32802-7

181 Chail, A., Saini, R. K., Bhat, P. S., Srivastava, K. & Chauhan, V. Transcranial magnetic stimulation: A review of its evolution and current applications. *Ind Psychiatry J* **27**, 172-180 (2018). https://doi.org:10.4103/ipj.ipj_88_18

182 Ishimura, K. *et al.* Quantitative analysis of the distribution of serotonin-immunoreactive cell bodies in the mouse brain. *Neurosci Lett* **91**, 265-270 (1988). https://doi.org:10.1016/0304-3940(88)90691-x

183 Shin, Y. *et al.* Characterization of fiber-optic light delivery and light-induced temperature changes in a rodent brain for precise optogenetic neuromodulation. *Biomed Opt Express* **7**, 4450-4471 (2016). https://doi.org:10.1364/BOE.7.004450

184 Castagne, V., Moser, P., Roux, S. & Porsolt, R. D. Rodent models of depression: forced swim and tail suspension behavioral despair tests in rats and mice. *Curr Protoc Neurosci* **Chapter 8**, Unit 8 10A (2011). https://doi.org:10.1002/0471142301.ns0810as55

185 Fosque, B. F. *et al.* Neural circuits. Labeling of active neural circuits in vivo with designed calcium integrators. *Science* **347**, 755-760 (2015).

https://doi.org:10.1126/science.1260922
186 Wan, J. *et al.* A genetically encoded sensor for measuring serotonin dynamics. *Nat Neurosci* **24**, 746-752 (2021). https://doi.org:10.1038/s41593-021-00823-7
187 Lei, T. *et al.* Rislenemdaz treatment in the lateral habenula improves despair-like behavior in mice. *Neuropsychopharmacology* **45**, 1717-1724 (2020). https://doi.org:10.1038/s41386-020-0652-9
188 Can, A. *et al.* The tail suspension test. *J Vis Exp*, e3769 (2012). https://doi.org:10.3791/3769
189 Zheng, Z. *et al.* Hypothalamus-habenula potentiation encodes chronic stress experience and drives depression onset. *Neuron* **110**, 1400-1415 e1406 (2022). https://doi.org:10.1016/j.neuron.2022.01.011
190 Yankelevitch-Yahav, R., Franko, M., Huly, A. & Doron, R. The forced swim test as a model of depressive-like behavior. *J Vis Exp* (2015). https://doi.org:10.3791/52587
191 Zheng, J. *et al.* An insular cortical circuit required for itch sensation and aversion. *Curr Biol* **34**, 1453-1468 e1456 (2024). https://doi.org:10.1016/j.cub.2024.02.060
192 Li, X. Y. *et al.* TGR5-mediated lateral hypothalamus-dCA3-dorsolateral septum circuit regulates depressive-like behavior in male mice. *Neuron* **112**, 1795-1814 e1710 (2024). https://doi.org:10.1016/j.neuron.2024.02.019
193 Xian, Q. *et al.* Protocol for the sonogenetic stimulation of mouse brain by non-invasive ultrasound. *STAR Protoc* **2**, 100393 (2021). https://doi.org:10.1016/j.xpro.2021.100393
194 Bittar, T. P. & Labonte, B. Functional Contribution of the Medial Prefrontal Circuitry in Major Depressive Disorder and Stress-Induced Depressive-Like Behaviors. *Front Behav Neurosci* **15**, 699592 (2021). https://doi.org:10.3389/fnbeh.2021.699592
195 Son, H. *et al.* Glutamine has antidepressive effects through increments of glutamate and glutamine levels and glutamatergic activity in the medial prefrontal cortex. *Neuropharmacology* **143**, 143-152 (2018). https://doi.org:10.1016/j.neuropharm.2018.09.040
196 Tervo, D. G. *et al.* A Designer AAV Variant Permits Efficient Retrograde Access to Projection Neurons. *Neuron* **92**, 372-382 (2016). https://doi.org:10.1016/j.neuron.2016.09.021
197 Sjulson, L., Cassataro, D., DasGupta, S. & Miesenbock, G. Cell-Specific Targeting of Genetically Encoded Tools for Neuroscience. *Annu Rev Genet* **50**, 571-594 (2016). https://doi.org:10.1146/annurev-genet-120215-035011
198 Kovacs, K. J. Measurement of immediate-early gene activation- c-fos and beyond. *J Neuroendocrinol* **20**, 665-672 (2008). https://doi.org:10.1111/j.1365-2826.2008.01734.x
199 Seewoo, B. J. *et al.* Validation of Chronic Restraint Stress Model in Young Adult Rats for the Study of Depression Using Longitudinal Multimodal MR Imaging. *eNeuro* **7** (2020). https://doi.org:10.1523/ENEURO.0113-20.2020
200 Stachniak, T. J., Ghosh, A. & Sternson, S. M. Chemogenetic synaptic silencing of neural circuits localizes a hypothalamus-->midbrain pathway for feeding behavior. *Neuron* **82**, 797-808 (2014). https://doi.org:10.1016/j.neuron.2014.04.008
201 Atchison, W. *Comprehensive Toxicology*. (2010).
202 Jurga, A. M., Paleczna, M. & Kuter, K. Z. Overview of General and Discriminating Markers of Differential Microglia Phenotypes. *Front Cell Neurosci* **14**, 198 (2020).

https://doi.org:10.3389/fncel.2020.00198

203 Zhang, S., Wu, M., Peng, C., Zhao, G. & Gu, R. GFAP expression in injured astrocytes in rats. *Exp Ther Med* **14**, 1905-1908 (2017). https://doi.org:10.3892/etm.2017.4760

204 Norden, D. M., Trojanowski, P. J., Villanueva, E., Navarro, E. & Godbout, J. P. Sequential activation of microglia and astrocyte cytokine expression precedes increased Iba-1 or GFAP immunoreactivity following systemic immune challenge. *Glia* **64**, 300-316 (2016). https://doi.org:10.1002/glia.22930

205 Urban, D. J. *et al.* Elucidation of The Behavioral Program and Neuronal Network Encoded by Dorsal Raphe Serotonergic Neurons. *Neuropsychopharmacology* **41**, 1404-1415 (2016). https://doi.org:10.1038/npp.2015.293

206 Hamani, C. *et al.* Antidepressant-like effects of medial prefrontal cortex deep brain stimulation in rats. *Biol Psychiatry* **67**, 117-124 (2010). https://doi.org:10.1016/j.biopsych.2009.08.025

207 Fu, W. *et al.* Chemical neuroanatomy of the dorsal raphe nucleus and adjacent structures of the mouse brain. *J Comp Neurol* **518**, 3464-3494 (2010). https://doi.org:10.1002/cne.22407

208 McDevitt, R. A. *et al.* Serotonergic versus nonserotonergic dorsal raphe projection neurons: differential participation in reward circuitry. *Cell Rep* **8**, 1857-1869 (2014). https://doi.org:10.1016/j.celrep.2014.08.037

209 <serotonin receptors.pdf>.

210 Dana, H. *et al.* Sensitive red protein calcium indicators for imaging neural activity. *Elife* **5** (2016). https://doi.org:10.7554/eLife.12727

211 Li, Y. Q., Li, H., Kaneko, T. & Mizuno, N. Morphological features and electrophysiological properties of serotonergic and non-serotonergic projection neurons in the dorsal raphe nucleus. An intracellular recording and labeling study in rat brain slices. *Brain Res* **900**, 110-118 (2001). https://doi.org:10.1016/s0006-8993(01)02272-7

212 Sabatini, B. L. & Regehr, W. G. Control of neurotransmitter release by presynaptic waveform at the granule cell to Purkinje cell synapse. *J Neurosci* **17**, 3425-3435 (1997). https://doi.org:10.1523/JNEUROSCI.17-10-03425.1997

213 Liu, T. *et al.* Sonogenetics: Recent advances and future directions. *Brain Stimul* **15**, 1308-1317 (2022). https://doi.org:10.1016/j.brs.2022.09.002

214 Blackmore, D. G., Razansky, D. & Gotz, J. Ultrasound as a versatile tool for short- and long-term improvement and monitoring of brain function. *Neuron* **111**, 1174-1190 (2023). https://doi.org:10.1016/j.neuron.2023.02.018

215 George, M. S. *et al.* Daily left prefrontal transcranial magnetic stimulation therapy for major depressive disorder: a sham-controlled randomized trial. *Arch Gen Psychiatry* **67**, 507-516 (2010). https://doi.org:10.1001/archgenpsychiatry.2010.46

216 Williams, L. M. *et al.* Identifying response and predictive biomarkers for Transcranial magnetic stimulation outcomes: protocol and rationale for a mechanistic study of functional neuroimaging and behavioral biomarkers in veterans with Pharmacoresistant depression. *BMC Psychiatry* **21**, 35 (2021). https://doi.org:10.1186/s12888-020-03030-z

217 Planchez, B., Surget, A. & Belzung, C. Animal models of major depression: drawbacks and challenges. *J Neural Transm (Vienna)* **126**, 1383-1408 (2019). https://doi.org:10.1007/s00702-019-02084-y

218 Chan, K. Y. *et al.* Engineered AAVs for efficient noninvasive gene delivery to the central and peripheral nervous systems. *Nat Neurosci* **20**, 1172-1179 (2017). https://doi.org:10.1038/nn.4593

219 Ye, D. *et al.* Incisionless targeted adeno-associated viral vector delivery to the brain by focused ultrasound-mediated intranasal administration. *EBioMedicine* **84**, 104277 (2022). https://doi.org:10.1016/j.ebiom.2022.104277